NOTICE

AVIS

The quality of this microform is heavily dependent upon the quality of the original thesis submitted for microfilming. Every effort has been made to ensure the highest quality of reproduction possible.

La qualité de cette microforme dépend grandement de la qualité de la thèse soumise au microfilmage. Nous avons tout fait pour assurer une qualité supérieure de reproduction.

If pages are missing, contact the university which granted the degree.

S'il manque des pages, veuillez communiquer avec l'université qui a conféré le grade.

Some pages may have indistinct print especially if the original pages were typed with a poor typewriter ribbon or if the university sent us an inferior photocopy.

La qualité d'impression de certaines pages peut laisser à désirer, surtout si les pages originales ont été dactylographiées à l'aide d'un ruban usé ou si l'université nous a fait parvenir une photocopie de qualité inférieure.

Canadä

SMALL STOICHIOMETRIC FLAMES
FOR THE GAS CHROMATOGRAPHIC
DETERMINATION OF ORGANOMETALLICS

by

Nancy B. Lowery

*Submitted in partial fulfilment of the requirements
for the degree of Ph.D. in chemistry*

at

*Dalhousie University
Halifax, Nova Scotia*
August, 1995

The author has granted an irrevocable non-exclusive licence allowing the National Library of Canada to reproduce, loan, distribute or sell copies of his/her thesis by any means and in any form or format, making this thesis available to interested persons.

L'auteur a accordé une licence irrévocable et non exclusive permettant à la Bibliothèque nationale du Canada de reproduire, prêter, distribuer ou vendre des copies de sa thèse de quelque manière et sous quelque forme que ce soit pour mettre des exemplaires de cette thèse à la disposition des personnes intéressées.

The author retains ownership of the copyright in his/her thesis. Neither the thesis nor substantial extracts from it may be printed or otherwise reproduced without his/her permission.

L'auteur conserve la propriété du droit d'auteur qui protège sa thèse. Ni la thèse ni des extraits substantiels de celle-ci ne doivent être imprimés ou autrement reproduits sans son autorisation.

ISBN 0-612-08774-3

Canadä

Name _Nancy B. Lowery_

Physical Sciences; Pure Sciences - Chemistry (Analytical) |0|4|8|6| U·M·I

SUBJECT TERM   SUBJECT CODE

Subject Categories

THE HUMANITIES AND SOCIAL SCIENCES

COMMUNICATIONS AND THE ARTS
Architecture 0729
Art History 0377
Cinema 0900
Dance 0378
Fine Arts 0357
Information Science 0723
Journalism 0391
Library Science 0399
Mass Communications 0708
Music 0413
Speech Communication 0459
Theater 0465

EDUCATION
General 0515
Administration 0514
Adult and Continuing 0516
Agricultural 0517
Art 0273
Bilingual and Multicultural 0282
Business 0688
Community College 0275
Curriculum and Instruction 0727
Early Childhood 0518
Elementary 0524
Finance 0277
Guidance and Counseling 0519
Health 0680
Higher 0745
History of 0520
Home Economics 0278
Industrial 0521
Language and Literature 0279
Mathematics 0280
Music 0522
Philosophy of 0998
Physical 0523

Psychology 0525
Reading 0535
Religious 0527
Sciences 0714
Secondary 0533
Social Sciences 0534
Sociology of 0340
Special 0529
Teacher Training 0530
Technology 0710
Tests and Measurements 0288
Vocational 0747

LANGUAGE, LITERATURE AND LINGUISTICS
Language
  General 0679
  Ancient 0289
  Linguistics 0290
  Modern 0291
Literature
  General 0401
  Classical 0294
  Comparative 0295
  Medieval 0297
  Modern 0298
  African 0316
  American 0591
  Asian 0305
  Canadian (English) 0352
  Canadian (French) 0355
  English 0593
  Germanic 0311
  Latin American 0312
  Middle Eastern 0315
  Romance 0313
  Slavic and East European 0314

PHILOSOPHY, RELIGION AND THEOLOGY
Philosophy 0422
Religion
  General 0318
  Biblical Studies 0321
  Clergy 0319
  History of 0320
  Philosophy of 0322
Theology 0469

SOCIAL SCIENCES
American Studies 0323
Anthropology
  Archaeology 0324
  Cultural 0326
  Physical 0327
Business Administration
  General 0310
  Accounting 0272
  Banking 0770
  Management 0454
  Marketing 0338
Canadian Studies 0385
Economics
  General 0501
  Agricultural 0503
  Commerce-Business 0505
  Finance 0508
  History 0509
  Labor 0510
  Theory 0511
Folklore 0358
Geography 0366
Gerontology 0351
History
  General 0578

Ancient 0579
Medieval 0581
Modern 0582
Black 0328
African 0331
Asia, Australia and Oceania 0332
Canadian 0334
European 0335
Latin American 0336
Middle Eastern 0333
United States 0337
History of Science 0585
Law 0398
Political Science
  General 0615
  International Law and
    Relations 0616
  Public Administration 0617
Recreation 0814
Social Work 0452
Sociology
  General 0626
  Criminology and Penology ... 0627
  Demography 0938
  Ethnic and Racial Studies 0631
  Individual and Family
    Studies 0628
  Industrial and Labor
    Relations 0629
  Public and Social Welfare 0630
  Social Structure and
    Development 0700
  Theory and Methods 0344
Transportation 0709
Urban and Regional Planning 0999
Women's Studies 0453

THE SCIENCES AND ENGINEERING

BIOLOGICAL SCIENCES
Agriculture
  General 0473
  Agronomy 0285
  Animal Culture and
    Nutrition 0475
  Animal Pathology 0476
  Food Science and
    Technology 0359
  Forestry and Wildlife 0478
  Plant Culture 0479
  Plant Pathology 0480
  Plant Physiology 0817
  Range Management 0777
  Wood Technology 0746
Biology
  General 0306
  Anatomy 0287
  Biostatistics 0308
  Botany 0309
  Cell 0379
  Ecology 0329
  Entomology 0353
  Genetics 0369
  Limnology 0793
  Microbiology 0410
  Molecular 0307
  Neuroscience 0317
  Oceanography 0416
  Physiology 0433
  Radiation 0821
  Veterinary Science 0778
  Zoology 0472
Biophysics
  General 0786
  Medical 0760

EARTH SCIENCES
Biogeochemistry 0425
Geochemistry 0996

Geodesy 0370
Geology 0372
Geophysics 0373
Hydrology 0388
Mineralogy 0411
Paleobotany 0345
Paleoecology 0426
Paleontology 0418
Paleozoology 0985
Palynology 0427
Physical Geography 0368
Physical Oceanography 0415

HEALTH AND ENVIRONMENTAL SCIENCES
Environmental Sciences 0768
Health Sciences
  General 0566
  Audiology 0300
  Chemotherapy 0992
  Dentistry 0567
  Education 0350
  Hospital Management 0769
  Human Development 0758
  Immunology 0982
  Medicine and Surgery 0564
  Mental Health 0347
  Nursing 0569
  Nutrition 0570
  Obstetrics and Gynecology .. 0380
  Occupational Health and
    Therapy 0354
  Ophthalmology 0381
  Pathology 0571
  Pharmacology 0419
  Pharmacy 0572
  Physical Therapy 0382
  Public Health 0573
  Radiology 0574
  Recreation 0575

Speech Pathology 0460
Toxicology 0383
Home Economics 0386

PHYSICAL SCIENCES

Pure Sciences
Chemistry
  General 0485
  Agricultural 0749
  Analytical 0486
  Biochemistry 0487
  Inorganic 0488
  Nuclear 0738
  Organic 0490
  Pharmaceutical 0491
  Physical 0494
  Polymer 0495
  Radiation 0754
Mathematics 0405
Physics
  General 0605
  Acoustics 0986
  Astronomy and
    Astrophysics 0606
  Atmospheric Science 0608
  Atomic 0748
  Electronics and Electricity 0607
  Elementary Particles and
    High Energy 0798
  Fluid and Plasma 0759
  Molecular 0609
  Nuclear 0610
  Optics 0752
  Radiation 0756
  Solid State 0611
Statistics 0463

Applied Sciences
Applied Mechanics 0346
Computer Science 0984

Engineering
  General 0537
  Aerospace 0538
  Agricultural 0539
  Automotive 0540
  Biomedical 0541
  Chemical 0542
  Civil 0543
  Electronics and Electrical 0544
  Heat and Thermodynamics ... 0348
  Hydraulic 0545
  Industrial 0546
  Marine 0547
  Materials Science 0794
  Mechanical 0548
  Metallurgy 0743
  Mining 0551
  Nuclear 0552
  Packaging 0549
  Petroleum 0765
  Sanitary and Municipal 0554
  System Science 0790
Geotechnology 0428
Operations Research 0796
Plastics Technology 0795
Textile Technology 0994

PSYCHOLOGY
General 0621
Behavioral 0384
Clinical 0622
Developmental 0620
Experimental 0623
Industrial 0624
Personality 0625
Physiological 0989
Psychobiology 0349
Psychometrics 0632
Social 0451

To my family

TABLE OF CONTENTS

Chapter 1.   INTRODUCTION

Chapter 2.   EXPERIMENTAL

Chapter 3.   FLAME INVESTIGATIONS

Chapter 4.   HOLOPHOTAL FLAME PHOTOMETRIC DETECTION

Chapter 5.   AUXILIARY SECOND CHANNELS FOR SINGLE-CHANNEL FLAME PHOTOMETRIC DETECTORS

Chapter 6.   MEASUREMENT OF FPD-ACTIVE ELEMENTS IN THE SMALL STOICHIOMETRIC FLAME

Chapter 7. SPECTRA DETERMINED WITH NON-STOICHIOMETRIC FLAMES

LIST OF FIGURES

LIST OF TABLES

ABSTRACT

A small, stoichiometric flame for a commercial gas chromatographic-flame photometric detector has been investigated using a variety of main group and transition elements. It was highly successful for the determination of most of the organometallic compounds, improving detection limits in almost all cases.

In addition to changes in traditional flame-gas flows, modifications were made to the same flame photometric detector so that a larger fraction of its luminescence would reach the photomultiplier tube. Tests with compounds of lead and osmium resulted in up to fifty times enhanced light transmission. Because of the square-root dependence of quantum noise, the signal-to-noise ratios improved about sevenfold.

To this modified version of the flame photometric detector was added a second channel, so that there would be two channels, with high sensitivity, operating simultaneously. Two alternate designs for the secondary channel were tested with compounds of osmium, lead, sulfur and phosphorus. Both the new primary channel and either one of the two second-channel designs yielded higher light throughput and lower detection limits than the original, conventional channel.

Using the stoichiometric flame and the two major modifications, a number of organometallic compounds were determined with detection limits that were significantly better than could be detected with conventional flame photometric techniques. In addition, Si, W, Mg and Bi, previously undetected using gas chromatographic-flame photometric detection, were found to respond favorably to these new conditions.

ABBREVIATIONS AND SYMBOLS[a]

σ	- standard deviation (85)
AW	- acid washed (30)
ECD	- electron capture detector (11)
FID	- flame ionization detector (5)
FPD	- flame photometric detector (1)
FPD-GC	- flame photometric detector-gas chromatography (12)
FWHM	- full width at half maximum (100)
i.d.	- inner diameter (30)
IR	- infrared (99)
LP	- long pass (35)
MDL	- minimum detectable limit (13)
MIP	- microwave induced plasma (12)
MMT	- (methylcyclopentadienyl)manganese tricarbonyl (20)
PMT	- photomultiplier tube (3)
p-p	- peak to peak (38)
RC	- resistor capacitor (31)
RMS	- root-mean-square (85)
S/N	- signal/noise (3)

---

[a]The number in parenthesis indicates the page number where the abbreviation first appears.

UV   - ultraviolet (93)

WB   - wideband (90)

ACKNOWLEDGEMENTS

Chapter 1.   INTRODUCTION

Since its initial development by Brody and Chaney[1] in 1966, flame photometric

detection of gas chromatographic effluents has been the subject of well over 250 citations[2]

and at least 16 published reviews in journals and books.[3-18] This obviously successful and

highly utilized technique has withstood rigorous examination with few modifications and

still remains today one of the most frequently used detectors in gas chromatography,

especially for sulfur and phosphorus compounds. A variety of manufacturing companies

such as: Tracor, IBM Instrumental, Varian, Shimadzu, Pye-Unicam, Carlo Erba and

Perkin-Elmer have marketed their own versions, all claiming ease of operation, good

stability, sensitivity and selectivity. In the following account, an attempt is made to trace

the evolution of the FPD and at the same time describe its basic function, working

parameters, advantages and disadvantages and finally relate its role in present and future

research.

1.1   ORIGINAL FPD

Brody and Chaney[1] were the first to use the chemiluminescent phenomena

produced by a cool air-hydrogen flame operating in a hydrogen-rich atmosphere as an

emission detector to monitor gas chromatographic effluents. Their actual flame assembly,

shown in Figure 1.1, was adapted from a flame ionization detector with the outer housing

1

glass window

optical filter   mirror

photomultiplier tube

hydrogen in

burner

oxygen in

column effluent
(nitrogen)
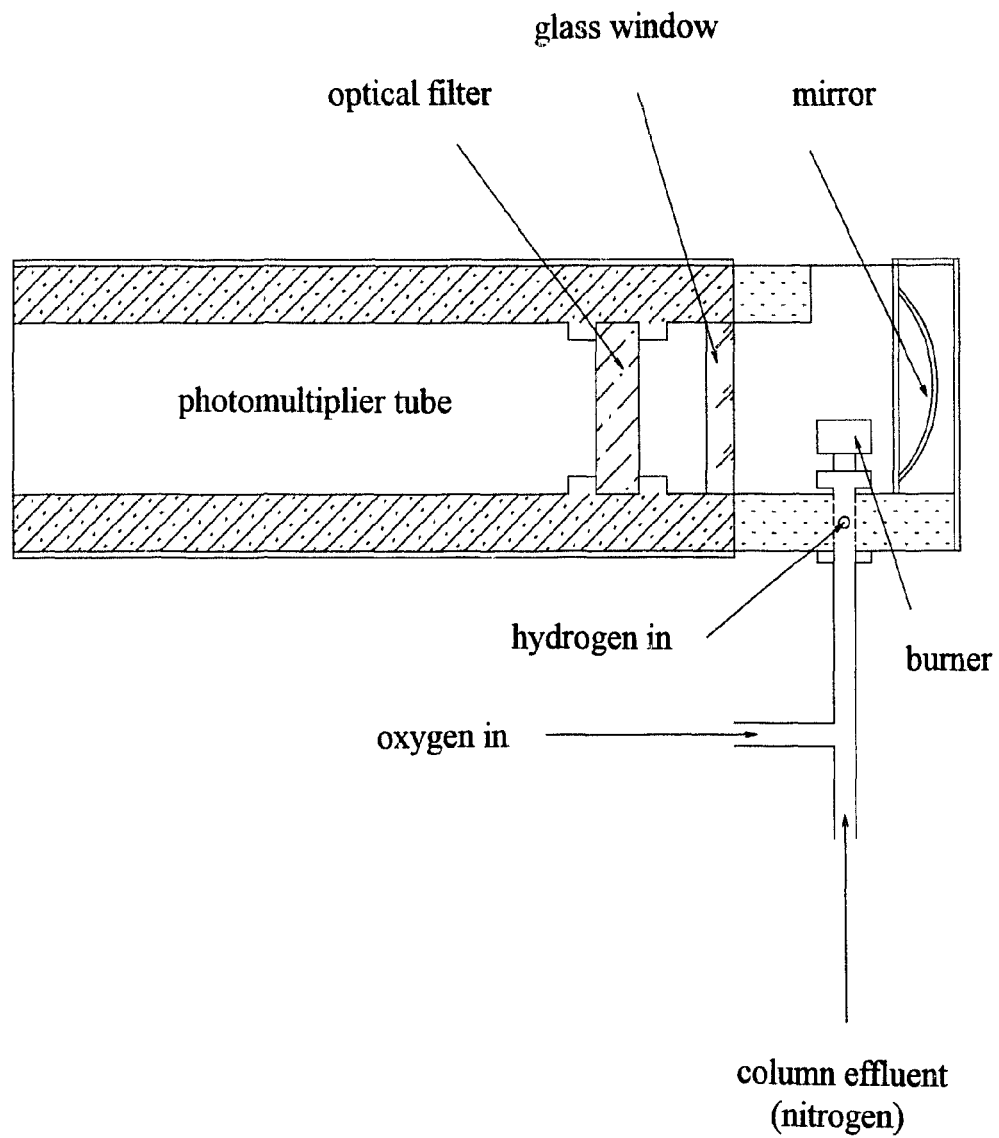
Figure 1.1   Simple schematic of the original FPD of Brody and Chaney.

and collector probe removed. Oxygen was mixed at the column exhaust with the carrier gas, nitrogen, to approximate their ratio in air. The hydrogen was not combined with this mixture but was brought directly to the burner head which was shielded from the optical system. A mirror (later removed as it failed to improve detection limits) was placed behind the flame while a window separated the optical filter and the photomultiplier tube (PMT) from the flame gases. The eluted species would thus pass into a fuel-rich hydrogen/oxygen or hydrogen/air flame and the emission bands of phosphorus and sulfur were monitored by means of appropriate interference filters and the PMT.

The problem of flame-extinction upon injection of an organic solvent larger than 1 μL was overcome by turning off the hydrogen flow (which cooled the igniter coil) for 15-20 seconds. With carrier gas and oxygen flowing, the hydrogen was then brought up to 200 mL/min with the igniter coil on until the flame was successfully ignited. Carrier gas up to 160 mL/min was used with the detector with the ratio of nitrogen carrier gas to oxygen kept at 4 to 1 (total nitrogen + oxygen + air = 200 mL/min). Optimum PMT voltage was found to be 750 V using a signal to noise ratio (S/N) for calibration.

The response to phosphorus at 526 nm (now attributed to HPO emission) provided a minimum detectability of 1×10^{-12} g of P over a four-order linear range. The response to sulfur at 394 nm was not linear but varied approximately as the square of the concentration (S_2 species) with a concentration of 0.6 ppm being easily detected.

1.2   EARLY MODIFICATION TO THE FPD

The FPD was welcomed as a novel means of detecting sulfur and phosphorus with much greater sensitivity than previous detection methods, however, it soon became apparent that there existed a number of drawbacks:

1.   "flame-out" when injection samples exceeded 1 µL

2.   at high concentrations sulfur compounds interfered with phosphorus detection using a 526 nm filter

3.   sulfur response was typically nonlinear

4.   optimum flow rates of feed gases were different for sulfur- and phosphorus-containing compounds and also seemed to vary with detector design

5.   interference from hydrocarbons (CO_2 and H_2O as well) caused decreased sensitivity

To combat these difficulties inherent in the original, "Melpar" FPD of Brody and Chaney, a variety of suggested improvements were soon forthcoming.

1.2.1   Alterations to the Spectral System

Shortly after Brody and Chaney's publication, Zado and Juvet[18] introduced a combination of monochromator and optical system that they used with gas chromatography to successfully analyze transition metal halides, chelates and organic compounds. Their burner apparatus, however, was much larger than the traditional FPD and used far greater, air-rich gas flows. In 1968 Bowman and Beroza[19] constructed a dual detection system which enabled the detection of sulfur and phosphorous at the same time. They evaluated the relative response characteristics of phosphorus and sulfur (R_p/R_s) and

found that $R_p/(R_s)^{1/2}$ was more appropriate because of the non-linear S_2 response. In 1970

a three-channel FID/FPD[20] was employed (similar to Bowman and Beroza's dual-channel

detector) which, using signal to noise values in FID/FPD ratios, could distinguish

phosphorus and sulfur compounds from hydrocarbons.

Another of the early changes in design was the elimination of the mirror at the rear

of the detector as, according to Selucky[6], it made no contribution to detector

performance. Also, to increase response by noise reduction, cooling coils were placed

around the photomultiplier.[5,6] Fiber optics [21] were also used (although not too effectively)

to isolate the phototube from the flame.

1.2.2 Flow Modifications

To overcome the serious problem of flame extinction, automatic ignition systems

and solvent venting valves were introduced.[22] Selucky[6] later concluded that "the tendency

to extinguish the detector when a larger volume of solvent vapour enters the burner

depends much on the operating conditions, i.e., on the ratio of gases in the mixture burned

at the jet". He suggested that the problem can be easily eliminated by introducing a micro-

volume exhaust valve between the column outlet and the detector.

Moye[23], in an earlier attempt to address this same problem, constructed a modified

flow system. He attributed the success of this design to the pre-mixing of combustion

gases in a mixing chamber before meeting the carrier gas at the torch tip (see Figure 1.2b).

The pre-mixed H_2/air did not combust until it exited the torch tip where it was mixed with

carrier. Excess solvent in the carrier could not flash back and extinguish the flame as there

was no available oxygen for combustion. Around the entire burner Moye also added a

a

H$_2$

O$_2$ +N$_2$

Original flame jet
of Brody and Chaney

b

H$_2$ +air

N$_2$

Torch tip burner
of Moye

c

H$_2$ + N$_2$

O$_2$

Ermeto cross-
burner of Gibbons
and Goode

d

O$_2$/air

H$_2$ + N$_2$

Burgett and Green:
Oxygen-hyperventilated Flame

e

H$_2$ + N$_2$

air

Greenhalgh and Wilson:
Pye FPD-Glass and Metal Jet
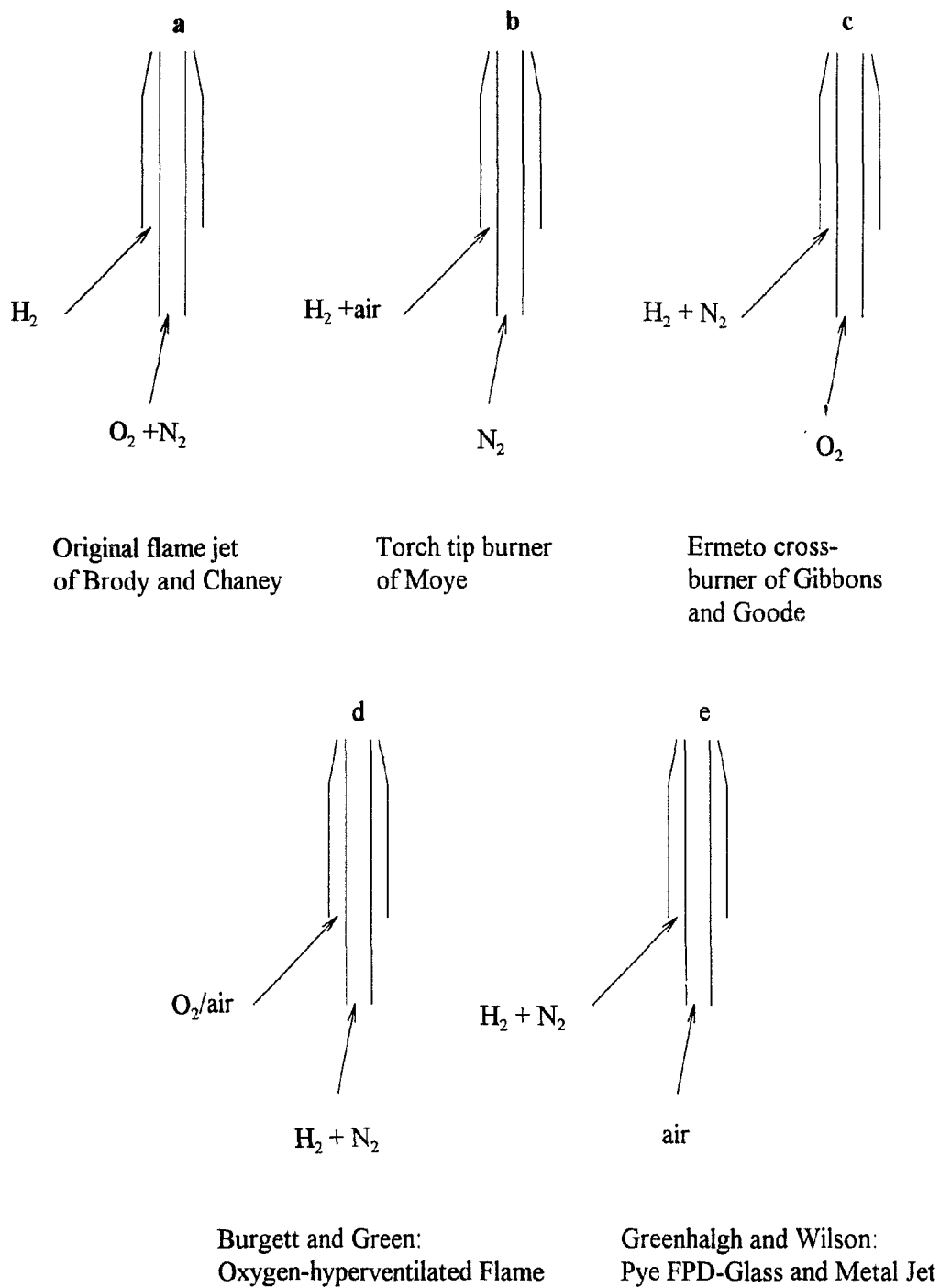
Figure 1.2 Flow modifications: variation in gas supply lines.

glass envelope, tightly fitting at the base and with an exhaust vent at the top. Sevcik[16]

explained the function of this glass shield was to suppress the detector background current

by absorbing wavelengths shorter than 370 nm. However, he also pointed out that the

overall FPD signal would be lower with the shield since the emission intensity of the flame

and the sample would be decreased.

In addition, Selucky[6] described the "Ermeto cross burner" of Gibbons and Goode[24]

(Figure 1.2c) which, unlike Moye's burner, had hydrogen and nitrogen premixed with

oxygen fed separately to the burner tip. Burgett and Green[25], also interested in the

"solvent flameout", reversed the hydrogen and air/oxygen gas inlets (Figure 1.2d) to form

an "oxygen-hyperventilated flame" and evaluated this system by optimizing for response to

both sulfur and phosphorus.

Greenhalgh and Wilson[26] used a Pye FPD, developed in 1974 (Figure 1.2e), which

had a jet composed of concentric glass and metal tubes. The outer tube supplied the

hydrogen and column effluent while the centre tube fed the air. This permitted small

hydrogen flows which in turn eliminated solvent flameout.

The similarity of many of the above systems soon revealed that the flame-

extinction was, indeed, dependent on the manner in which gas flows entered the detector

jet and the problem was virtually eliminated.

1.2.3 Burner Modifications

Besides obvious design enhancement, researchers soon focused their attention on

another aspect of FPD, that of interferences or "quenching". Sevcik[16] described this

process as a "non-radiative de-excitation" which is caused by the absorption of the energy

of excited molecules during collision with other molecules of organic substances.

Rupprecht and Phillips[27] found that when sample mixtures of sulfur and hydrocarbons (or carbon dioxide to a lesser extent) were injected together, the response for sulfur was less than for sulfur alone. As the amount of hydrocarbon was increased, the sulfur response decreased and eventually was completely suppressed. To overcome the effect of this hydrocarbon quenching they opted to remove the interfering hydrocarbons by combustion and to convert the separate sulfur compounds into one compound. In order to do this they constructed a dual-flame FPD. The analyte (hydrocarbons plus sulfur compound) was oxidized in an initial oxygen-rich flame while the second flame, hydrogen-rich, was used to detect the subsequent sulfur emission.

Hasinski[28] also designed a dual-flame system that, in addition to reducing hydrocarbon quenching, would also help to control signal-to-noise ratios, background noise and solvent flameout. He attributed the success of this burner to the geometrical design where the luminescence and burner are separated by a thermal insulation plate. Excess hydrogen was used in both flames. Another dual-flame system was designed by Joonson and Loog[29] which focused on several of the limitations of the FPD. With their separate combustion chamber, they not only eliminated flameouts, they also found equal optimum flow rates for phosphorus- and sulfur-containing compounds. Then, with electrical damping, they could eliminate the "cross-talk" problems between phosphorus and sulfur.

Patterson and coworkers[30], as well, discussed hydrocarbon quenching and solvent flame-out. They used hydrogen-rich flames in both cases to simplify the ignition system

and also found that a metallic structure, rather than glass, eliminated interference from alkali impurities. In a "companion" paper Patterson[31] compared the quenching effects in single- and dual-flame photometric detectors.

An interesting study by McGaughey and Gangwall, published in 1980[32], compared three commercially available detectors in the sulfur mode with respect to dynamic range, linearity, minimum detection limit, sensitivity, peak shape, selectivity and ease of operation. The three detectors, two single-flame and one dual-flame were not significantly different and "none of the systems proved to be superior in all categories".

1.3 FPD DEVELOPMENT POST 1980

After the initial inundation of *improvements*, there still remained only two basic kinds of flame photometric detectors, single-flame and dual-flame. There have been a few alterations in the eighties but most recent development entails more novel application with only minor instrumental changes. In general, the majority of research efforts concentrated on sulfur related work, optimizing, explaining operating parameters and suggesting mechanisms.

Fredriksson and Cedergren[33] discussed optimal flame parameters based on two different burner configurations, again illustrating the success of reversed air and hydrogen inlets. Using a Pye-Unicam FPD they designed a new burner-furnace combination. This modified, now dual-flame, burner was found to be equally effective, with respect to quenching, as the double-burner design of Patterson et al.[30,31] This similarity was

attributed to the fact that the sulfur compounds were converted to SO_2 and the hydrocarbons to CO_2, which reduced compound dependence and hydrocarbon quenching.

Barinaga and Farwell[34], in 1986, described the "simple addition of a small glass tube or chimney over the FPD's jet tip" which they claimed reduced the total dead volume, improved flow streamlining, minimized absorptive detector surface area and lowered detection limits. This was not a completely new concept (earlier studies made use of such devices[21,24,35,36,37]), however, they compared an open mode or standard mode with a 4 mm and a 6 mm glass chimney to try and enhance the limiting parameters of open tubular capillary column gas chromatography. Liu et al[38] also were interested in chimneys and flame profiles in their FPD determination of sulfur. They emphasized the need to maintain an air tight seal at the base of the chimney as air could be "sucked in", thereby decreasing sensitivity significantly. They also addressed the problem of adsorption losses within detectors by placing inactive linings in the carrier gas channel. A new shield ring design was chosen to reduce the background noise but it was found that varying the position of this ring on the flame jet had virtually no effect on the overall S/N. Jiang et al[39] constructed their own detector system, with a quartz tube assembly, specifically to determine butyltins in mussel, using the blue surface-induced luminescence discovered in 1977.[35]

Driscoll and Berger[40] described, in detail, a new type of optical filter, constructed using rare earth glasses which function by ionic absorption. In their FPD studies of sulfur, they used this rare-earth glass filter instead of the traditional interference filter, claiming increased sensitivity with more control of quenching.

In 1987 Wakayama and coworkers[41] applied a modulated magnetic field to a FPD

burner in the detection of phosphorus. This allowed the selective detection of the HPO

emission increasing sensitivity by a factor of five. More recently, Cheskis, Atar and

Amirav[42] devised a pulsed-flame photometer to be used with capillary columns. It used a

"self-terminating flame" that operated in a periodic manner. They cited a variety of

advantages including: higher sensitivity, improved selectivity, additional heteroatom

selective detection modes, less gas consumption, reduced quenching, no flameout and

solvent problems, and increased level of information. Two disadvantages were described

as column flow effects and combustor surface effects.

The above description of FPD development entails only those advancements

directly related to the design of the detector itself. Much progress has also been

accomplished by automation[43], or by coupling FPD techniques with other analytical

systems such as high-resolution gas chromatography[44], supercritical fluid

chromatography[45,46], and series-coupled capillary columns[47], not to mention digital

processing[48]. Earlier papers describing combinations with FID, ECD systems etc. are too

numerous to include in this brief review.

1.4   CHEMILUMINESCENCE

Design improvement and technical advancement have not been the only focus for

FPD research as a significant number of responsive elements have been added to the

original sulfur and phosphorus.[49] While it still remains impossible to predict which

elements emit or which should be more responsive, it is apparent, in view of the low temperatures of the flame (typically 300-600 °C), that chemical excitation, not thermal, is responsible.

Alkemade et al.[50] use the term chemiluminescence to describe "any process whereby species are excited to produce light emission as a result of a chemical reaction in which part of the chemical energy is directly converted into electronic excitation energy." If "these processes should lead to suprathermal emission", then they "refer to this emission as suprathermal chemiluminescence". This suprathermal chemiluminescence is further subdivided into "hard" and "soft" where the hard includes higher excitation energies up to 9 eV where the soft is less than 5 eV. Furthermore, they disregard the soft as a nuisance which may "cause serious errors" and state that "this effect is of no practical use in analytical chemistry". However, soft, suprathermal chemiluminescence (labelled more simply as chemiluminescence in FPD-GC literature), when used in conjunction with gas chromatography, has been found to be extremely successful for a variety of elements. The FPD has, in fact, been used to determine not only main group elements but also a number of transition metals and often with better results than the best high-energy (thermal) sources such as the microwave induced plasma (MIP).

The following account will attempt to give a very brief summary of all "FPD-active" elements with respect to four specific areas:

1. optimal analytical conditions (i.e. compounds, temperatures, gas flows, etc.)

2. calibration (linear range)

3. minimum detectable limit (MDL) with $S/N_{p-p} = 2$

4. spectral information

Although sulfur and phosphorus have traditionally been linked together, it may be more interesting for the purpose of this study to place them and the other elements in their own families or periodic groups.

1.5 MAIN GROUP ELEMENTS

The absence of response from a particular compound does not necessarily indicate a lack of response from the element in question. It may simply mean that the chosen compound perhaps did not behave well chromatographically; thus, the availability of suitably volatile analytes often dictates the response of an element. The alkali and alkaline earth metals have remained so far untested, perhaps for this very reason, but the main group families 13 to 17 all have at least one member that responds favourably.

1.5.1 Boron

In the early seventies Sowinski and Suffet[51,52] analyzed boron compounds in a Melpar FPD. Optimum flame gas flows were found at a ratio of oxygen to hydrogen of 0.58, i.e., almost stoichiometric conditions. The minimum detectable limit for decaborane was reported as 0.72 ng or -log(mole B/s) ~ 11. No actual spectra were published but using a 546 nm bandpass filter (halfwidth = 10 nm) they determined the emitting species to be BO*.

Aue et al[53] included boron as one of the main group elements in their FPD study on

selectivity, spectra and computer-generated specificity. Their interest lay not in

optimization of boron but rather in using it as an example of a dual emission, BO* and

BO_2^*. Two spectra were given, one at 200 mL/min of hydrogen and 45 mL/min of air and

the other at almost stoichiometric conditions. They found the presence of BO* dominates

at hydrogen-rich flows but BO_2^* at stoichiometric.

1.5.2 Carbon

Group 14 elements show a great diversity in both chemical and physical properties

and their response characteristics in the FPD are no exception. Carbon compounds

traditionally have a very low response, a fortunate property since they constitute the major

portion of many typical "FPD" standard compounds, e.g., t-butyldisulfide,

triethylphosphate, n-tetrabutyltin. However, unless an element responds significantly

larger (at least an order of magnitude) than the expected carbon response, then the

element response cannot be considered conclusive. Sun and Aue[54], recognizing this need

for comparison, were the first to obtain calibrations and spectra of carbon at relevant FPD

operating conditions. They used three different standard carbon compounds, an alkane, an

aliphatic ether and an aromatic in order to simulate the organic portion of the various

organometallic analytes. The linear range was between two and two and a half orders of

magnitude with an MDL of 9.2 (-log[mole C/s]). The spectra, although obtained at very

low light levels, showed a definite peak at 430 nm, probably from CH. Spectrally the

aromatic was not only stronger than the aliphatics, it was also slightly different.

1.5.3 Germanium and Tin

Unlike carbon (and silicon which has not been detected by FPD), germanium and tin have responded with exceptionally high sensitivity with detection limits in -log(mole/s) of 16 for germanium and 17.3 for tin.[48] Kapila et al[2] give a brief review of the work done with tin and germanium but most of the work on these compounds has been done by Aue and co-workers.[35,55,56,57,58] They found, in addition to the red or "gas phase" luminescence of tin, there was a more intense blue "surface" emission that was up to one hundred thousand times larger than for the corresponding hydrocarbons. Calibration curves showed that the tin response was linear over more than two orders of magnitude but became slightly exponential at a higher range. The spectra depended on the type of emission and, as well, the operating conditions. Using the constricted quartz flame enclosure (blue emission), and "normal" conditions, the spectra consisted of a broad, featureless emission with a maximum at 390 nm. If the detector was over-loaded, a broad, featureless emission appeared at 480 nm but there was a sharp band at 610 nm attributed to SnH. Aue and Flinn[55] also found that germanium responded in a similar fashion with both red and blue emission, the latter being stronger with a maximum around 615 nm.

1.5.4 Lead

Lead has been successfully analyzed in the filter-less mode, introduced by Aue and Hastings[49], with a minimum detectable limit of about 30 ng (under unoptimized conditions). Calibration appeared linear and the selectivity against hydrocarbons was about two orders of magnitude. Additional work by Aue and coworkers[53] showed a spectrum of tetraethyllead at flows of 200 mL/min of hydrogen and 45 mL/min of air

(common and not optimized conditions). Low light levels prevented accurate assignment of features but two maxima occurred between 480 and 640 nm. Further unpublished work by members of this group may provide supplementary information.

1.5.5 Nitrogen

Nitrogen was analyzed under the same conditions as outlined for lead[53]. Again, optimizations and calibrations were not the purpose of this study but spectral data under common analyte conditions were obtained. The luminescence was weak but injections of indole clearly showed an unidentified maximum around 460 nm.

1.5.6 Phosphorus

The response characteristics of phosphorus have been described extensively in the literature[3-18] and, therefore, will be discussed only briefly. The spectrum consisted of three main bands between 500 and 600 nm (due to HPO^*) with the largest found at around 526 nm. Calibrations were usually linear over more than three orders of magnitude and the MDL, as -log(mole/s), was 14.4.[48] The selectivity against hydrocarbons was over 10^4.

1.5.7 Arsenic, Antimony and Bismuth

Arsenic and antimony have also been the subject of a number of emission studies involving cooler flames. In their 1973 paper using a filterless FPD, Aue and Hastings[49] measured the response of triphenyl derivatives of arsenic, antimony and bismuth. At flow rates in mL/min: hydrogen 140, oxygen 27, air 60 and nitrogen 15, the arsenic gave the best result of the three. Both arsenic and antimony were linear over almost two orders with MDLs around 30 ng. Bismuth was less sensitive at ~100 ng and was also only a little over ten times better than hydrocarbon model compounds under the same conditions.

Earlier work with a number of different fluorides, using a low-temperature

diffusion flame, produced spectra of both arsenic and antimony.[59] Arsenic was described

as a broad continuum, due to an unidentified species, over the range of 360 to 600 nm.

Antimony was also portrayed as a broad continuum but from 440-700 nm with a

maximum about 580 nm, attributed to the SbO species. Several years later, Kapila and

Vogt[60], using a dual-flame burner in single mode and optimum flow conditions of 60

mL/min of hydrogen and 110 ml/min air, obtained a minimum detectable amount of 0.5 ng

of triphenylarsenic. The response was linear over three decades and the selectivity, As/C,

was over a thousand. The spectrum (band pass = 3 nm) was a broad continuum from 400

to 625 nm with AsO being a possible emitter. These spectra were very similar to previous

results obtained by molecular emission cavity analysis.[61]

Aue and co-workers[53] under the "common" conditions for their study of some

main-group elements, also included a spectrum of arsenic (for comparison purposes only)

which appeared to be very similar to the known continuum. In addition, they showed the

spectrum obtained from injections of triphenylantimony, a slightly narrower band starting

at 500 nm with a maximum at around 600 nm which was also similar to that obtained by

Dagnall and co-workers.[59] Analysis of triphenylbismuth was attempted but was

discontinued because of experimental difficulties.

1.5.8 Sulfur

Sulfur, like phosphorus, has been well documented in the literature. Because of its

quadratic or almost quadratic response, mechanisms and models have been difficult to

establish. Kapila et al.[2] gave a summary of both historical and up-to-date publications

I

involving most aspects of FPD sulfur analysis, much of which is based on a review by

Farwell and Barinaga.[13] Therefore, as with phosphorus, just a brief description will

suffice. To monitor the S_2 species the emission band at 324 nm is usually selected.

Optimum conditions vary widely in the literature but cool hydrogen-rich flames are used

for maximum response. Minimum detectable limits vary, according to Dressler[17], from

2×10^{-12} to 5×10^{-11} g S/s while the linear range is approximately two orders of magnitude.

The selectivity is highly dependent on experimental conditions. Aue and Sun[62] described a

linear emitter that exhibited a response about five times larger than the quadratic mode

with a linear range of four decades. The spectrum occurred in the 600 to 850 nm region

and was a first order process.

1.5.9 Selenium and Tellurium

Aue and Flinn [63,64] recorded results very similar to that of quadratic sulfur for both

selenium and tellurium. Compounds of both Te and Se were analyzed in the

picogram/second range and spectral information suggested that Se_2^* and Te_2^* were

probably the emitting species. A method for linearizing chalcogen response (S, Se and Te)

was also developed.

1.5.10 Halogens

The halogens have successfully been determined with the FPD but only when

sensitized with copper or indium. Kapila et al.[2] discussed these methods but found that

the overall sensitivity and stability of these "FPD" halogen detection systems were not as

good as those of the electron capture detector or the electrolytic conductivity detector.

1.6 TRANSITION METALS

Chemiluminescence in GC-FPD analysis has recently been developed as a highly intriguing and also unpredictable means of detection for a variety of transition metals.[54] Why such responses occur or how they occur in these cool, hydrogen-rich flames remains, for the most part, pure speculation. As in traditional flame spectroscopy, some of these heavy metals do display atomic lines. Unlike in hotter flames, molecular bands seem to be responsible for some of the stronger emitters. There are also other emitters, less strong, yet still significant, that display large continua. Despite the low temperature of the flame, these chemiluminescent responses have demonstrated both good selectivity and high sensitivity. A brief summary follows of FPD-active transition metals, classified according to their periodic group. Groups 3-5, however, have shown little response, which again may be due to a lack of a sufficiently volatile compound that can be chromatographed.

1.6.1 Chromium and Molybdenum

Chromium was the first transition metal to be analyzed in the FPD. Ross and Shafik[65], using chromium trifluoroacetylacetonate and a 425.4 nm filter found only a range of 2.5 to 90 ng of Cr and no spectral information was obtained. Burgett and Green[66], several years later selected the chromium emission at 520 nm with optimum flow ratios of: 70 mL/min of hydrogen, 50 mL/min air and 50 mL/min oxygen. They found a linear response from 50 pg to 500 ng which was ten thousand times larger than for hydrocarbor ι.

In a filterless, hydrogen-rich mode (hydrogen 300 mL/min and air 55 mL/min),

using hexacarbonylchromium, Sun and Aue[54] obtained a minimum detectable amount of

5×10^{-14} mole Cr/s. They measured spectra at these conditions as well as at stoichiometric,

obtaining essentially the same results. They were able to observe both atomic

contribution, with small sharp peaks at about 359 nm and 427 nm, and broad features as

well. In addition, the spectrum for molybdenum was obtained by injecting the

hexacarbonyl derivative. The response was much weaker than chromium (MDL = 2×10^{-12}

mole Mo/s) and the spectrum was measured with less resolution. Although relatively

close to the response of hydrocarbons, a sharp peak appeared around 420 nm while

broader maxima occurred around 500 nm and 600 nm.

1.6.2 Manganese and Rhenium

In Group 7 both manganese[67] and rhenium[54] have been shown to respond

favourably. The minimum detectable amount of manganese, as (methylcyclopentadienyl)-

manganese tricarbonyl (MMT) was reported as 2×10^{-14} mole/s at hydrogen flows of 300

mL/min, air 80 mL/min and extra nitrogen, added to the air stream, of 20 mL/min. The

linear range for the manganese compound was over 4 orders of magnitude while

selectivity ratios of three to six orders of magnitude were obtained compared to lead,

phosphorus, sulfur and carbon (using dual-channel differential modes). The spectrum

obtained at these same conditions showed a sharp maximum at 403 nm, corresponding to

the atomic manganese, while another sharp feature was observed at 540 nm, also a

probable atomic transition.

The minimum detectable amount for rhenium[54], injected as dirheniumdecacarbonyl

was reported as 6×10^{-13} mole Re/s with a linear range over three decades. The spectrum

was found to be basically continuous with maxima around 600 and 650 nm.

1.6.3 The Iron Family

Iron[68], ruthenium[69] and osmium[70] have all responded well in the FPD, and ruthenium, bis(cyclopentadienyl)ruthenium in particular, has been shown to be highly sensitive with the MDL around 1×10^{-15} mole/s. The linear range was well over four orders of magnitude while the elemental selectivity, ruthenium /carbon, was 4×10^5. Optimal gas flows in mL/min (no filter, no chimney) were hydrogen 300, air 80 and extra nitrogen (in the air supply) 20. At these conditions the spectrum showed an unidentified emission source (perhaps RuH) with two sharp peaks at 484 nm and 528 nm. The emissions between 350 nm and 400 nm corresponded to known atomic Ru lines; however, the other two features were much stronger.

Iron was also chromatographed as the metallocene and responded with an MDL of 5.4×10^{-14} mole/s. The linear range was similar to ruthenocene and was 1.5×10^4 times stronger than a corresponding hydrocarbon. These results were obtained at the following optimized conditions: hydrogen 370 mL/min, air 60 mL/min and extra nitrogen in the air, 23 mL/min. Spectral data using ferrocene were obtained at three different flame conditions. At close to optimal conditions a spectral scan showed peaks between 330 and 400 nm (345, 373 and 387 nm) which were attributed to atomic transitions. At flows of hydrogen 260 mL/min and air 81 ml/min, the spectrum changed slightly. The 373 nm feature increased and a broad feature between 400 and 600 nm appeared. At almost stoichiometric conditions the "atomic" portion was less clearly defined and there was a large maximum between 460 and 580 nm.

Optimal conditions for Os response (using osmocene) were 300 mL/min of

hydrogen and 60 mL/min of air with 20 mL/min of extra nitrogen. The minimum

detectable amount (-log[mole Os/s]) was 12.8 and the linear range extended about three

orders of magnitude.

1.6.4 Cobalt

Sun and Aue[54] used dicyclopentadienylcobalt to obtain a linear calibration and a

spectrum for cobalt but the luminescence was only about an order of magnitude stronger

than that of naphthalene. The main emission appeared around 400-420 nm and again,

with its similarity to carbon, no conclusive information was obtained.

1.6.5 Nickel

Nickel (as nickelocene) has been reported to be a relatively sensitive metal[48,54] with

-log(mole Ni/s) equal to 13.9. Calibration curves showed a linear range over four orders

of magnitude and the overall response was 10^3 larger than carbon. The interesting

spectrum, in addition to some atomic lines, contained a number of unidentified features

quite possibly due to NiH and NiO systems. No further elements in group 10 responded,

nor were any metals in groups 11 or 12 found to be FPD-sensitive.

1.7 RESEARCH OBJECTIVES

As mentioned earlier, analytical emission spectrometry involves thermal excitation,

as opposed to the chemiluminescent excitation produced by the cool, very small flames of

the FPD. Chemiluminescent spectroscopy or "suprathermal excitation of the first kind"[50]

(up to 5 eV and typically involving atomic recombination) is generally dismissed as an

"interference" of little interest to analytical spectroscopy. Yet, as demonstrated in the

preceding summary, this excitation system, when used in conjunction with gas

chromatography, has been found to be extremely successful with a variety of elements.

Nevertheless, most of these detector responses are largely empirical and require much

more investigation to be fully understood. Outlined below are some research objectives

that were originally planned to further investigate the role of the traditional FPD.

1.7.1 New Chemical Systems

The optimal conditions for much of the work above have been found using a

"normal" FPD flame, i.e., air fed through a centre jet, and nitrogen (carrier), hydrogen and

analyte directed to the outside in a diffusion-type flame. In an attempt to change the

chemistry of the flame and/or the nature of the emitter, several proposals were considered.

First, a premixed flame versus the diffusion flame should be checked in case there may be

spectral differences. In addition, optimizations could be carried out with a variety of flame

types based on not only different gas flow modes but nozzle designs as well.

1.7.2 Fast and Flexible Spectral Measurement

Routine spectral measurements can be very time consuming not only because of

actual sample injection time but also because of the necessity to adapt spectrometers to

the existing apparatus. It was decided to assemble a variable interference filter

monochromator, with a range of 400 to 1000 nm, that could be quickly and efficiently

installed on existing apparatus. Although it would not provide the spectral resolution of a

quarter-meter grating monochromator, it could be used to easily measure spectra of

intermediate or low intensity (often beyond the ability of conventional grating

monochromators). Furthermore, it could give a preliminary scan of more sensitive

elements which would later make measurement with a quarter-meter grating

monochromator easier.

1.7.3 Optical Enhancement of Light Throughput

As just mentioned above, one of the problems with spectral analysis using the

FPD-GC system is the low response of some of the emitters reported. Arguments can

logically be made that part, if not all, of the response of a weak emitter could be attributed

to the hydrocarbon portion of the analyte. Also the fragile nature of any spectral

measuring device (including the variable filter suggested above) means there must be

adequate separation from the hot detector body of the FPD. This, in turn, means reduced

light levels. It was, therefore, necessary to increase light throughput to the variable

interference filter by improving the basic optical system. Among the possible

improvements were the installation of a taller, centred burner, addition of a mirror system

and/or lens, adjustment of the length of the light path (including a special cooling section)

and finally the insertion of a highly polished cylinder in the pathway to help in collecting all

possible light.

1.7.4 Search for New FPD-active Elements

The absolute light level of most FPD-active elements is unquestionably low but,

with the enhancement of light throughput, there is a distinct possibility that more elements

do exist that previously could not be determined. Once these elements are detected it is

necessary to optimize, calibrate and obtain useful spectral information. Also, it may prove

interesting to further investigate those elements that, because of their weak response, were dismissed as being not conclusively different from carbon.

The proposals outlined above follow some the same themes as that of previous FPD-related research, improvement of existing techniques and application of these systems to our understanding of spectral analytical chemistry. With hindsight, it is possible to say that most of the objectives were carried out but not always with anticipated results. Successes (like the development of an auxiliary second channel described in Chapter 5) are recorded in detail but an attempt is also made to describe any lesser achievements that may help to better define the capabilities of the FPD-GC system.

Chapter 2.   EXPERIMENTAL

2.1   GENERAL DESCRIPTION

The original chromatographic system was set up using a 1990 Shimadzu GC-8APF$_p$. Six basic units constituted the main body of this model:

1. column oven
2. flow control
3. basic control
4. power control
5. detector control
6. detector

Of these six units only the column oven and the basic control were left unaltered. The original GC gave excellent performance both in isothermal or programmed temperature mode, however, special needs arising from various research projects dictated a number of changes.

2.1.1   Column Oven

The oven could accommodate different sizes of column depending on the type, i.e., stainless steel, glass or capillary. However, only 100 x 0.3 cm Pyrex columns were used in this work. The upper temperature range rarely exceeded 250 °C, far from the maximum of 400 °C listed for the isothermal mode. Temperature control precision was ± 0 .1 °C and the programming rate was variable from 0.5 to 32 °C/minute.

2.1.2   Flow Control

The original flow control system included pressure regulators with gauges reading

26

kg/cm² for both nitrogen, the carrier gas and for the flame gases, hydrogen and air. To obtain more control and accurate measurement of flow in mL/minute, three significant steps were taken: rotameters were installed, in-line-regulators (0-10 psi) were added and the restrictors in the air and hydrogen inlet lines were removed. A flow controller and a rotameter were also installed on the carrier line. An angle metering valve (B-SS2-A, Nupro Company, 4800 East 345th Street, Willoughby, Ohio, 44094) controlled the air supply but for hydrogen (which needed to be controlled to very low values) a two valve system was installed. First there was a straight metering valve (B-SS2) followed by a double pattern model with a vernier on one end (B-SS2-A), both from Nupro.

2.1.3 Basic Control

The basic control unit supplied the power to the entire instrument. It controlled the injection/detector temperature (always about 30 to 50 °C higher than the column) and the oven as well. Temperature readouts, pilot lights, programming rates were all part of this unit.

2.1.4 Power Control

The FPD control was essentially an electrometer which processed the detector signals. Included in this section were range control (1 to 10^3) , attenuation (1 to 1024), zero adjust (fine and coarse) and high voltage supply. The electrometer components were not altered with the exception of the zero adjust. Here the resistance was changed in the basic electric circuit to provide a larger bucking range.

2.1.5 Detector Control

The light detector, a head-on photomultipler, was originally supplied with a

maximum dynode voltage of -700 V. This high voltage supply was replaced with a lab-made, -70 to -1270 V power unit.

2.1.6 Detector

The original detector unit is shown in Figure 2.1. This detector was modified a number of times and the changes, designed mostly to enhance the light through-put, are described in the appropriate sections. Optical filters were from either Ditric (no longer in business) or Oriel (250 Long Beach Blvd., P.O. Box 872, Stratford, CT. USA 06497). Specific information about the spectral characteristics of these optical filters (only long pass filters were used) is summarized in Appendix I.

Most of the work was performed with either an R-1104 or an R-2228 photomultiplier tube with occasional use of an R-268 or R-316, all from Hamamatsu (Hamamatsu Corporation, 250 Wood Avenue, Middlesex, NJ, 08846). Table 2.1 outlines the nominal range and wavelength of maximum yield of each of these photomultipliers.

Table 2.1

PMT Range and Yield

PMT Model	Nominal Range (nm)	Wavelength of Maximum Yield (nm)
R 1104	180~850	420
R 2228	300~900	650
R 268	300~650	420
R 316	400~1200	800
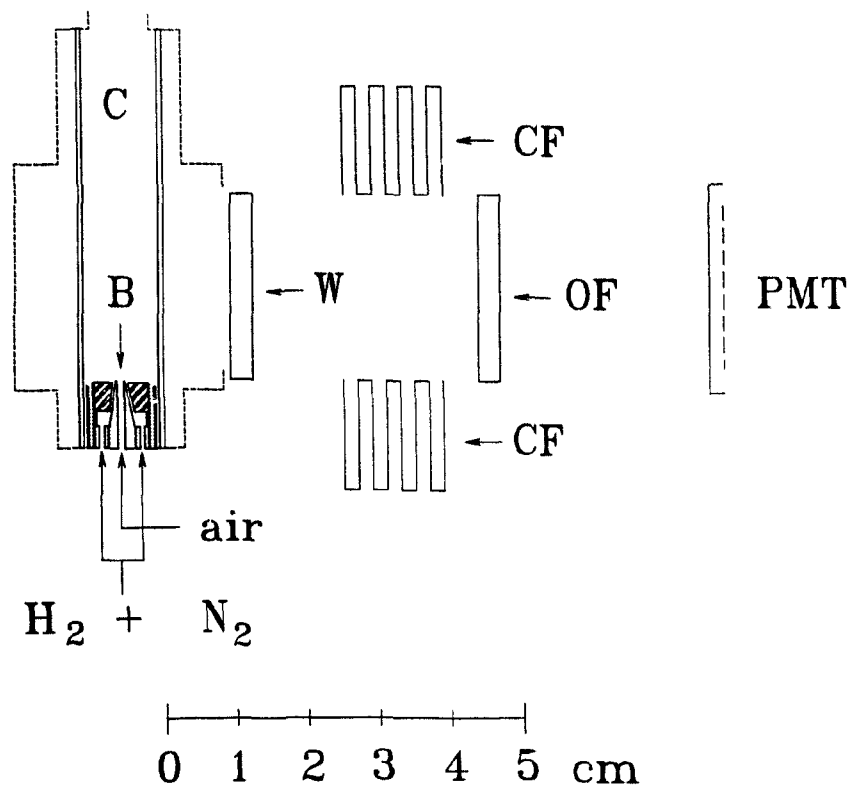
Figure 2.1 The original detector unit of the Shimadzu GC-8APF$_p$. Legend: C = chimney, B = burner, CF = cooling fins, W = quartz window, OF = optical filter, PMT = photomultiplier tube.

2.2   GASES AND REAGENTS

The carrier gas was prepurified nitrogen from Linde (Linde Union Carbide Canada Ltd., Toronto, Ontario). It was passed through a hydrocarbon filter, model HT 200-2, from Chromatographic Specialties Incorporated, Brockville, Ontario and a glass moisture trap, G BMT-100-2, also from Chromatographic Specialties. The flame gases, hydrogen and air (Linde) were also prepurified and passed through similar purification devices. It was found that a slightly lower grade of hydrogen was adequate and less expensive.

A variety of standard analyte samples (at least 95 % pure) were used, all from commercial sources: Aldrich Chemical Company, Milwaukee, Wis.; Alfred Bader Library of Rare Chemicals, Division of Aldrich Chemical Company; Fluka Chemical Corp., Ronkonkana, N.Y.; Ventron Alfa Inorganics, Danvers, Ma.; K & K Laboratories, Division of ICN Biomedical Inc., Plainview, N.Y.; and Strem Chemicals Inc., Newburyport, Ma. Almost all samples were dissolved in acetone and stored in crimp-top glass vials with grey butyl rubber septa and aluminum seals at approximately 0 to 5 °C. Solutions of air-sensitive compounds like nickelocene and magnesocene were prepared and stored under nitrogen.

2.3   THE COLUMN

The chromatographic column was 100 x 0.3 cm i.d. Pyrex tubing packed with 5 % OV-101 on Chromosorb W (AW), 100-120 mesh (about 150-125 µm diameter particles).

A single, loose plug of silanized glass wool was used at the injector insert while several,

more densely packed plugs (~ 3 cm each) were placed at the column exit. Good sample

evaporation was obtained unless the inlet plug of glass wool became excessively dirty from

repeated large injections, contaminated samples or analytes that decomposed readily.

Care, therefore, was taken to replace glass wool after doing lengthy spectra

determinations that required many injections of large amounts of analyte.

2.4   RECORDING DEVICES

The signal from the electrometer output was fed to a Shimadzu millivolt recorder,

model R-112. A lab-made electronic filter with an RC time constant of one second was

used to reduce the peak-to-peak fluctuation of the baseline. A second channel signal was

monitored by a "dicorder", a lab-made read-out device containing simple dual-channel

amplifier circuits. After converting the signal from analog to digital, these circuits, with

the help of a microprocessor, fed moving-average noise filters and a conventional 8-point

dot matrix printer in real time. Additional information, describing this two-channel printer

recorder, has recently been published by B. Millier in a computer magazine. (See page 14

of *The Computer Applications Journal,* Issue #49, August 1994.)

Chapter 3.   FLAME INVESTIGATIONS

3.1   INTRODUCTION

Initially, in order to acquire a working knowledge of the Shimadzu GC-8APF$_p$, it was decided to operate the system using a current investigation of linear sulfur[62] as a model. Repeated attempts, however, to calibrate t-butyldisulfide in the linear mode at 590 and 620 nm failed to produce a consistent linear plot. Furthermore, the optimal gas flows were quite different from those of the original work. After eliminating syringe injection technique as a possible source of error, it was confirmed that neither the exact linearity nor the linear range, as determined on the older model Shimadzu[62], could be successfully reproduced. Upon close examination, it was observed that the flame jet on the older GC had been worn down over the years from repeated cleaning, producing perhaps a more "premixed-type" flame than on the newer model where the flame is essentially "pure" diffusion. This prompted a detailed investigation into premixed- and diffusion-type flames which included the actual design of several new burners and caps as well as a special venting system.

With the topic of "flame chemistry" still in mind, gas flow modes seemed the next logical step for investigation. A number of modified flow systems were examined and doping techniques were applied as well. An unusual blend of very low, almost stoichiometric flame gas flows turned out to be highly favourable and will be discussed in

detail in this and subsequent chapters.

3.2   PREMIXED VERSUS DIFFUSION

Moye[23] described a burner design where hydrogen and air/oxygen were premixed

in a mixing chamber with the intent of creating a system in which sample injection did not

extinguish the flame. The purpose of this study, however, was to explore analyte response

and its behaviour in a premixed flame and compare this to similar work in a diffusion

flame.

3.2.1   Experimental

The original FPD burner, illustrated in Figure 3.1(a), consisted of three sections:

the jet which was screwed tightly into the base of the detector, and a two piece adjustable

cap which fitted (rather loosely) over the detector base. This cap was, essentially, just a

stainless steel cylinder with threads on the inside to accommodate the diffusion insert, also

made of stainless steel. This threaded insert fitted closely to the upper jet so that there

was no mixing of the hydrogen (which was supplied with carrier gas though two small

holes in the detector base) and the air (supplied though the centre of the jet). The cylinder

could be raised above the mouth of the jet so as to block the lower portion of the flame

(that may produce unwanted flame emission), yet not affect the emission of sulfur or

phosphorus above the shield. It was found in this study that the shielding was not

necessary and the outer cylinder was used only as a holder for the inserts. Figure 3.1(b)

shows the stainless steel premix insert which provided ample room for mixing of the flame

a

holder

diffusion
insert

assembled
diffusion
burner

jet

0   1   2   3   4   5   cm

b

premixed
insert

assembled
premixed
burner

0   1   2   3   4   5   cm
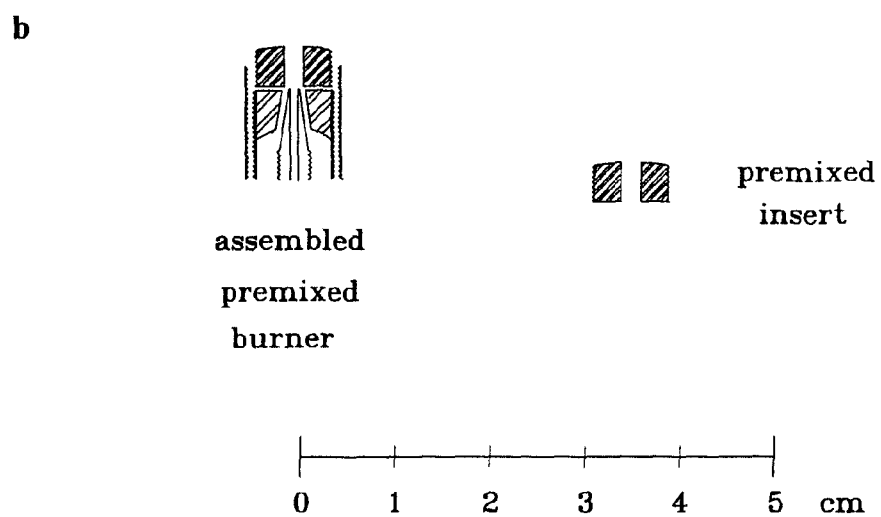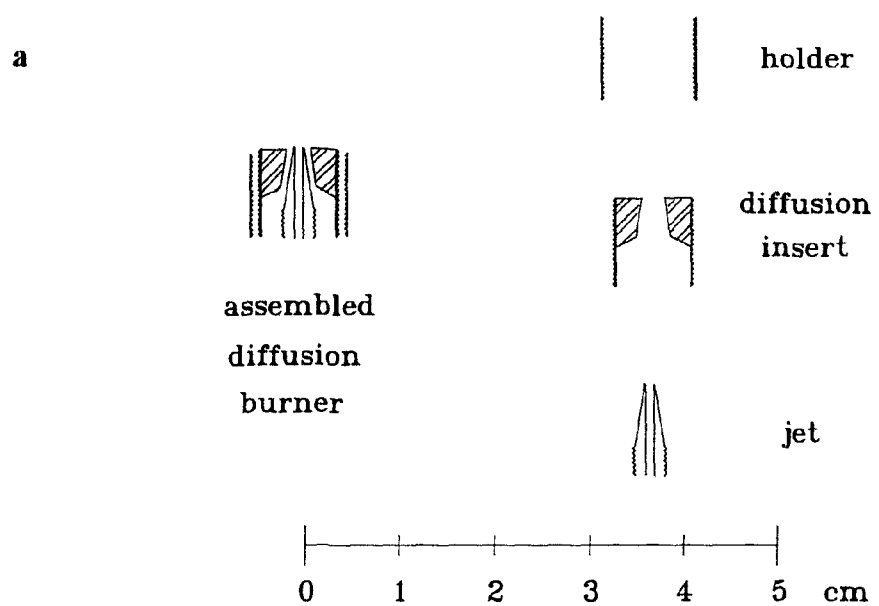
Figures 3.1 FPD burners: a. Original diffusion burner; b. Premix burner.

gases. The size of the mixing chamber soon proved to be of little significance as long as the flame gases met before the jet tip. In preliminary work, the premixed nozzle was simply screwed into the very upper portion of the holder without the diffusion cap in place. Later, to try and improve response, a new, taller holder was machined so that the premixed section sat on top of the diffusion cap. The premixed mode, with the inclusion of the diffusion insert, was marginally better than without, but more care had to be taken as sometimes there was a tendency for the flame to burn between the two inserts.

Also, during preliminary work using premixed conditions, there appeared to be difficulty in effectively removing waste products from the flame chamber. Either moisture build-up or fluctuation of waste gases caused flame flicker and often flame out. A special aluminum cylinder (Figure 3.2), designed to fit tightly over the detector vent, alleviated this problem to some extent. The upper end of this cylinder was grooved in three places to provide adequate space for gases to escape between the cylinder and the cap. The cap inserted into the cylinder and over the saw-tooth edge of the cylinder but had drilled holes across the gap. This allowed the gases to escape, yet, kept the detector light tight. In addition, a Swagelok bulkhead union was drilled out and inserted into the cap, providing easy access to the flame for venting tubes, thermocouples, etc.

Before testing the performance of the new premixed nozzle, the original diffusion system was examined once again for the optimization of the linear-sulfur mode. Using an R-1104 photomultiplier tube, no chimney and a 620 nm long pass (LP) filter, 20 ng t-butyl-disulfide was injected while first keeping the air flow constant and varying the hydrogen, then keeping the hydrogen constant and varying the air. Following this

vent cylinder

cap

grooves

1/4 " Swagelok
bulkhead union

side view
cross section

bottom view

drilled holes across gap
to allow gases to escape
(while keeping detector
light tight)

0   1   2   3   4   5   cm
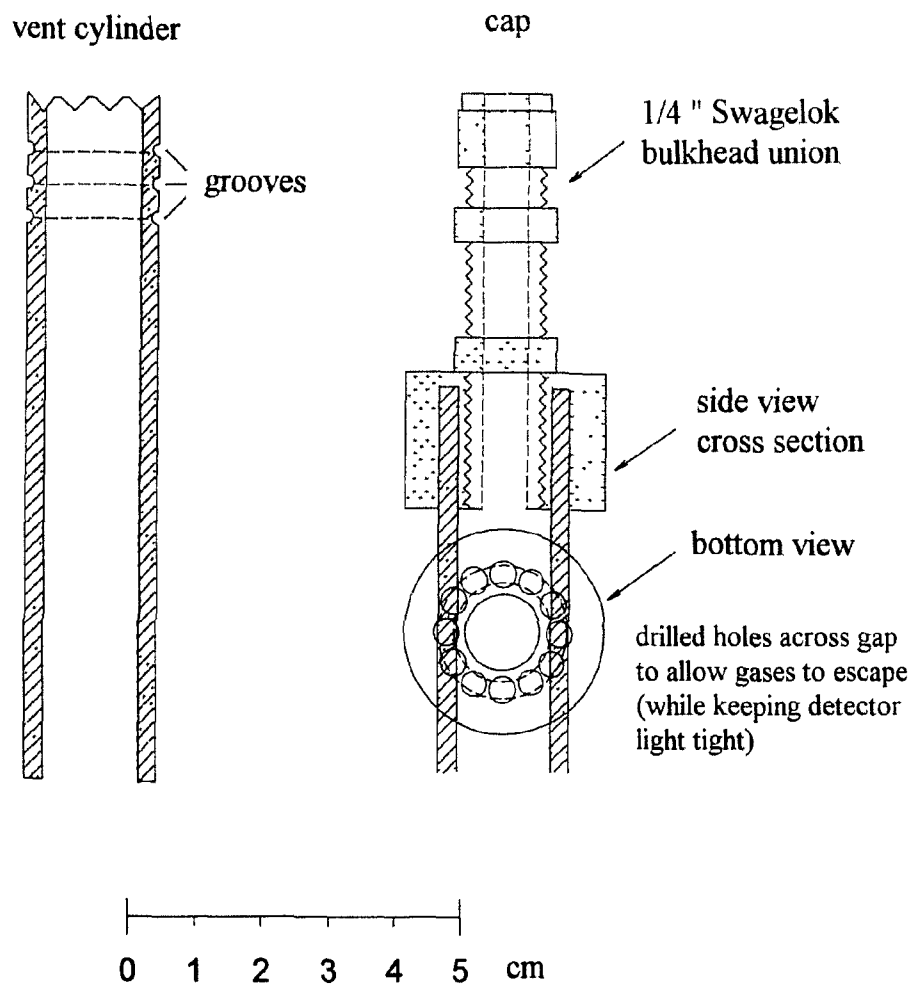
Figure 3.2   Aluminum vent cylinder and cap

optimization, the effect of hydrogen flows and the choice of filter on the calibration curves

of the t-butydisulfide were studied, still with the diffusion flame. The entire procedure

was repeated with the premixed nozzle except 100 ng of sample were introduced for the

optimization when a 640 nm (LP) filterwas used. Calibrations were then carried out at

optimum air conditions while hydrogen flow and filter wavelength were varied.

3.2.2 Results

In Figure 3.3 the ratio of signal to noise (peak-to-peak) was plotted against the

hydrogen flow in mL/min at three different air flows to define the optimum flows for the

diffusion-type flame. Each point is usually the average of three or more injections.

Injection error was typically less than 2 %; i.e., repeated injection of at least six samples of

analyte would produce a response that varied only about 2 %. More important, the trends

of the optimization plot were identical to those found earlier and were again confirmed

about a year later. It was found that the optimum flow conditions were hydrogen 200

mL/min, and air 20-30 mL/min (approximately half those of the older Shimadzu).

"Diffusion" calibration curves with a range of optical filters and hydrogen flows are

shown in Figure 3.4. The air was set at 30 mL/min and the hydrogen flows selected at

100, 200 and 400 mL/min. With a 640 nm long pass filter, the sulfur response was linear

at a hydrogen flow from 100 to 200 mL/min but at higher flows it began to deviate (i.e.,

log/log slope >1). Using the 620 nm long pass filter, the 100 mL/min flow provided an

almost linear plot but at 200 and 400 mL/min the slope increased. The plots with filters of

560 and 500 nm were not linear and the slopes were greater with higher flows.

Figure 3.5 shows that the optimal flow conditions were substantially altered upon
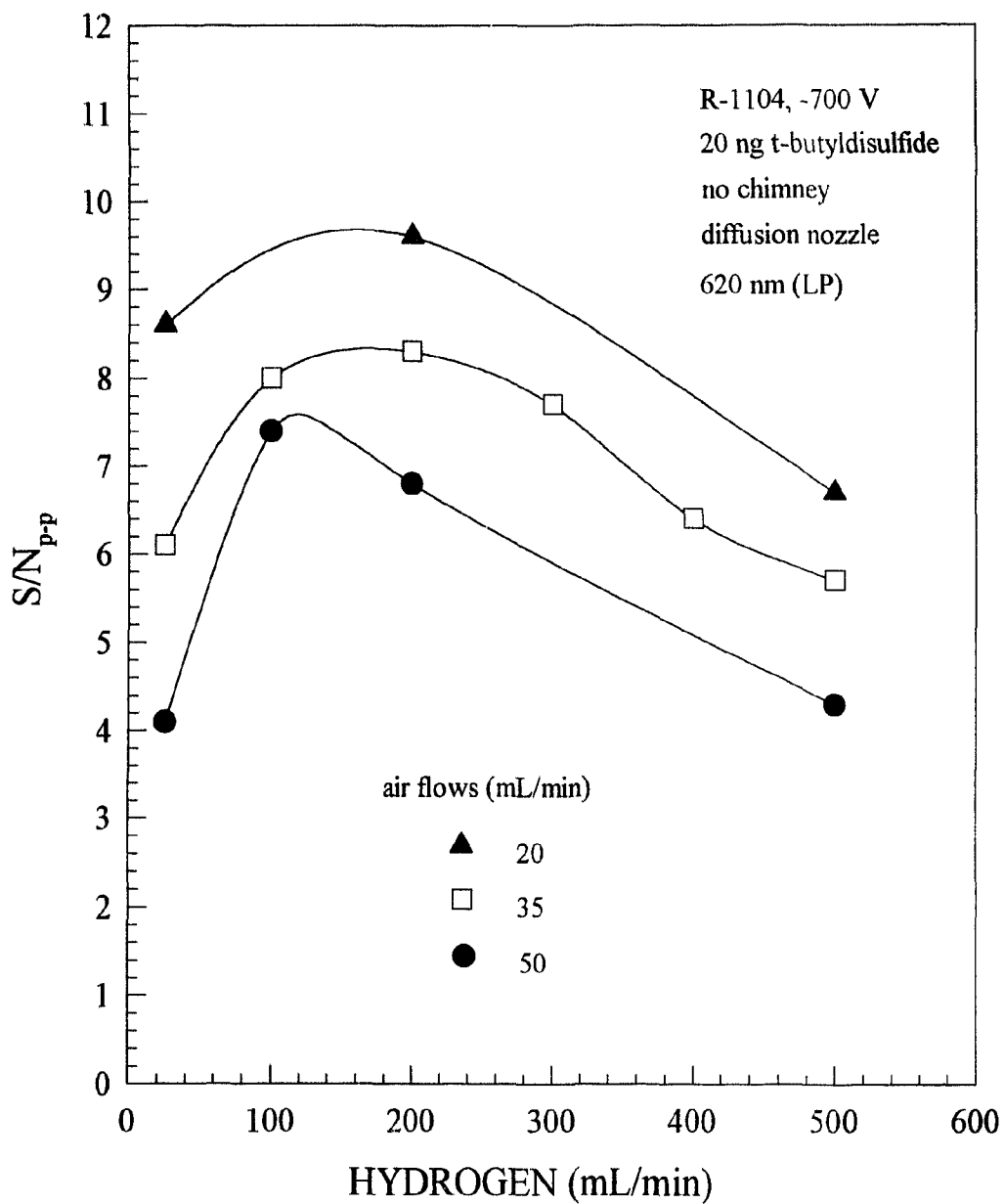
**Figure 3.3** Optimization of gas flows for linear sulfur (diffusion nozzle).
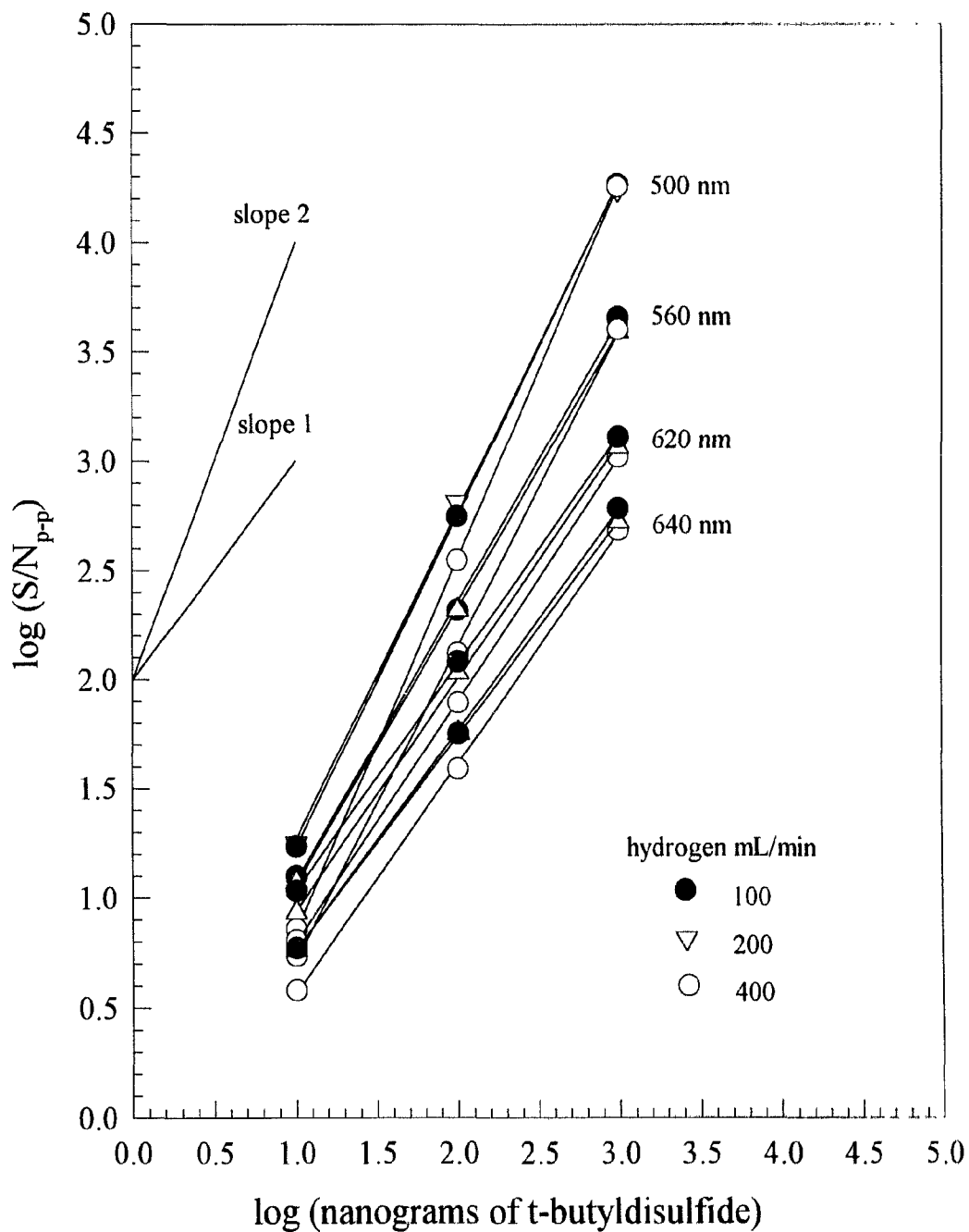
Figure 3.4   Influence of wavelength and hydrogen flow on linear sulfur (diffusion nozzle): R-1104, -700 V; t-butyldisulfide; no chimney; N_2 20 mL/min; air 30 mL/min; column 110 $^{\circ}$C.
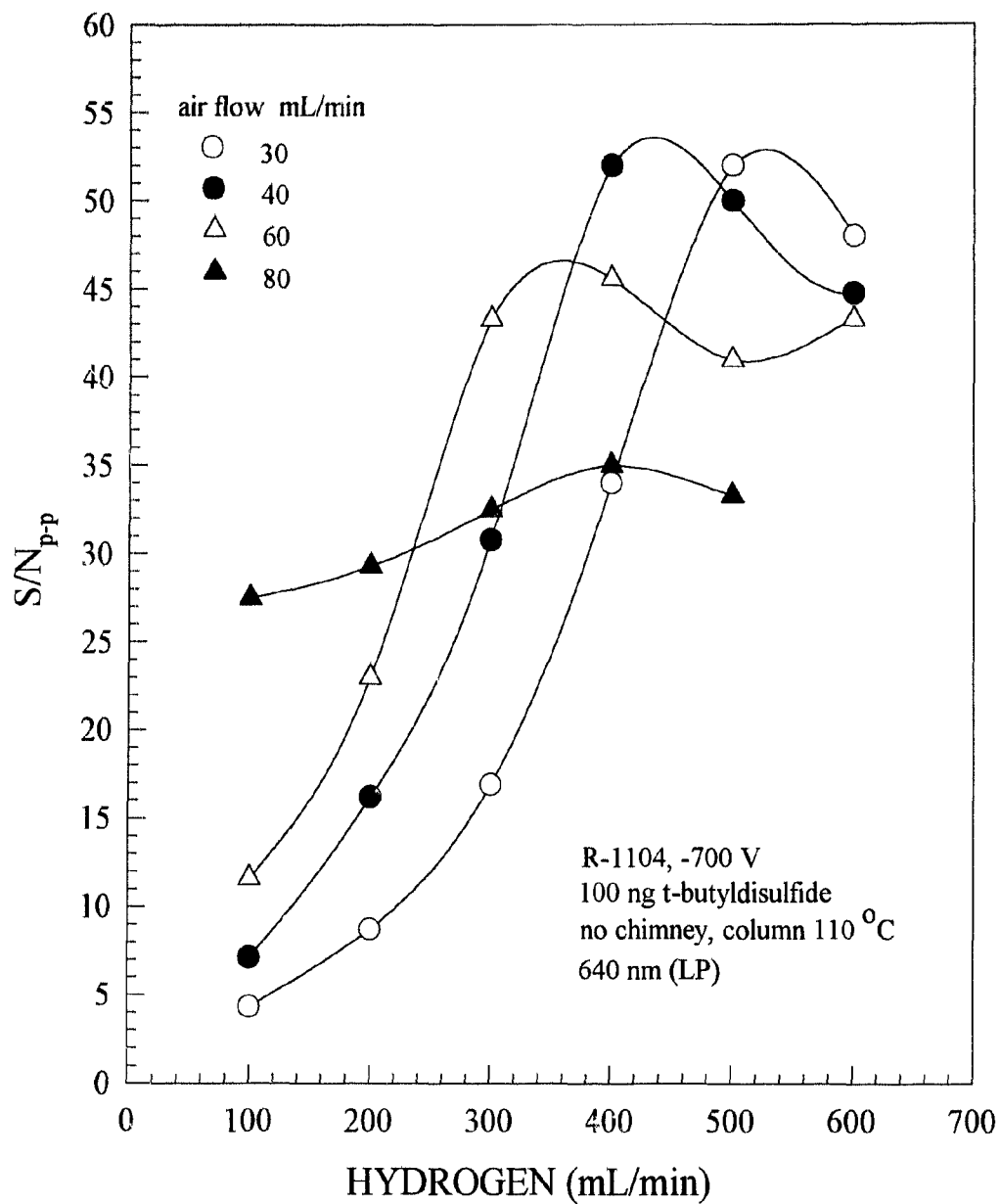
Figure 3.5 Optimization of gas flows for linear sulfur (premix nozzle).

installation of the premixed nozzle. Optimum flows appeared to occur between 400 and 500 mL/min of hydrogen and 30 to 40 mL/min of air which is in agreement with the initial study of the linear-sulfur mode.[62] (The rise at air 60 and hydrogen 600 mL/min was not investigated as the flame no longer resembled the small, cooler flame of a typical FPD system.) Using a 640 nm long pass filter, a linear plot was obtained at a hydrogen flow of 500 mL/min, air 30 mL/min and, as well, at hydrogen 400 mL/min with air equal to 40 mL/min. It can be seen in Figure 3.6 that there was only a very slight difference between the two perfectly linear plots. Hydrogen/air flows of 400/40 mL/min with a 590 and 570 nm filter also produce a linear sulfur plot. Measurements at 560 nm were approximately linear but with the 500 nm filter there was a marked deviation.

3.3   NEW NOZZLE DESIGNS

In addition to the premix, there were two other, more novel designs: a circular 6-hole insert and a 5-hole fan-shaped insert illustrated in Figure 3.7. Like the premix, they were machined from stainless steel and threaded to fit on top of the original diffusion insert. Both were, essentially, "premix" burners.

3.3.1   Experimental

Ferrocene, ruthenocene and osmocene were selected to test each of the flame types described above: diffusion, premixed, circular 6-hole and fan-shaped 5-hole. This initially was part of another study (involving other transition elements as well) to investigate some previously observed responses in the red and very near infrared.[54] As a
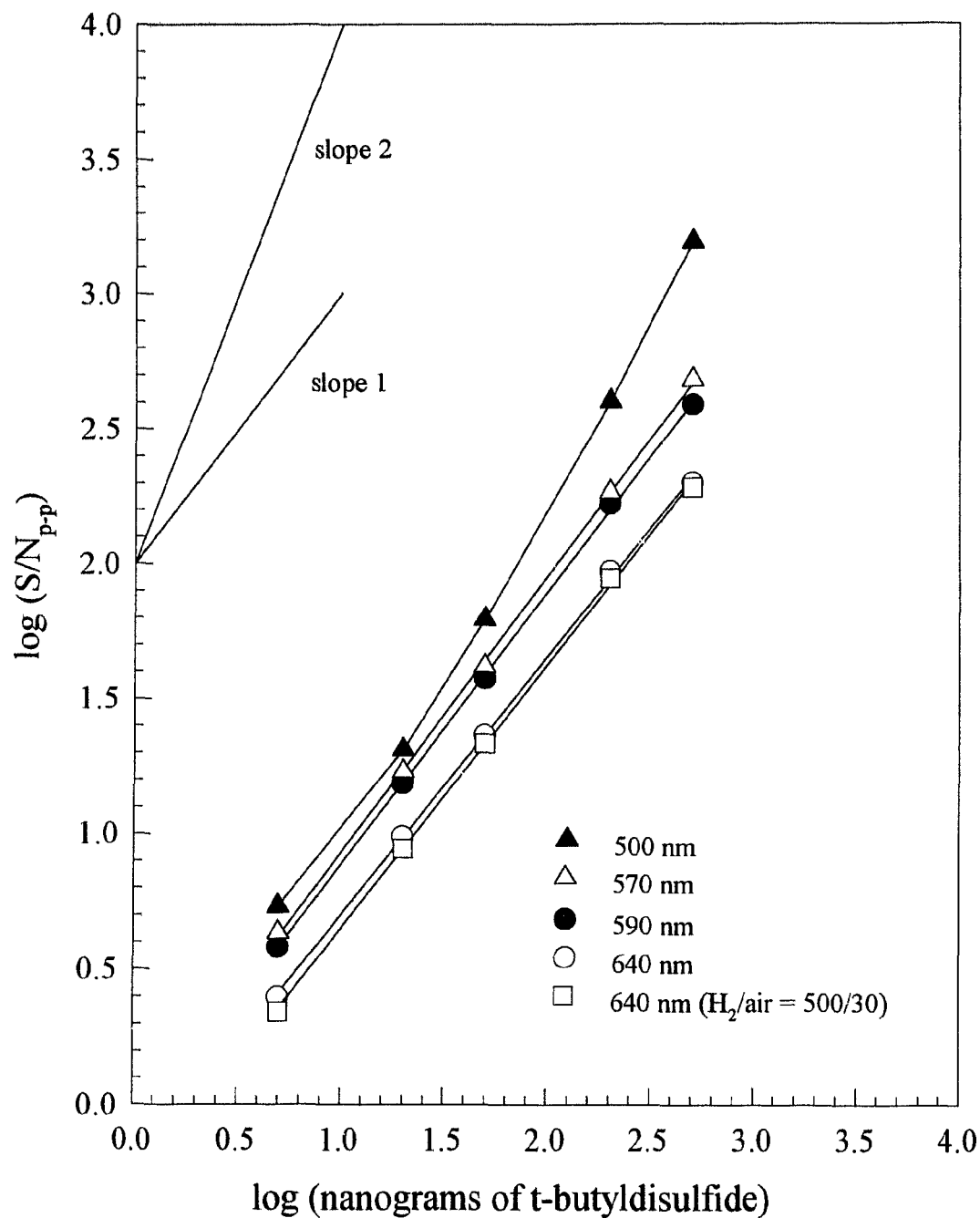
Figure 3.6   Influence of wavelength and hydrogen flow on linear sulfur (premix nozzle): R-1104, -700 V; t-butyldisulfide; no chimney; N_2 20 mL/min; air 40 mL/min; hydrogen 400 mL/min, column 110 ^{O}C.

circular six-hole   five-hole fan-shaped
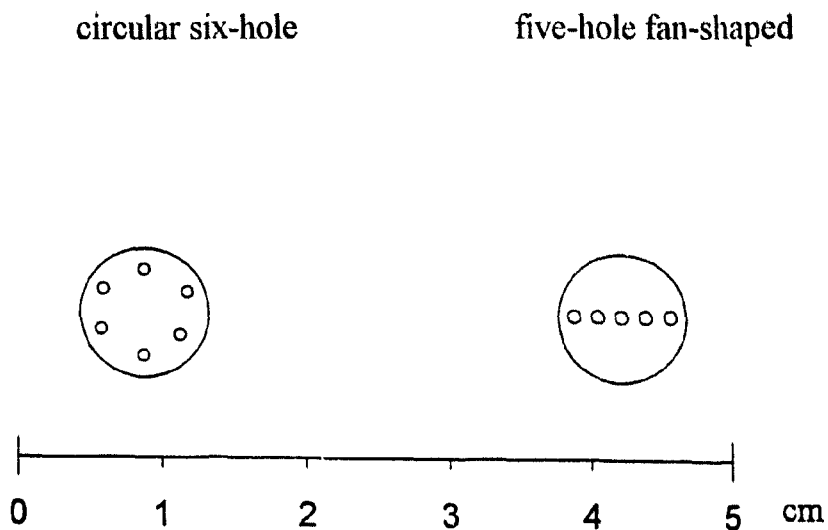
Figure 3.7   New nozzle designs.

consequence, the optimizations were all executed using an R-2228 PMT (range 180 to

850 nm) and a 630 nm long pass filter. Column temperatures varied according to the

compound: ferrocene 140 °C, ruthenocene 170 °C and osmocene 180 °C. The usual

procedure was followed: keep one flame gas at constant flow and vary the other while

measuring the corresponding S/N_{p-p} ratio for a given amount of analyte. (The peak-to-

peak noise was an average of the baseline fluctuation excluding spikes and drift.) Nitrogen

flows were kept at 25-30 mL/min.

3.3.2 Results

Figures 3.8-3.11 show the optimization curves for ferrocene only, as the results for

ruthenocene and osmium were similar with respect to the comparison of flame types. The

curves themselves, as actual optimizations, are rather meaningless since the choice of

optical filter was incorrect, as will be discussed later. Relatively speaking, however, the

diffusion flame performed the best with the premixed flame being the least sensitive.

Figure 3.8 shows the response of 20 ng of ferrocene in the diffusion flame being roughly

ten times larger than the premixed example in Figure 3.9 where 200 ng of ferrocene were

injected. The peculiar curve at low hydrogen flows and air 20 mL/min (or higher air

which will be discussed shortly) was reproducible for not only ferrocene but ruthenocene

and osmocene as well. On the other hand the "premixed" response appears to get larger

and larger with increasing hydrogen but the flame is no longer the small, cool,

characteristic FPD flame. It should be mentioned here, as well, that several bore sizes

were used for the premixed insert but no difference was observed among them.

The circular 6-hole design (Figure 3.10), with optimum flows of hydrogen = 100

mL/min and air = 200 mL/min, produced a response very similar to that of the diffusion

flame and at a lower PMT voltage (-700 V as opposed to -900 V). When examined

visually, there appeared to be six, tiny individual flames burning. However, this mode was

much noisier and had a number of inherent difficulties. Often a second flame would occur

between the diffusion insert and the premix (see Figure 3.1b), severely reducing the signal.

Removal of the diffusion insert prevented the second flame phenomenon and the noise

level was marginally reduced. This flame was also difficult to light and the range of gas
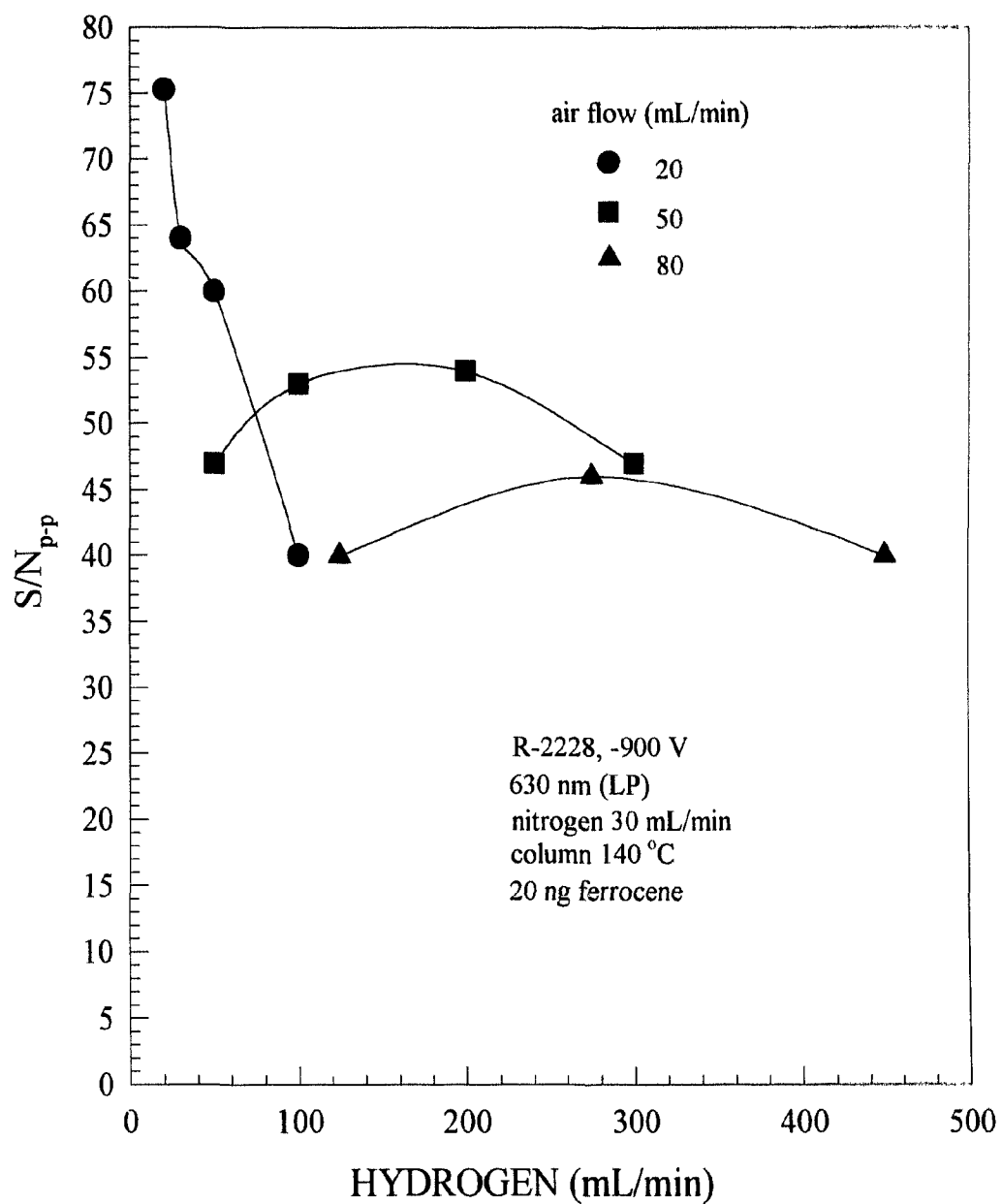
**Figure 3.8**   Optimization of ferrocene (diffusion nozzle).
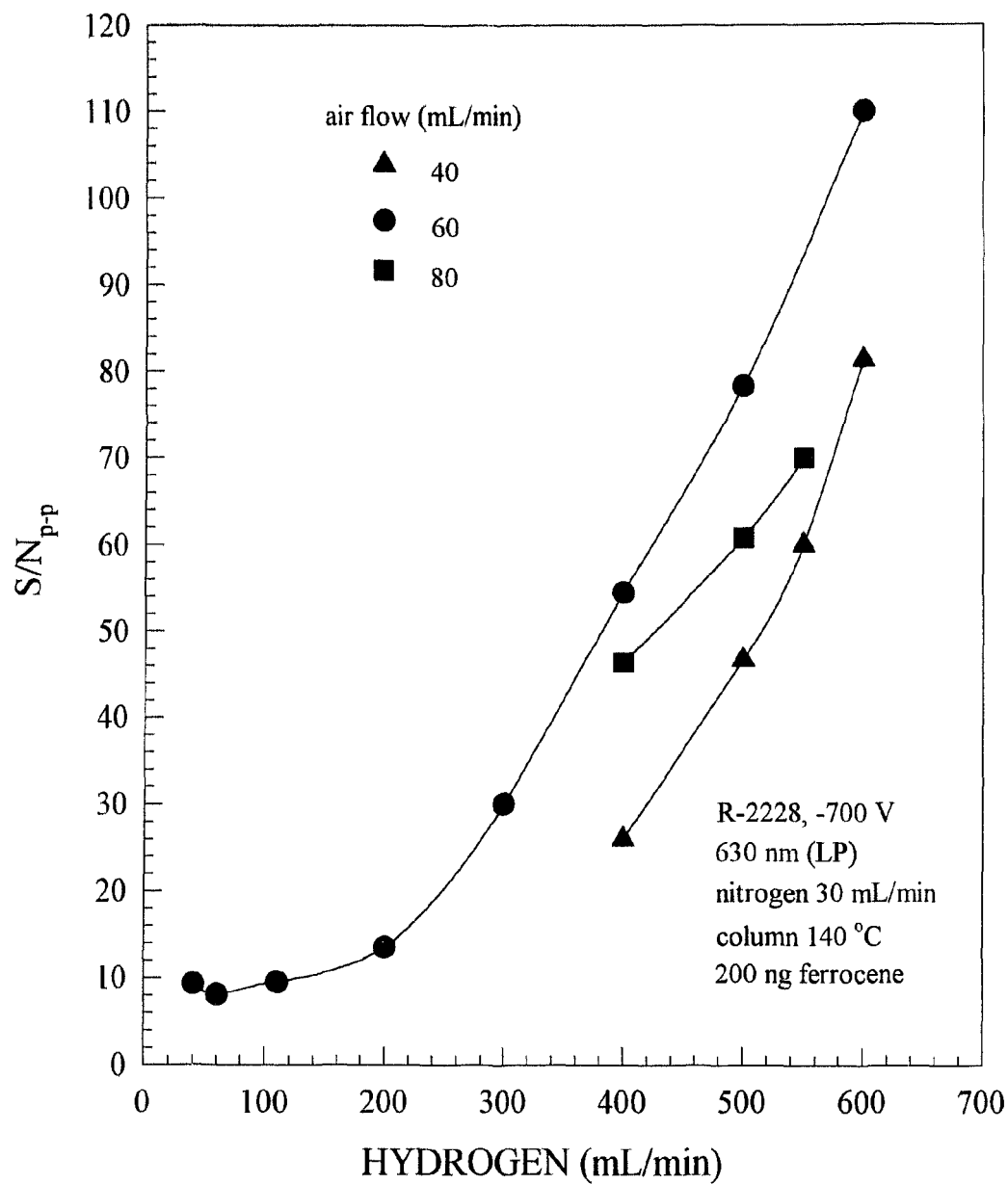
**Figure 3.9**   Optimization of ferrocene (premix nozzle).
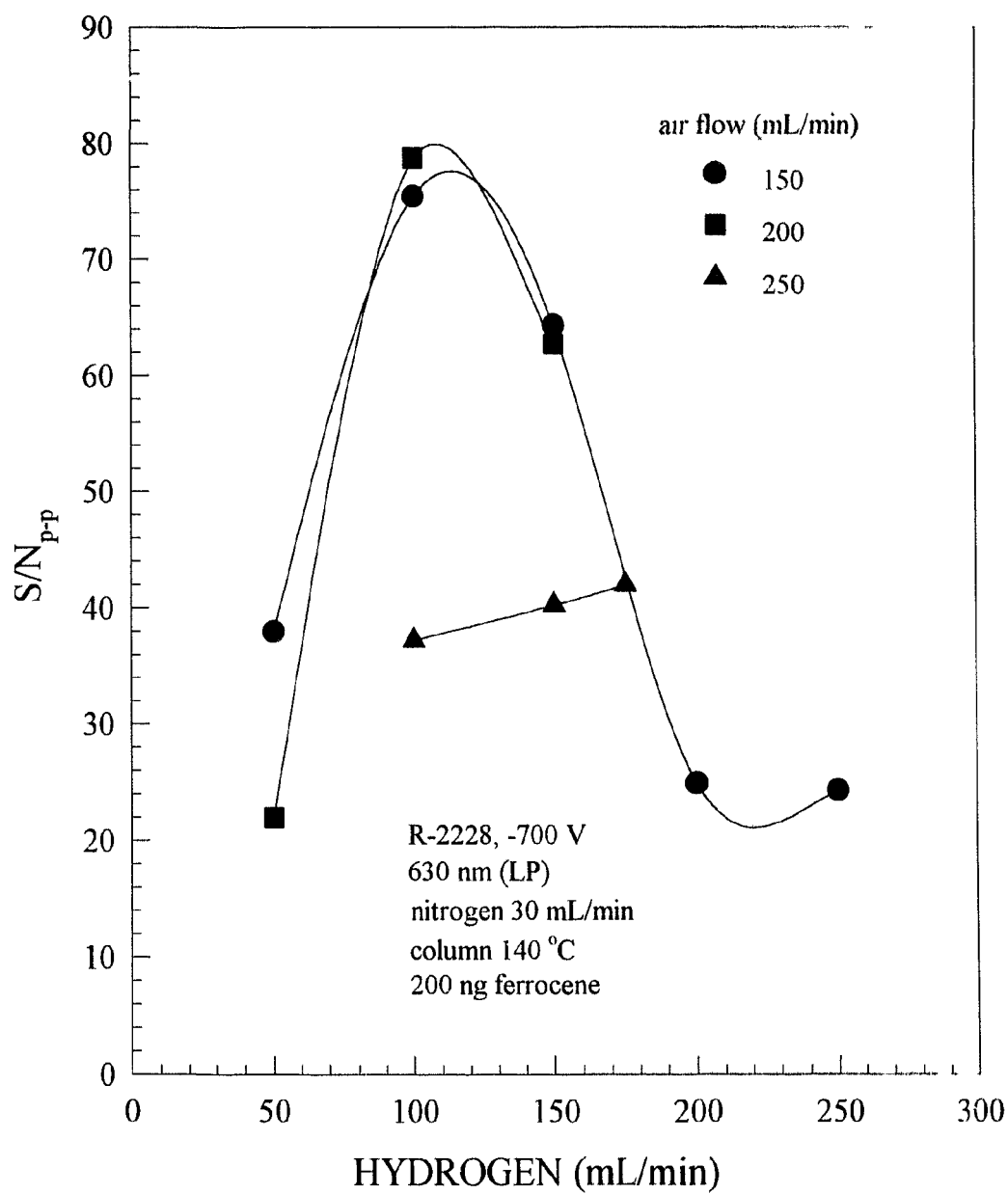
**Figure 3.10**   Optimization of ferrocene (circular six-hole nozzle)
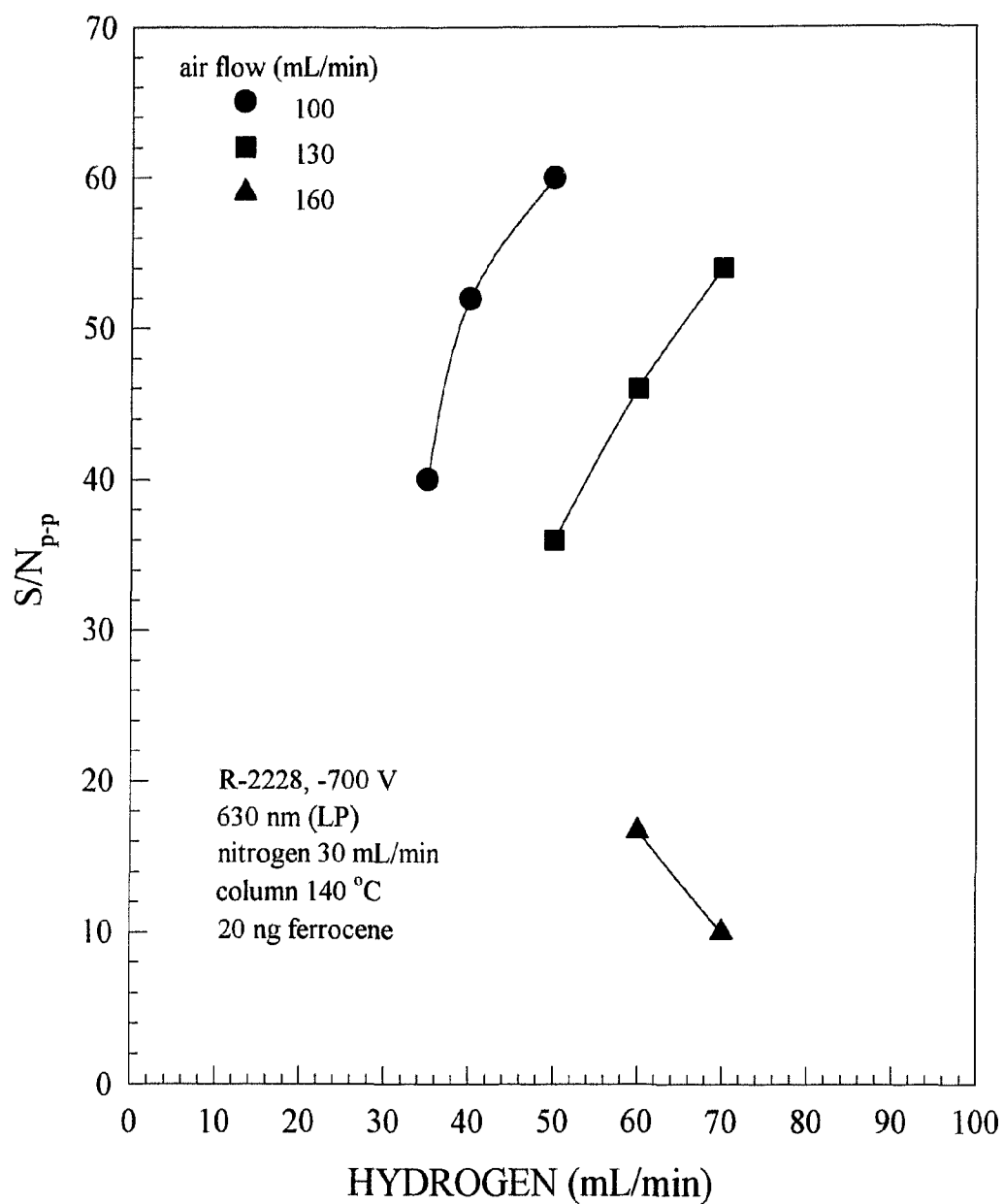
Figure 3.11   Optimization of ferrocene (fan-shaped five-hole nozzle).

flows was limited compared to the diffusion flame and the premixed.

The fan-shaped 5-hole did produce a fan-shaped flame which was examined, both with holes parallel and perpendicular to the PMT. The poor optimization plots revealed in Figure 3.11 indicate the difficulty maintaining the flame itself. Only a very narrow range of air/hydrogen combinations could be used without the flame going out, a second flame often occurred, similar to the premix system, and the PMT had to be set at -700 V, like with the 6-hole nozzle. In addition, the flame was extinguished upon injection of analyte and had to be ignited again before elution of the peak. The five holes were originally drilled to 0.500 mm and then increased to 0.635 mm with little improvement in performance, so no further increase was attempted.

3.4   GAS FLOW MODES

Figure 1.1 described the gas flow system of the original FPD system of Brody and Chaney[1], accompanied by different variations in supply lines suggested by other researchers. These modifications were designed primarily to overcome the problem of flame-out upon injection of sulfur and phosphorus compounds. The question arose whether or not similar changes to the Shimadzu's gas flow system could be achieved and whether they could perhaps be used to make the detector more responsive or even more selective.

3.4.1   Experimental

There were basically six different experimental gas-flow modes (see Figure 3.12),
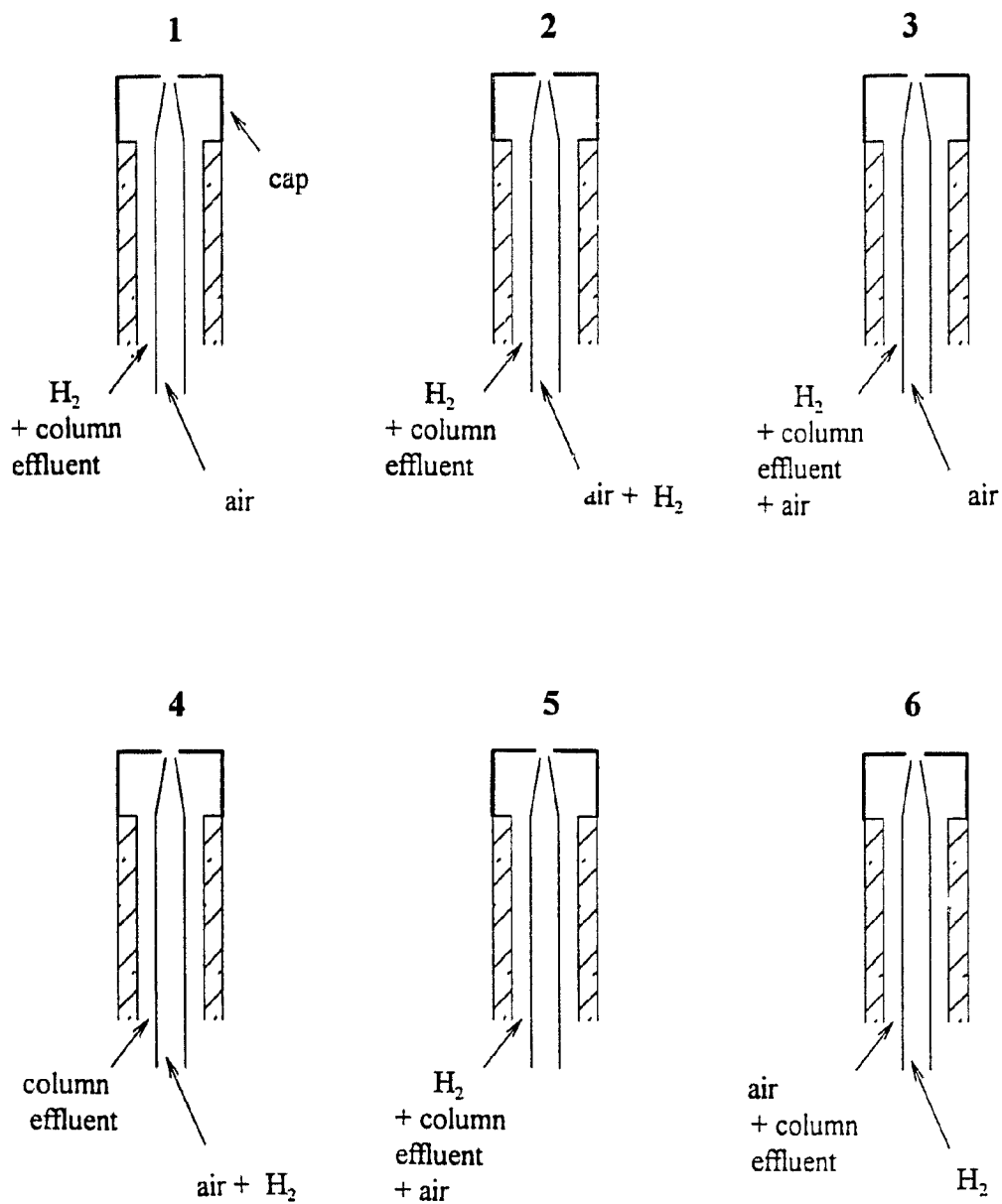
Figure 3.12 Experimental gas flow modes: **(1)** normal **(2)** normal (H_2-doped)
(3) normal (air doped) **(4)** central **(5)** hydrogen line **(6)** reverse normal.

all centred around the original diffusion burner of the Shimadzu G.C.:

1. Normal: air in the center with hydrogen fed to either side

2. Normal (H_2-doped): normal configuration but with extra hydrogen added to the central air

3. Normal (air-doped): normal configuration but with extra air added to the hydrogen supply at the sides

4. Central: hydrogen and air are supplied through the centre only

5. Hydrogen Line: hydrogen and air are supplied through the hydrogen lines only

6. Reverse Normal: hydrogen is supplied through the air line and air through the hydrogen line

Initially, all of the above flow modes were tested without sample injection, i.e., flame stability was determined by PMT noise level, bucking control, and ultimately whether or not the flame was extinguished. Following this preliminary investigation, a comparison of S/N_{p-p} was undertaken for modes 1-6 using the same experimental conditions: PMT, R-1104, -650 V; 640 nm (LP) filter; nitrogen, 20 mL/min; 5 µL of 100 ng/µL t-butyldisulfide; column temperature, 120 °C. Lastly, very rough optimizations of the normal mode were made for ferrocene, ruthenocene and hexacarbonylchromium using modes 2 and 3 (doping with hydrogen and air).

3.4.2 Results

Table 3.1 gives a summary of the initial flame tests done without sample injection. The normal modes 1, 2 and 3 were the most stable while 4, 5 and 6 were essentially unworkable.

Table 3.1

Summary of Gas Modes Without Sample

Mode	Air (mL/min)	H₂ (mL/min)	+ H₂ (mL/min)	+ Air (mL/min)	Flame
1. normal	30	50	0	0	best for lighting; can't light at higher flows
	30	30-600	0	0	stable
	20-300	30	0	0	stable
2. normal (H₂-doped)	30	125	10-150+	0	works well; 150 is not the maximum
3. normal (air-doped)	30	125	0	5-33	works well
4. central	30	0	350+	0	stays lit but un-stable; no bucking
	40	0	12	0	stays lit but un-stable; no bucking
5. H₂ line	0	125	0	33	requires high H₂ flows; unstable
6. reverse normal	0	0	20	40	lights but back-ground is too high; no bucking

Not unexpectedly, then, for actual injection of the sulfur analyte, modes 1 to 3

were much more stable and sensitive than 4 to 6. It must be noted that during these

investigations using the various modes, periodic checks were made to insure that the

detector sensitivity was not altered by any residues from incomplete combustion. In mode

2, with 0-15 mL of extra hydrogen added to the air/hydrogen flows, the response was decreased while flows greater than 15 ml/min of the extra hydrogen extinguished the flame.

Figure 3.13 shows the results of adding air to the hydrogen line (mode 3). At flows of air/hydrogen of 30/500, a slight addition of air to the hydrogen line increased the response by a factor of 1.6. At flows of 40/400 this enhancement was reduced to a factor of 1.2 (see Figure 3.14). Although actual response varied over time, this actual ratio did not, nor was it due simply to the increase in total air flow. Mode 2 (hydrogen added to the air line) produced a slightly decreased signal at a hydrogen/air ratio of 30/500 and extra hydrogen flow from 0-15 mL/min. Above 15 mL/min, the flame was extinguished.

Very rough optimizations using the normal mode (air in centre, hydrogen at sides) were made for ferrocene, ruthenocene and hexacarbonylchromium. The optimizations of the chromium compound were not very reproducible but in all cases the addition of extra air or hydrogen produced no enhancement or a definite decrease in signal. With ferrocene (air/hydrogen = 25/100), extra hydrogen produced a decrease in S/N_{p-p} while addition of 5 mL/min or less of air in the hydrogen line produced a response about 4 times larger than normal.

3.5   STOICHIOMETRIC FLAMES

As mentioned previously in section 3.3.2, the optimization of ferrocene revealed a peculiar increase in sensitivity with low hydrogen flow combined with high air flow.
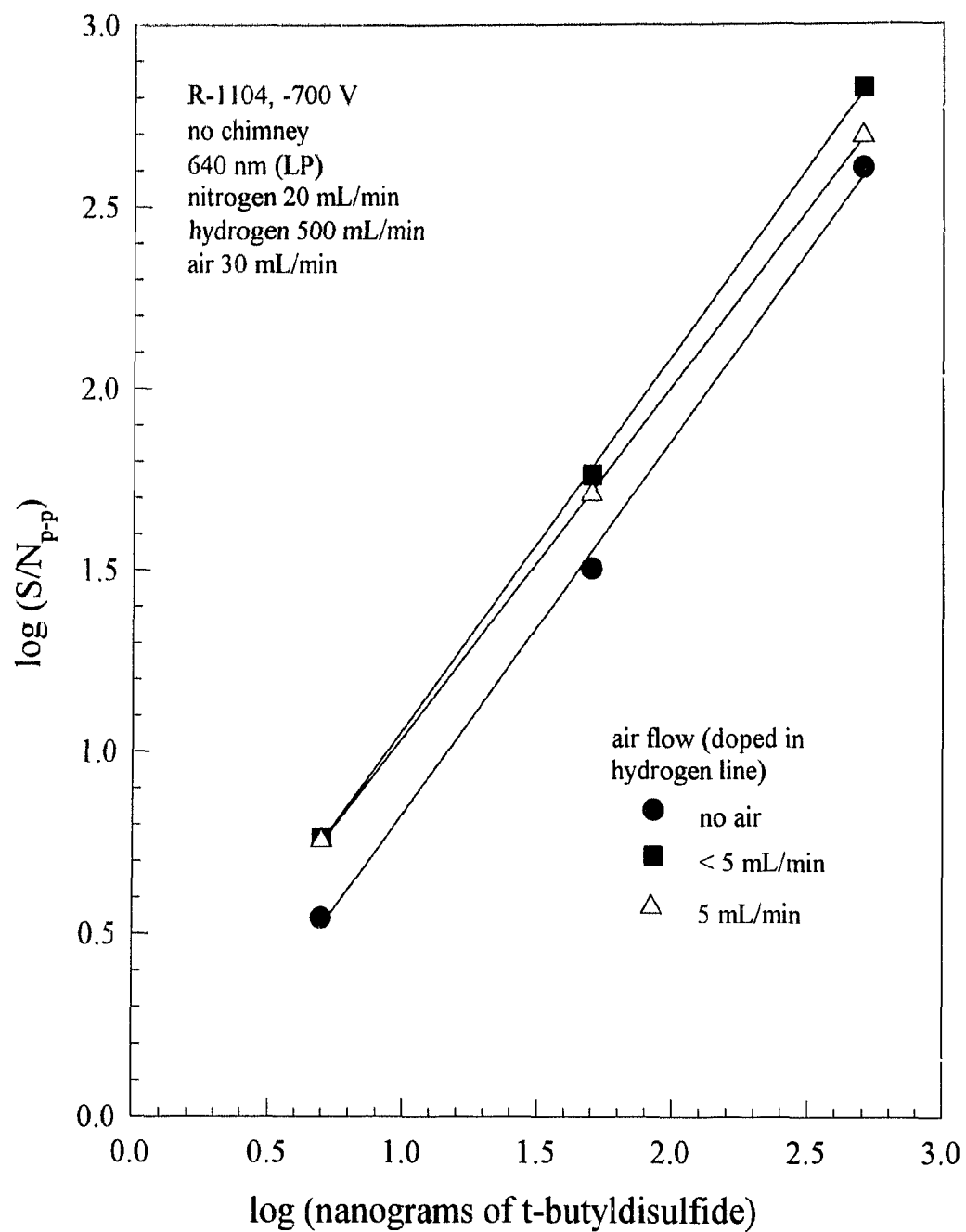
**Figure 3.13** Sulfur response in mode 3: hydrogen/air = 500/30.
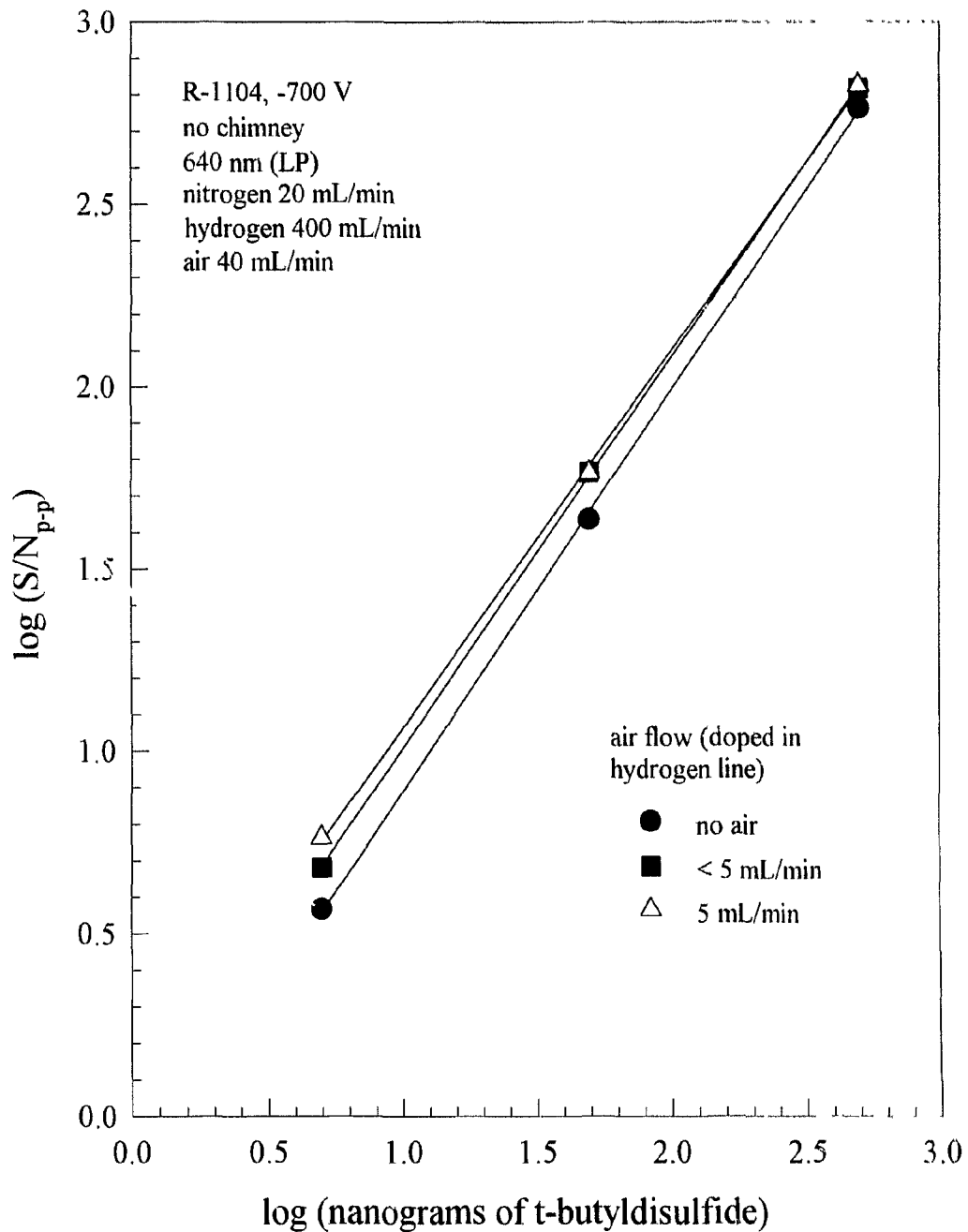
Figure 3.14 Sulfur response in mode 3: hydrogen/air = 400/40.

Ruthenocene also exhibited this behaviour (see Figure 3.15), and so did osmocene. To determine just how sensitive these conditions were, rough minimum detectable limits were measured for these compounds. Ruthenium was slightly less sensitive than best literature values, iron was about six times better, and osmium was over one and a half *orders* of magnitude better. Other elements Cr, Mo, Re, Mn, and even W (whose response had previously been classified as too weak to be significant) also seemed to respond favourably, although with less consistency. The above discussion is mainly qualitative in nature because the original range for calibration of the flow meters was too large for the required low flows of hydrogen. For fear of disturbing the system at this point in time, recalibration was postponed and further qualitative investigations were carried out. A number of noteworthy features soon became apparent. The supply of ambient air around the burner played a crucial role in obtaining optimum flows. Very inconsistent results were obtained because of the loose fit between the burner and the detector base. (Asymmetrically shaped flames due to irregularities in air supply were easily visible.)

The cleanliness of both the burner and the column (especially the glass wool insert at the inlet) were almost as important as optimum flows for obtaining sensitivity. Optimum gas flows seemed to coincide approximately with a maximum background from the flame. In order to obtain a rough value it was necessary to simply set the air to a particular value and slowly lower the hydrogen until the background (observed from the recorder trace) reached a maximum as well. Oddly enough, the flame was just on the verge of being extinguished at *the best* conditions, i.e., the most stable and sensitive ones. Nitrogen, as the carrier, also seemed to play a vital role. Possibly, if increased, the
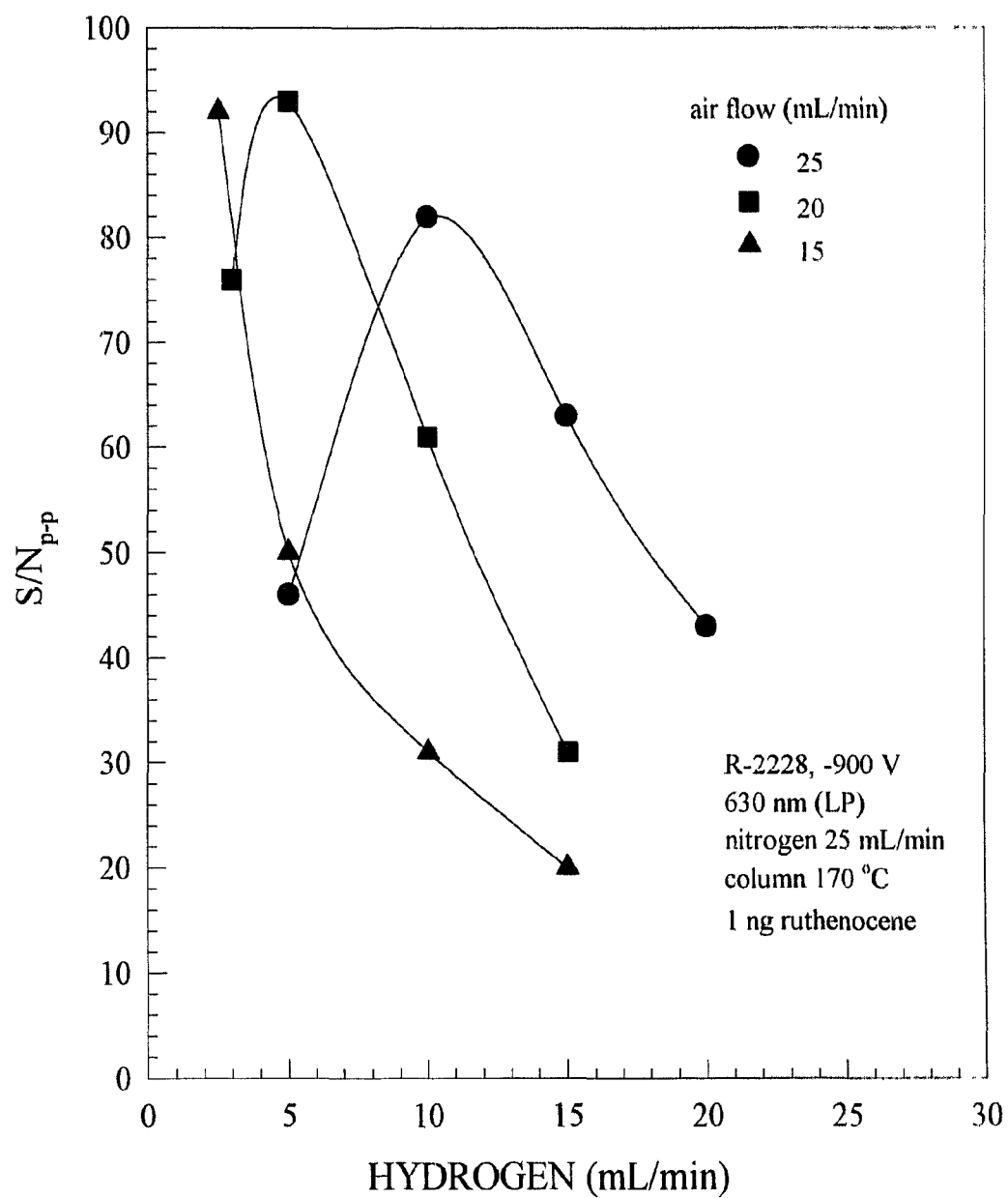
Figure 3.15 Optimization of ruthenocene (diffusion nozzle).

nitrogen could further dilute an already very small flow of hydrogen. With carrier flows

around 20-25 mL/min, it appeared that the actual ratio of air to hydrogen, which provided

maximum response, was essentially stoichiometric. Similar results could be obtained with

a range of hydrogen from 10 to 15 mL/min and air around 25 to 40 mL/min, as long as the

ratio of air to hydrogen was in the vicinity of 2.5 (stoichiometric).

To provide more accurate assessment of flame gas flows, the back pressure

regulators were reset at lower pressures and the rotameters recalibrated. Now, on

optimizing, there was a definite maximum in the optimization profile. At very low

hydrogen flows the response of analyte would definitely drop but the actual change in

hydrogen was too minuscule to record accurately each time, even with the addition of fine

gas control valves. Consistently, the easiest way to obtain optimum conditions was to use

the "background" method and then adjust the hydrogen very slightly to give the maximum

response. These flows were used very successfully with the *holophotal* method [71]

described in detail in the next chapter. Because of the need for a chimney when using

holophotal flame photometric detection, air control around the flame jet was much more

reliable. The addition of a Teflon gasket at the base of the burner (where it met the

detector base) also helped to keep the gas exchange with the surrounding atmosphere to a

minimum. The ratio of air to hydrogen flow of 40/16 (2.4) was almost invariably the ratio

of choice, with small variations usually due to the influence of nitrogen flows. The two

main exceptions to this rule were the optimum flows for sulfur and phosphorus

compounds. Tin also did not perform well under these conditions.

While the stoichiometric flame produced increased sensitivities for many elements,

the absolute light level of the chemiluminescence had to be still very low, especially

considering the tiny flame. Solvent emission appeared as an intense bluish ball of light

(See Figure 3.16), followed by the analyte, not so intense but with a similar shape. The

flame itself could be seen, but more as a very small, unfocussed light that appeared slightly

smaller than the average FPD flame. As shown in Figure 3.16, however, the temperatures

may be a little higher. Normally flame temperatures measure roughly 300 to 600 °C but a
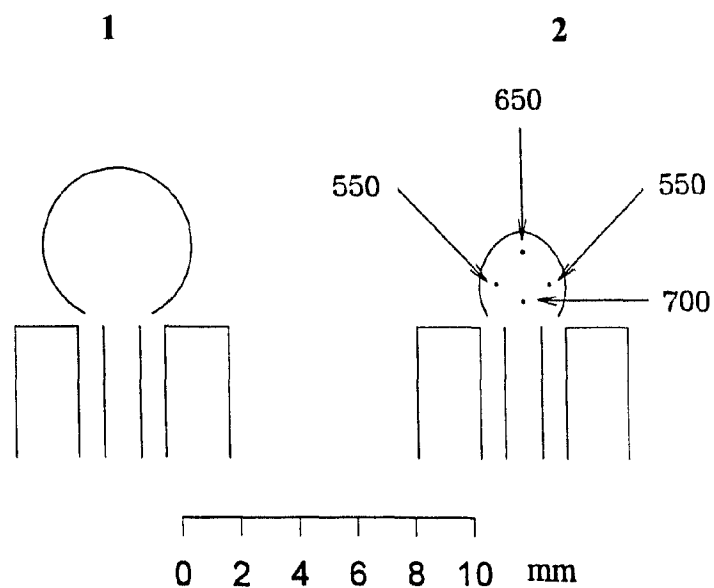
Figure 3.16 The small stoichiometric flame (1) typical ball-like shape of actual emission; (2) "flame" shape with approximate thermocouple temperatures in °C.

temperature profile of the stoichiometric flame shows an approximate range between 500

and 700 °C . Perhaps the increased sensitivities are in some way related to these higher

temperatures.

Like the normal FPD flame, the stoichiometric version produces a very wide range

of elemental response intensities that appear totally unpredictable. Often selectivity

depends more on response intensity than on spectral resolution. However, in Chapter

6 there will be given more experimental spectral data (in addition to calibration and MDL

information) using stoichiometric flames that hopefully will lead to more selective

determination of FPD-active elements.

Chapter 4. HOLOPHOTAL FLAME PHOTOMETRIC DETECTION[71]

4.1 INTRODUCTION

The flame photometric detector of Brody and Chaney[1] (Figure 1.1) originally included a mirror behind the burner assembly, supposedly to enhance the overall sensitivity of the instrument, but there was no discussion given about its purpose or ultimate effect on the optical system. Several years later, however, Selucky[6] came to the conclusion "that this mirror does not contribute to detector performance" and "consequently it has been omitted in the more recent detector types". Again, no experimental data or explanations were forthcoming but Selucky, also in this particular publication, noted that the limiting factor for detector sensitivity is detector *noise*. This provides, perhaps, a possible clue as to the failure of the mirror. Noise can come from a variety of sources including the electronics, filters, the PMT and, in particular, the flame itself. The noise can be "multiplicative" where it is proportional to light throughput or it can be "fundamental" where it is proportional to the square root of the light throughput. If the major source of noise in Brody and Chaney's system was multiplicative, then any optical enhancement, like a mirror or a lens, would fail to improve the response (measured as signal/noise).

A recent publication has shown that the noise of a flame photometric detector was predominantly shot noise limited.[72] This being the case, the S/N_{p-p} is proportional to

the square root of the light intensity reaching the photomultiplier tube (PMT).

Consequently, improving the light throughput of the FPD should, in theory, improve the

S/N_{p-p}, providing the square-root relationship endures.

The conventional FPD used for this study has an acceptance cone of about 16

degrees (see Figure 4.1) which means that only about 0.5 % of the light emitted by the

flame reaches the photocathode of the PMT (calculated from a simplified formula for the

surface area of a spherical section: $r_p^2/4r^2$ x 100 %). This percentage is approximate only,

also since it assumes that the flame emits equally in all directions, and since it neglects

such effects as light reflection off existing walls. In addition, it overlooks the significant

absorption by the interference filter. In spite of these approximations, it is still quite

evident that only a small fraction of the generated light reaches the PMT. If it is assumed

that all of this light reaches the PMT, then an S/N_{p-p} dominated by photon shot noise

should improve by a factor of $(4r^2\pi/r_p^2\pi)^{1/2}$ or $2r/r_p$, which theoretically turns out to be 14

times. This value can also be obtained from the given percentages, i.e., $(100/0.5)^{1/2} = 14$

It would be highly improbable that perfect holophotal performance could be

achieved in view of the obvious physical limitations. Mechanical obstructions and optical

imperfections are unavoidable, as are absorption, transmission and reflection losses. In

addition, shapes of luminescence differ for different elements and different flame

conditions. There is also the possibility that the square-root law might not be completely

valid, or perhaps applicable only to certain flames. Only carefully controlled experimental

measurement can hope to define how much actual improvement can be obtained by

simple optical modifications.
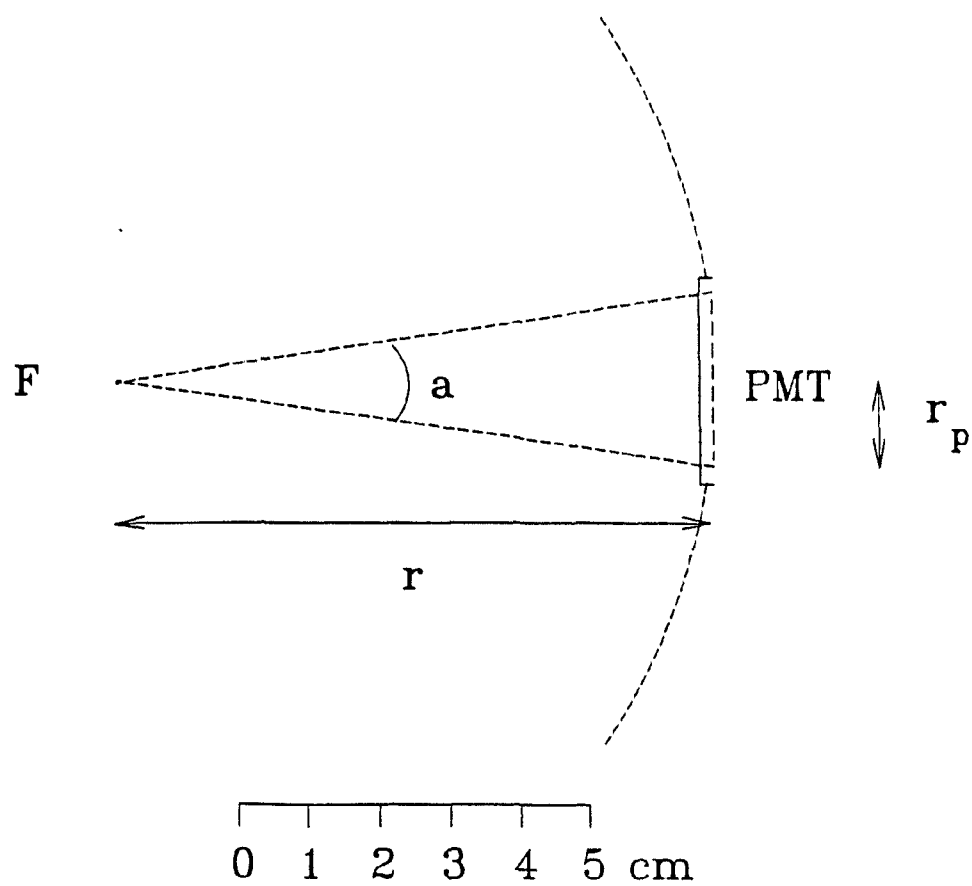
Figure 4.1 Acceptance cone of the Shimadzu GC-8APF$_p$ where r = 8.5 cm, r$_p$ = 1.2 cm and a = 16°, F = flame and PMT = photomultiplier tube.

The remainder of this chapter describes these optical changes and attempts to provide

reliable and relevant data in order to evaluate their effect. Some experimental

work pertaining to part of this project was corroborated by that of a coworker.[73] Thus,

two essentially identical instruments were tested by two different operators with two

different types of test compound, but under individually optimized conditions.

4.2   EXPERIMENTAL

Two essentially identical Shimadzu gas chromatographs were used, both models

GC-8APF$_p$ with single-channel FPD. Modifications that had earlier been made to one or

both units included the substitution of a variable PMT power supply, the provision of a

larger bucking current, the removal of in-line flow restrictors, the installation of wider-

range flow controllers and rotameters, the replacement of the detector cap by a differently

shaped one, and the insertion of a Teflon gasket into the detector base (to keep gas

exchange with the atmosphere to a minimum in that region of the detector). A simple

three-pole RC filter was also used.

These early modifications, however, were solely to accommodate a variety of

research projects that demanded unconventional conditions and in no way were a

reflection upon the quality of the two Shimadzu units which gave very satisfactory

performance. Since the earlier changes did not alter the basic performance of the

instruments, they were left in place for the present study. It is also important to note at

this point, that these modifications did not change the character of the noise.

Modifying the FPD for higher light throughput started by raising the flame, on a thinner jet, to the center of the light path (the optical axis). A parabolic mirror was installed with the flame at its focal point. It had been lathed into a 1-inch aluminum rod, which was then inserted through the unused second opening of the detector. The parabolic mirror was drilled perpendicular to its optical axis and centered at its focal point in order to accommodate the detector jet and its quartz chimney. Both the jet and the chimney were more slender than in the original FPD, although at the base they were still the same size in order to fit on the detector.

Since the two flames were of different size and shape, their centers (their visually observable locations of highest analyte emission intensity) were made to coincide with the focal point of the parabola. The Pb luminescence was relatively tall, tapering at the top, while that of osmium resembled a small sphere. For the osmium determination, therefore, the actual jet was about 2 mm taller.

A simple planoconvex lens of 50 mm focal length (Edmund Scientific Co., 101 East Gloucester Pike, Barrington, NJ, 08007-1380, USA) was fitted into a threaded support which replaced the conventional window. An aluminum tube was then screwed firmly against an o-ring seal and the window, eliminating any chance of water vapour escaping from the burner chamber. The tube was also thin-walled to minimize heat conduction, and had been internally polished to a mirror surface. All of the above optical components are illustrated schematically in Figure 4.2 along with some lightpaths used in the "conventional", "holophotal" and "comparative" FPD measurements. There were also two "intermediate" modes which are simply variations of these three configurations and
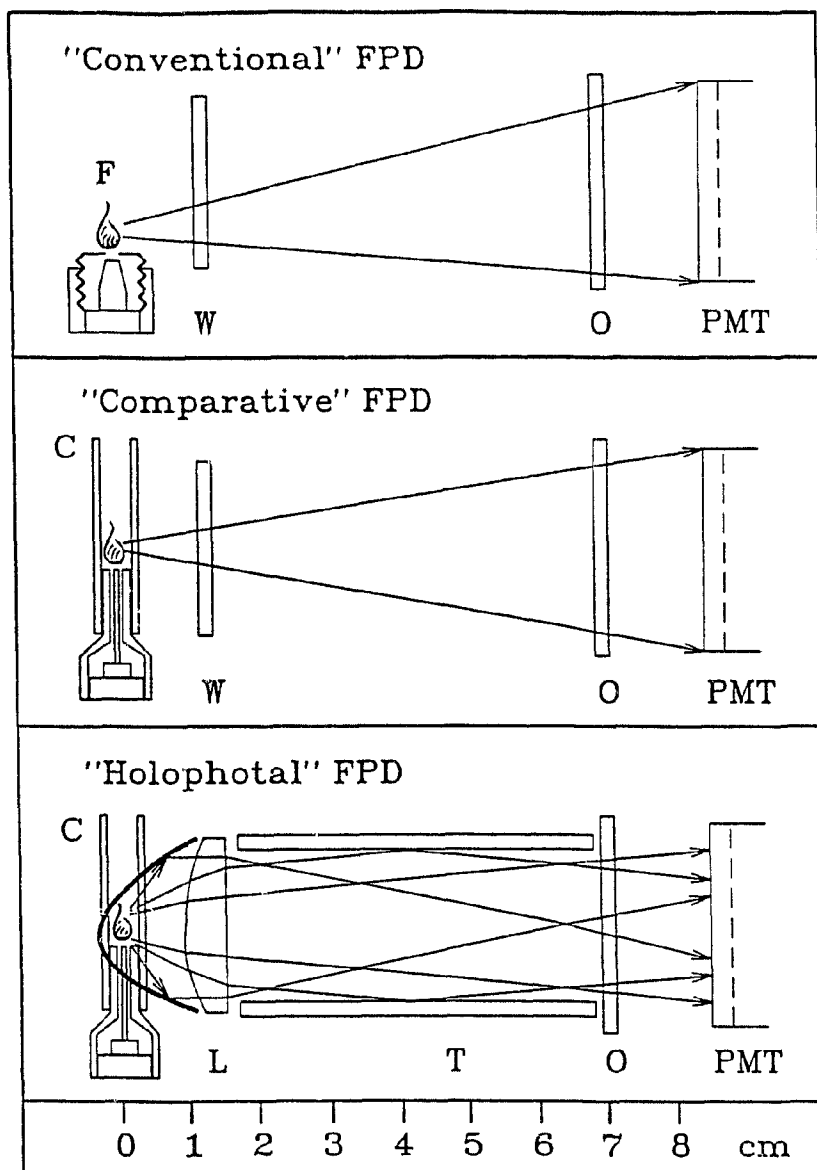
Figure 4.2   Optical layout of "conventional", "comparative" and "holophotal" FPD configurations. C = glass or quartz chimney; F = flame; L = planoconvex lens, focal length 5 cm; O = optical filter; PMT = photocathode; T = internally polished aluminum tube; W = quartz window. Not labelled but shown in bold line: aluminum parabolic mirror, focal length ca. 2.5 mm. In the holophotal configuration, the top of the jet is slightly lower than shown for Pb, and slightly higher for Os (see text for explanation of the ca. 2 mm difference.)

will be described later.

The "conventional" measurements were done with the original detectors, except

for the modifications previously mentioned which did not affect the noise character of the

instruments. The only other change was the removal of the commercial quartz chimney

which inexplicably results in a larger analyte signal. This gain in signal, previously

observed[54], was not confirmed (see Table 4.3) when the experimental response for

hexacarbonyltungsten was examined with and without the presence of a quartz chimney.

The "holophotal" measurements were carried out on the detectors supplied with the

greatest possible optical enhancement: parabolic mirror, centered slender jet and chimney,

reflecting tube, etc. The "comparative" measurements were performed with the detectors

using the light path of the conventional mode, but the jet and chimney of the holophotal

mode. The purpose of this version was merely to provide reliable determination of the

light throughput ratio.

Each of the configurations were tested under conditions optimized for the

individual detector, analyte, and analyst. The author of this thesis tested the FPD versions

with the π-bonded osmocene (dicyclopentadienylosmium) while the second study by J.A.

Gebhardt used the σ-bonded tetraethyllead. It should also be pointed out that the two

analysts exchanged analytes briefly, confirming that results were the same regardless of

operator or instrument.

The tetraethyllead determination was carried out on a 100 x 0.3 cm i.d.

borosilicate column packed with 5 % OV-101 on Chromosorb W, AW, 100-120 mesh

(about 150-125 μm diameter particles), at 130 °C. Flows were nitrogen 30, hydrogen 73

and air 13 mL/min, i.e., strongly hydrogen-rich. Emissions were detected using a

Hamamatsu R-1104 PMT at -650 V and a 665 nm longpass colored-glass filter (Oriel

Corporation, 250 Long Beach Blvd., Stratford, CT, 06497, USA, item # 51,330). The

injected amounts of tetraethyllead were 10 ng for the "holophotal", 10 and 20 ng for

various "intermediate", 50 ng for the "comparative", and 100 ng for the "conventional"

configuration. All data, however, are reported as "per 100 ng".

The osmocene determination was carried out on a 100 x 0.3 cm i.d. borosilicate

column packed with 5 % OV-101 on Chromosorb W, AW, 100-120 mesh, at 180 °C.

Approximate flows were nitrogen 25, hydrogen 16 and air 40 mL/min (i.e., stoichiometric

or close to it). A Hamamatsu R-2228 PMT was used at -900 V, with a 630 nm longpass

colored-glass filter (Oriel, item # 51,320). The amount of osmocene injected was 5 ng for

all configurations.

The two independent sets of experiments shall be distinguished by the symbols of

the FPD-active elements involved, i.e., "Pb" and "Os".

4.3   RESULTS AND DISCUSSION

The compounds tetraethyllead and osmocene were selected for the holophotal

project mainly because they were two quite differently behaved analytes which could be

used to conduct two independent test series with similar optical objects. It was also a

matter of convenience as they were already being used in the on-going theses projects of

the two analysts. The FPD's response to the main-group element lead and the transition

metal osmium was published in earlier work by group members, as has already been

discussed briefly.[53,2] J.A. Gebhardt has reported more information on lead in her recently

published thesis[73] while osmium will be discussed in more detail in following chapters.

Essentially, the purpose of this study was to discover if light throughput and

signal-to-noise can be significantly improved by optical means. One of the problems in

assessing improvement fairly in this situation is to ensure that both the holophotal and the

conventional mode are studied with the same light source and under identical conditions.

The holophotal effect obtained by the insertion of the parabolic mirror is most effective if

its focal length is kept to a minimum which in turn causes extreme perturbation in the

flame. A chimney is thus a necessity. The question then arises, should the conventional

mode be tested with or without the chimney. The wider, commercial chimney of the

conventional design may also pose a problem for the intended comparison. Furthermore,

in the commercial design the flame is situated considerably lower than the "centered"

flame of the holophotal configuration.

In order to provide a reasonably unbiased comparison, it was decided to use a *best*

holophotal mode and compare it to a *best* conventional configuration with several

comparative versions to determine the actual effect of the optical enhancements. In this

manner, then, the direct measurement of the light throughput can be achieved and, at the

same time, a comparison can be made between the theoretical and the experimental S/N_{p-p}

improvement. Table 4.1 presents the relative light intensity as measured both from the

baseline (baseline current minus dark current) and from a peak (peak apex current minus

baseline current). Also listed are the experimental S/N_{p-p} values for Pb and Os for five

Table 4.1

Comparison of Different FPD Configurations

Tetraethyllead (100 ng)

Mode	Dark Current (A)	Baseline Current (A)	Peak Current (A)	$S/N_{p\text{-}p}$
Holophotal	2.8×10^{-9}	1.6×10^{-7}	3.8×10^{-7}	340
Intermediate (I) (Lens/Al tube)	7.6×10^{-9}	2.8×10^{-8}	1.2×10^{-7}	210
Intermediate (II) (Parabola)	1.6×10^{-9}	5.8×10^{-8}	1.6×10^{-8}	114
Comparative	1.4×10^{-9}	2.4×10^{-9}	7.4×10^{-9}	48
Conventional	1.4×10^{-9}	5.1×10^{-9}	8.0×10^{-9}	35

Osmocene (5 ng)

Mode	Dark Current (A)	Baseline Current (A)	Peak Current (A)	$S/N_{p\text{-}p}$
Holophotal	1.1×10^{-9}	1.2×10^{-7}	1.3×10^{-7}	230
Intermediate (I) (Lens/Al tube)	2.8×10^{-9}	3.4×10^{-8}	2.5×10^{-8}	87
Intermediate (II) (Parabola)	2.8×10^{-10}	3.5×10^{-8}	4.5×10^{-8}	160
Comparative	3.5×10^{-10}	5.2×10^{-9}	4.0×10^{-9}	37
Conventional	2.8×10^{-10}	3.5×10^{-9}	3.5×10^{-9}	32

different configurations.

The overall improvement of the holophotal configuration is dependent on interpretation of the data. If, for example, the light throughput is calculated using simply the baseline current (with or without the dark current) the agreement with experimental improvement is not as good as when peak currents are used. Best agreement, as expected, is obtained when the change in signal for a particular mode, compared to the holophotal, is divided by the square root of the corresponding change in noise. These comparisons of "improvements" are summarized in detail in Table 4.2. In columns 1-3 the improvement factor (IF) for S/N_{p-p} values is given for each of the modes using first baseline currents (BC) only, then baseline current with dark current (DC) included and third, the peak currents (PC). The fourth column shows the improvement factors calculated using the ratio of the improvement in signal or peak current (IPC) to the increase in total noise (IN_{tot}) for each of the modes. The measured improvement factors (IF_{exp}) are presented in the fourth column.

There appears to be a discrepancy in peak currents for the parabola-Pb mode which is possibly due to a recording or experimental error. Apart from this incongruity the data remain fairly consistent. Baseline calculations, both with and without corrections for dark current, show the poorest agreement which is not surprising. Peak heights are generally much larger than baseline signals and therefore less susceptible to interferences such as PMT dark current or stray light. However, even with dark current correction the S/R values do not improve significantly, if any. Another possible factor is that the baseline noise is a square root function in the calculations whereas the signal is not. S/N_{p-p} values

Table 4.2

Improvement Factors for S/N$_{p\text{-}p}$ Values

Tetraethyllead

Mode	IF (BC)	IF (BC + DC)	IF (PC)	IPC/ IN$_{tot}$	IF$_{exp}$
Intermediate I (Lens/Al tube)	2.4	2.1	1.8	1.5	1.6
Intermediate II (Parabola)	1.7	1.7	4.9 (?)	14.4 (?)	3.0
Comparative	8.2	6.5	7.2	7.8	7.1
Conventional	5.6	5.0	6.9	9.5	9.7

Osmocene

Mode	IF (BC)	IF (BC + DC)	IF (PC)	IPC/ IN$_{tot}$	IF$_{exp}$
Intermediate I (Lens/Al tube)	0.62	1.8	2.3	2.9	2.6
Intermediate II (Parabola)	2.0	1.9	1.7	1.6	1.4
Comparative	1.8	1.5	5.7	7.0	6.2
Conventional	2.0	1.9	6.1	6.6	7.2

predicted on peak currents provide much better correlation, but when the ratios of signal improvement to the square root of total noise is calculated, good agreement with the measured S/N_{p-p} is obtained.

Although this demonstrates that the square root relationship is truly valid under these conditions, it is interesting to note that the lead and the osmium study do differ in actual numbers. In particular, the parabola improves the light throughput more than the Al cylinder in the osmium study while the opposite is the case for lead. This may be due to normal changes in operation such as dirt deposits on chimneys or mirrors, light leaks or changes in gas flows over time. More likely it is because experimental optimum conditions vary considerably, i.e., gas flows, column temperatures. Even the shape of the analyte luminescences are different, as previously mentioned, which may contribute to observed discrepancies between the two analytes.

It is interesting, as well, that significant improvement can be achieved simply with the insertion of a small lens and a shiny aluminum tube in the light path. Several combinations of this unit were investigated before arriving at the design illustrated in Figure 4.3. At first a plain a quartz window was used. Then two planoconvex lenses of 25 mm focal length (Edmund 45 098) were inserted instead of this window but the best arrangement turned out to be the lens with the 50 mm focal length. The actual contribution from the lens was found to be minimal in the holophotal system, but as it also adequately isolated the flame chamber from either air leaking in or moisture leaking out, it was left in place. The major improvement in the Intermediate I mode (lens plus tube) is mostly attributed to the highly polished aluminum tube. It allowed the easy exchange of
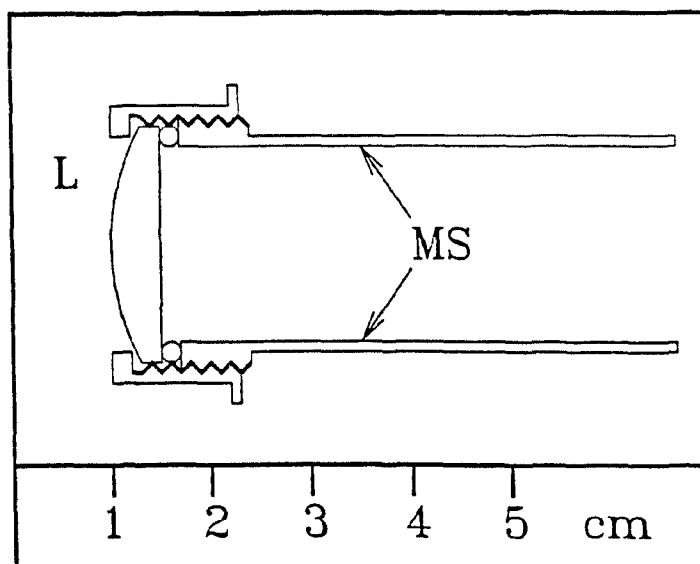
Figure 4.3 Mechanical details of light-propagating tube and modified window holder.
L = lens; MS = mirror surface.

window or lens and provided a simple means of adjusting the tension on the o-ring seal to keep it leak-tight. Another positive feature was that it very effectively shut out room light. Unquestionably it improved light throughput. Use of this unit alone increased the S/N_{p-p} ratio 4.4 times for lead and 2.4 times for osmium. Confirmation of these, apparently quite different, numbers was again made by an exchange of analytes on the two instruments. It was also observed that the improvements do not add up linearly. The tube is not nearly as effective when it is inserted with the parabola already in place. When the parabola is added to an installed tube, a similar observation is made: the parabola is less effective.

The optical system described above was the best out of a number of different designs. The parabola itself was eventually coaxially drilled to provide access for a 1/4 inch light conduit but this produced an almost negligible decrease in performance. Initially, however, a first surface mirror of 25 mm diameter and 10 mm focal length from Edmund (Edmund Scientific Co., Barrington, New Jersey, part no. 43464) was secured to a piston-like assembly to permit focussing. A new, higher jet (but the same width as the original) was also added to center the flame. A similar mirror was lathed into a one inch aluminum rod (like the parabola) and highly polished. After testing this unit, a 1/4 inch passage for a light conduit was drilled into the cylinder. In order to compare these different mirrors, the response of 50 ng, and then 500 ng of hexacarbonyltungsten, was observed with each of the mirrors both with and without a chimney. A summary is given in Table 4.3.

The same jet (the smaller, thin version made for the parabolic mirror) and light tube were used each time but gas flows had to be adjusted slightly each time to ensure

Table 4.3

Comparison of Commercial and Lab-Machined Mirrors

Mirror	S/N_{p-p} (with chimney)		S/N_{p-p} (without chimney)	
	50 ng	500 ng	50 ng	500 ng
commercial (no conduit hole)	110	140	110	140
machined parabola (with conduit hole)	120	140	flame out	flame out
machined circular (no conduit hole)	110	120	100	110
machined circular (with conduit hole)	93	94	flame out	flame out

maximum signal. In general, flows ranged between 14-18 mL/min for hydrogen and 40-42 mL/min for air. The parabola, with or without the conduit hole, performed almost the same with samples of osmium so this comparison was not repeated.

Except for the commercial mirror, all the mirrors functioned better with the chimney than without. Both the parabola and the circular mirror with hole could not be used without a chimney probably because of venting difficulties as well as any influence from the conduit hole. The choice of burner, i.e., the high and wide or the high and narrow, had virtually no effect on the performance of the commercial mirror. What did make a difference, however, was the size of the jet orifice. For a good, stable flame and maximum response, the size of the jet opening where the air comes through should be approximately 1 mm. The space between this jet and the outer burner, where the hydrogen meets the air is not crucial and can be 0.5 to 1 mm between the inner and outer tube. If the two sections are too close, then the flame has a tendency to burn at the base of the jet.

In summary, the *best* holophotal arrangement was the parabolic mirror, lab-machined, in combination with the lens/Al tube arrangement. With the observed square-root relationship between light throughput and S/N_{p-p}, such significant improvement in response was achieved that the holophotal technique became an integral part of the remainder of this thesis. An addition to this system, an auxiliary second channel will be described in the next chapter.

Chapter 5. AUXILIARY SECOND CHANNELS FOR SINGLE-CHANNEL FLAME PHOTOMETRIC DETECTORS[74]

5.1 INTRODUCTION

Brody and Chaney[1] were well aware that the addition of a second channel from their single burner design would increase the possible usefulness of their flame photometric detector. Quickly taking advantage of this concept, Bowman and Beroza[19] replaced the original mirror and metal plate assembly opposite the PMT with a second window and an additional PMT. Their primary aim was to simultaneously monitor the two different elements, sulfur and phosphorus, at two different wavelengths.

Dual-channel operation has since been developed further for a variety of purposes. Aue and coworkers in a series of papers have demonstrated improved detector selectivity by subtracting background, sample matrix, or interfering peaks.[67,75,53] Computer-based algorithms along with graphic displays of two-channel response ratios[76] have also been successfully applied. It has also been confirmed that these spectral response ratios remain constant[77] throughout the calibration or quenching ranges.[78] In a more simple context, the addition of a second channel can be valuable as a basic control for certain applications run on the first channel such as the measurement of spectra by repeated injection, an often time-consuming task. The simultaneous measurement of the analyte signal on both channels provides a response ratio which can be used to correct for injection error which

without the second channel could not be distinguished from any effect due to change in wavelength on the primary channel.

As described in detail in Chapter 4, the holophotal[71] system was capable of sending up to 50 times more light to the photomultiplier tube. Because the system was shot noise limited, the signal/noise ratios for compounds of lead and osmium correspondingly increased by the square root of 50, i.e., by over seven times. It soon became evident that the addition of a second channel would further improve an already successful holophotal mode for the FPD.

Dual channel instruments are initially very expensive and the addition of a commercial second channel to a single channel unit is costly as well. The original holophotal design was also such that a commercial second channel could not have been installed even if it had been available. The mirror, spherical or parabolic, blocked the light path to the second channel. A possible solution to this problem appeared to be to drill through it a small, co-axial hole for diverting a small fraction of the light. The overall light throughput should not be decreased significantly since the jet and chimney also prevent some of this light from reaching the PMT. Initial holophotal measurements were done using a first-surface mirror with 10 mm focal length. The surface of this mirror was very fragile and could not be cleaned if contaminated. Furthermore, several careful attempts to drill a hole though this type of mirror failed.

In the meantime, experimental results showed that the parabolic mirror machined from the one-inch aluminum cylinder performed as well as, if not better than, the commercial, spherical mirror. It was, then, a simple matter to drill the small hole in the

parabolic mirror. However, the injection port of the Shimadzu GC used in this study was located too close to the second channel opening on the detector itself. The hole could have been drilled perpendicularly to the optical axis of the parabola but it seemed easier to avoid major changes to the detector body. Still, to maintain convenient working conditions, the light had to be diverted at a right angle. Two different designs were developed to achieve this diversion. The first method (adopted in this study) used a light guide system while the second (used by J.A. Gebhardt[73]) depended on a lens and mirror combination. To both systems were added similar components necessary to complete the second channel: lab-made, inexpensive power supplies, "dicorders" described in Chapter 2, and finally the more costly photomultiplier tubes which, however, were assembled using lab-constructed housing and sockets. The total cost of the entire second channel assembly was estimated to be less than $1000 US.

Once this second channel was operational, it was necessary to determine if it was sufficiently sensitive. Furthermore, it was required to check if the sensitivity of the original holophotal channel was adversely affected. As in the original holophotal investigations, testing of this new system was carried out with two different instruments and two different operators. In the holophotal study using the two very different analytes, lead and osmium, general trends agreed but individual results seemed to depend on the analyte and their optimum flame conditions. It was decided, therefore, to use these same elements for test compounds once again, but sulfur and phosphorus, the *traditional FPD elements*, were included as well. These two elements in the form of thianaphthene and tris(pentafluorophenyl)phosphine would provide more a familiar basis for comparisons

with any FPD literature.

5.2   EXPERIMENTAL

The same two Shimadzu (GC-8APFp) gas chromatographs with single channel

FPD, described in Chapter 4, were used for this study. The columns, packings and

nitrogen flows (20 to 30 mL/min) remained unchanged. Each detector was equipped with

its holophotal assemblies[71], i.e., parabola, lens, light tube, etc. The only alteration to this

holophotal channel, which shall be designated channel 1, was the addition of a hole,

slightly larger than a 1/4 of an inch. It was drilled through the parabola along its optical

axis and could accommodate either a lens or some kind of light guide such as an image

conduit, a random optical fiber bundle or even a quartz rod.

5.2.1   The Lens/Mirror Channel

The lens, from Edmund Scientific Co. (101 E. Gloucester Pike, Barrington, NJ,

08007-1380, USA; item # 45,078), was 6 mm in diameter and had a 6 mm focal length. It

acted more as a protective window than an actual focussing device and was cemented in

place by a gas-tight seal of black, high-temperature epoxy ("Duralco 4525", maximum

temperature 260 °C; Cotronics Corp., 3379 Shore Parkway, Brooklyn, N.Y., 11235,

USA).

Figure 5.1 gives a scale-drawn illustration of the lens/mirror arrangement of the

second channel. Light coming from the flame through the lens and a highly polished light

tunnel was reflected through 90 ° which effectively solved the *injection port problem*. The
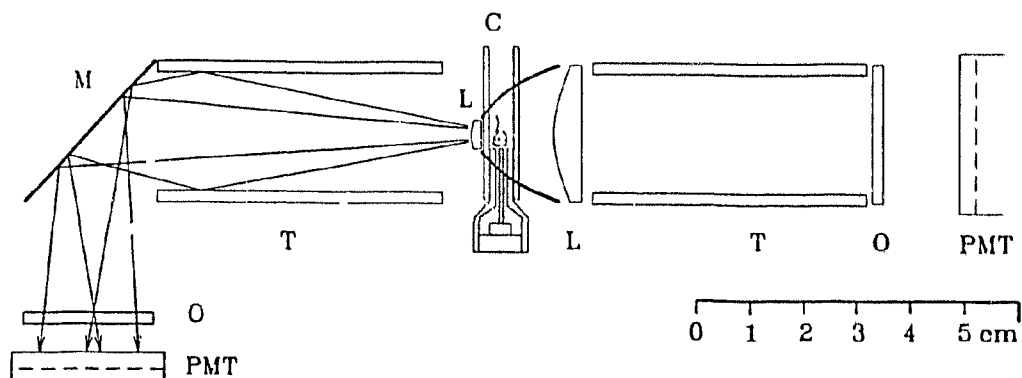
Figure 5.1 "Lens-mirror" arrangement of second channel. PMT = photocathode of head-on photomultiplier tube; O = optical filter; M = aluminum mirror, T = light-reflecting aluminum tunnel; L = planoconvex lens; C = borosilicate or quartz chimney.

reflector was cut at a 45-degree angle from a 1-inch aluminum rod and was also well

polished. Better light throughput could probably have been achieved with a slightly

concave surface but technical difficulties in lathing and polishing this piece were greater.

The mirror housing was constructed from an aluminum cube with two 1-inch openings and

two 40-mm horizontal openings, which carried ports with compressed, black o-rings for

inserts of the same size. The light tunnel from the detector block and the rod with the 45 °

mirror were inserted into the cube from opposite sides through the two 1-inch ports. The

second 40 mm port was used only as a holder for silica gel to keep the base of the

photomultiplier dry.

5.2.2 The Light-Guide Channel

A 6 x 1/4 inch diameter image conduit (Edmund Scientific, # 38,307) was bent to

almost 90 ° to accommodate the position of the injection port. A quartz rod of similar

shape was also fashioned in order to accommodate cases where UV light is important.

These rods were not cemented in the parabola opening but were carefully positioned so

that they touched the quartz chimney surrounding the flame. There was no need for the

1/4 inch opening to be gas-tight since the conduit at the exit end was sealed with a flat,

silicone rubber ring. Any exposed sections of the conduit were covered first by black tape

then wrapped in aluminum foil, but the quartz rod was wrapped carefully in aluminum foil

only. Figure 5.2 gives a schematic drawing of the main optical parts of this light-guide

arrangement.
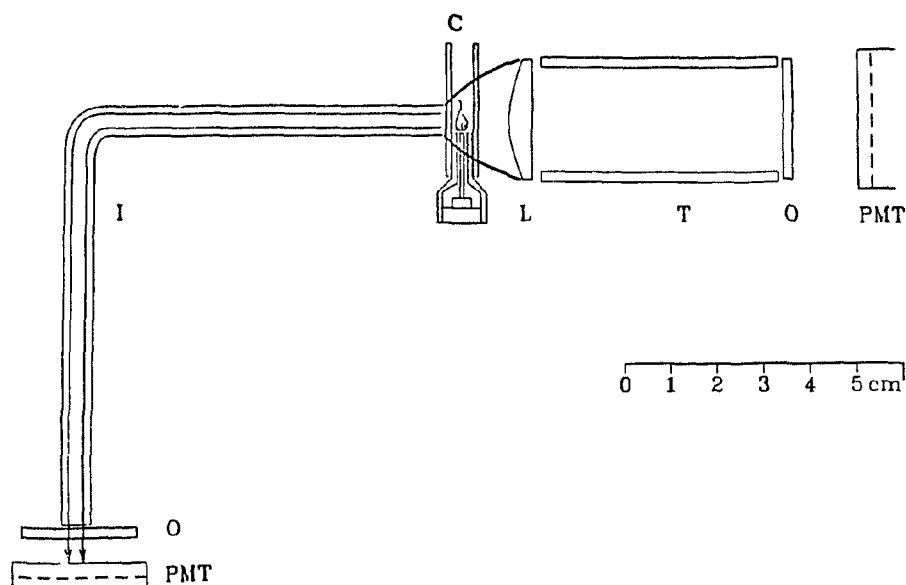
Figure 5.2 "Light-guide" arrangement of second channel. PMT = photocathode of head-on photomultiplier tube; O = optical filter; I = image conduit (or a more gently bent quartz rod); C = borosilicate or quartz chimney; L = planoconvex lens; T = light-reflecting aluminum tunnel.

5.2.3 Measurements

Three different channels were investigated using the four test compounds, tetraethyllead, osmocene, thianaphthene and tris(pentafluorophenyl)phosphine. The holophotal channel is designated as channel 1 while channel 2 corresponds to the new channel, either the lens/mirror design or the light guide arrangement. The third configuration refers to the unaltered, single channel version supplied with the original unit.

The signals for channels one and two were optimized, using the best combination of flame gases, PMT voltages and optical filters, to give a maximum signal/noise ratio for each of the test compounds. If necessary, the hydrogen and air flows for the conventional channel were adjusted slightly so that a better comparison of channels could be made. The optical conditions, however, including the voltage of the photomultiplier, were kept constant for each set of experiments using a particular element. In addition, all minimum detectable flows were made separately using the same Shimadzu electrometer and stripchart recorder which provided more precise noise measurement than the dicorder. The *baseline current*, measured from the dark-current level, gave the background intensity while the *peak current*, determined from the baseline level, was a measure of the peak-apex luminescence intensity. Values for signal/noise ratios were taken from the signal provided by the same quantity of analyte used to measure the peak currents. The noise (N_{p-p}) was measured as the peak-to-peak fluctuation of the baseline, with drifts and spikes excluded, at an analog filter (RC) time constant of 1 second.

Much smaller amounts of analyte were used for the measurement of the detection limits of the element so that the peak size and the noise level were more comparable in

size. The minimum detectable analyte flows were measured in -log(mole X/s), where X

corresponds to Pb, Os, S or P. The MDL is calculated using two different definitions[72]:

S/N_{p-p} = 2 and S/RMS = 3. The RMS refers to the root-mean-square (the standard

deviation, σ, in a Gaussian distribution) of the baseline fluctuation. The analog filter was

used to determine the detection limits but not to measure the S/N_{p-p} values.

5.2.4 Individual Analyte Conditions

Osmium, light-guide arrangement:

The flow rates in mL/min were: carrier, nitrogen 25, hydrogen 16 and air 40.

Temperatures in °C were: column 170 and detector 220. The R-1104 PMT was set at -540

V, while the optical filter used was a 475 nm long-pass colored-glass filter from Oriel

based on preliminary spectral data for osmium detection using stoichiometric conditions.

These optical conditions varied somewhat from the original holophotal study which used

an R-2228 PMT and 630 nm LP filter based on the original emission spectrum[70]. The

amount injected for measurements of peak current and signal/noise ratio was 5.0 ng of

osmocene in 1.0 µL of acetone. Measurements on the conventional channel were made

without a quartz chimney.

Lead, lens/mirror arrangement:

The flow rates in mL/min were: carrier, nitrogen 20, hydrogen 73, air 14. The

temperatures in °C were: column 140 and detector 180. The R-1104 PMT was set at -650

V, while the optical filter used was a 665 nm long-pass colored-glass filter from Oriel.

The amount injected for measurements of peak current and signal/noise ratio was 10.0 ng

of tetraethyllead in 1.0 µL of acetone.

Sulfur, light-guide arrangement:

The flow rates in mL/min were: carrier, nitrogen 20, hydrogen 14, air 18 (flows for the conventional channel varied slightly, with hydrogen at 16 and air at 20 mL/min). The temperatures in °C were: column 130 and detector 200. The R-1104 PMT was set at -400 V and no optical filter was used. The amount injected for measurements of peak current and signal/noise ratio was 5.0 ng of thianaphthene in 1.0 µL of acetone. For this particular measurement the detector conditions were very clean, as the detector had been thoroughly cleaned and left in a steady nitrogen flow for an extended period of time.

Sulfur, lens/mirror arrangement:

The flow rates in mL/min were: carrier, nitrogen 30, hydrogen 14, air 18 (the conventional channel varied slightly with hydrogen 16 and air 20). The temperatures in °C were: column 130 and detector 180. The R-1104 PMT was set at -500 V and no optical filter was used. The amount injected for measurements of peak current and signal/noise ratio was 5.0 ng of thianaphthene in 1.0 µL of acetone.

It should be noted that there were slight discrepancies between the conditions for the two different second-channel arrangements. Possible reasons include any slight contamination in the detectors, different flow control devices, etc. These small differences, however, had very little effect on the final results.

Phosphorus, light-guide arrangement:

The flow rates in mL/min were: carrier, nitrogen 30, hydrogen 60, air 30. The temperatures in °C were: column 190 and detector 230. The R-1104 PMT was set at -600 V and a 500 nm (nominal) wideband interference filter from Oriel was used. The

measured bandpass at half height was 515-575 nm. 1 0 ng tris(pentafluorophenyl)-

phosphine in 1.0 µL acetone was injected for measurements of peak current and

signal/noise ratio.

Phosphorus, lens/mirror arrangement:

The conditions were the same as the above except the PMT voltage was set at

- 550 V.

5.3 RESULTS AND DISCUSSION

The experimental data, summarized in Table 5.1 for lead and osmium, are

essentially a confirmation of the results presented in Chapter 4. Table 5.2 contains the

data for the elements sulfur and phosphorus. The S/N_{p-p} values can be compared with the

measurement of peak current and baseline currents and, again, the square-root dependence

under shot-noise conditions as discussed in Chapter 4 is evident[71]. The MDL

measurements which were made using the 3-pole RC filter were intended for comparison

with literature values. They were made using small amounts of analyte, of a peak size

comparable to the peak-to-peak noise and are, therefore, more representative than an

estimate based on the larger injection amounts used for S/N_{p-p} measurements. The MDL

is defined not as an amount of analyte, but rather as a flow, which can then be applied to

either a low or high resolution column. Often, detection limits can be calculated roughly,

using signal/noise ratios, especially for linear emitters, but not for this particular study.

This becomes quite evident if a comparison is made between the improvement ratios from

conventional to the holophotal mode. The MDL determinations show increases of 8, 8, 2, and 3-5 times (for Os, Pb, S and P respectively) while the S/N_{p-p} measurements give improvement ratios of 9, 7, 2-3 and 4-5.

The data presented in Tables 5.1 and 5.2 clearly show that the holophotal channel once more has the highest light throughput, much higher than the conventional. It is interesting, however, that in all cases except for the sulfur, the second channel is higher as well. This appears to be true for both the image conduit and the lens/mirror designs, even though their access to the flame luminescence is limited by a small tunnel about 6 mm at the most narrow part. In comparison, the limiting part of the holophotal and the conventional is about 20 mm. It appears that the determining factor is the distance from the flame, which is again considered to be a point source. The second channel, because of its proximity, has a larger *light cone* than the conventional.

The second channel, though, has a much smaller viewing area and, instead of the flame and a good part of the flame chamber, it is exposed to mostly just the flame. This observation provides a possible explanation for sulfur's better performance in the conventional as opposed to the second channel. It was noted in Table 5.2 that sulfur's response was mainly quadratic which means that a good portion of the actual luminescence probably occurred above the flame. Thus, the conventional channel, well-known for its ability to detect sulfur, is superior to the conduit or lens/mirror in this particular case.

The larger viewing area of the holophotal system can also have its disadvantages. Often the space above the flame, as well as the inner surface of the quartz chimney, can

Table 5.1

Currents, Signal/Noise Ratios and Detection Limits for Osmium and Lead

PMT, voltage, filter	Channel	Baseline current (A)	Peak current (A)	$S/N_{p\text{-}p}$[a]	MDL^b at $S/N_{p\text{-}p}=2$
Osmium (5 ng osmocene)[c]					
R-1104 -540 V 475 nm (LP)	1. Holophotal	2.7×10^{-7}	3.2×10^{-7}	910	14.7
	2. Image conduit	3.2×10^{-8}	8.6×10^{-8}	490	14.4
	Conventional[d]	1.3×10^{-8}	8.2×10^{-9}	100	13.8
Lead (10 ng tetraethyllead)					
R-1104 -650 V 665 nm (LP)	1. Holophotal	1.3×10^{-7}	2.6×10^{-8}	35	13.5
	2. Lens/mirror	1.8×10^{-8}	3.5×10^{-9}	14	13.0
	Conventional	5.3×10^{-9}	7.6×10^{-10}	5	12.7

[a]Peak height/peak-to-peak noise, no electronic filter.

[b]Minimum detectable limits of element X (X = Os, Pb, S or P), expressed as - log(mole X/s), for amounts of X close to detection limits at an RC = 1 second time constant.

[c]Amount injected for peak current and $S/N_{p\text{-}p}$ measurement.

[d]Without chimney.

Table 5.2

Currents, Signal/Noise Ratios, and Detection Limits for Sulfur and Phosphorus

PMT, voltage, filter	Channel	Baseline current (A)	Peak current (A)	$S/N_{p\text{-}}$[a]	MDL^b at $S/N_{p\text{-}p} = 2$
Sulfur-1^e (5 ng thianaphthene)^{e,f}					
R-1104 -400 V open	1. Holophotal	1.7×10^{-8}	9.3×10^{-8}	1800	13.7
	2. Image conduit	2.5×10^{-9}	1.3×10^{-8}	1200	13.5
	Quartz rod	1.9×10^{-9}	2.1×10^{-8}	380	13.0
	Conventional^d	1.1×10^{-9}	5.3×10^{-9}	550	13.4
Sulfur-2 (5 ng thianaphthene)					
R-268 -500 V open	1. Holophotal	7.6×10^{-8}	1.1×10^{-7}	870	13.4
	2. Lens/mirror	3.7×10^{-9}	$2.0 \times 10^{-}$	160	12.8
	Conventional	4.1×10^{-10}	3.5×10^{-9}	440	13.1
Phosphorus-1 (1 ng tris(pentafluorophenyl)phosphine)					
R-1104 -600 V 550 nm (WB)	1. Holophotal	1.6×10^{-7}	8.3×10^{-8}	200	15.1
	2. Image conduit	3.5×10^{-8}	2.2×10^{-8}	90	14.7
	Conventional	1.6×10^{-9}	2.2×10^{-9}	42	14.4
Phosphorus-2 (1 ng tris(pentafluorophenyl)phosphine)					
R-1104 -550 V 550 nm (WB)	1. Holophotal	2.4×10^{-8}	6.1×10^{-9}	150	14.9
	2. Lens/mirror	2.0×10^{-9}	7.1×10^{-10}	75	14.6
	Conventional	2.5×10^{-10}	2.9×10^{-10}	46	14.5

^{e} Thoroughly "clean" conditions after extended period of time.

^{f} Note: sulfur response is mostly quadratic.

also luminesce. This surface phenomena on the quartz chimney is responsible for an extremely sensitive method of tin detection but, for most cases, it simply increases baseline noise, severely affecting S/N_{t-p} ratios. This background luminescence (not as pronounced with the larger chimney in the conventional channel) is very unpredictable and changes appreciably with time and use. The second channel, then, with its limited view of the flame offers a less sensitive but a much more stable system.

It was noted in Table 5.2 that under extremely clean detector conditions, the light guide measurements were extraordinarily high. Usually the S/N_{p-p} ratios for the holophotal mode are about half those recorded. The detector *had* been cleaned and was allowed to rest in a low nitrogen flow at room temperature for about two weeks. Cleaning in this case involves complete removal of the chimney and burner. The chimney is either replaced with a new chimney, treated briefly with hydrofluoric acid, or with a *used* chimney which is heated in hot nitric acid for about five minutes and then scrubbed with distilled water and acetone. The burner jets, inner and out, often have a visible dark ring around the tip which is removed by polishing with fine sandpaper. The injection port and the small quartz tube at the column exit leading into the detector base are also cleaned regularly. However, one of the most important factors is the cleanliness of the plug of glass wool at the entrance of the column. If this is not replaced frequently, particularly after the repeated injections of large amounts of analyte for a spectrum, much higher peak-to-peak noise is observed, as well as decreased sensitivity.

If all these cleaning measures are completed, then the system is basically *clean* as opposed to *dirty* but this does not always ensure maximum sensitivity. Sulfur, and

phosphorus too, easily contaminate a chromatographic system so the two-week rest period after basic cleaning served to further remove additional background of sulfur. The practical nature of this cleaning regime, however, prevented its regular use so only normal cleaning was routinely performed.

As mentioned above, contamination (especially with the quartz chimney) is worse with some elements than others. Lead, for example, in the form of tetraethyllead, very quickly forms large black rings on the chimney with repeated injection, but background levels are substantially *reduced* while sensitivity is only slightly affected. Osmocene produced a film on the chimney only after prolonged injection but was very sensitive to change in hydrogen flows which seemed to change the *surface chemistry* of the chimney. Large amounts of sulfur and phosphorus compounds leave no visible deposit on the quartz but background levels often reach such proportions that bucking control is exceeded. (At one point, peak-to-peak noise was so high as a result of S_2 contamination that the blue luminescence in the chimney could actually be seen by the naked eye.) The compound tris(pentafluorophenyl)phosphine presented the reverse problem. Background levels seemed to continually decrease, often rapidly, which made the MDL measurements difficult. This was attributed to the possible formation of HF which provided a *self-cleaning* effect with the quartz chimney.

To avoid major problems in reproducibility with the phosphorus and, indeed, all the compounds in this thesis, several basic steps were followed. First, and most obvious, the detector, column and injection port were cleaned frequently. Before vital measurements were made the system was conditioned thoroughly, i.e., sufficient quantities

of analyte were added so that the background and peak-to-peak noise were stable and, hopefully, consistent during the investigation of that element. Generally, peak-to-peak noise was similar for most elements but actual backgrounds varied tremendously, especially in holophotal mode. Also, all measurements were made in as short a time frame as possible to prevent any changes in chimney, column etc. Although absolute measurements are always questionable, strict adherence to these precautions made reproducibility quite good.

It is evident now that the second channel, although lower in sensitivity, is not nearly as susceptible to many of the problems discussed above. The light guide mode is also not restricted to the image conduit which was selected mainly because it could be easily shaped to fit the design and also could withstand the temperatures and conditions of the FPD. It was also relatively inexpensive. Table 5.2 includes results obtained using a similar size guide made of quartz rod. It did not perform quite as well but it could be of value when measuring emissions in the UV. A plain glass rod gave much lower transmission so was not included as part of this study but, nevertheless, it did work. A specially designed guide was made out of a number of small quartz rods that were fused together but this proved too fragile. A similar construction was encased in glass tubing and fused at the ends. It could also transmit light through the sharp angle but since the commercial conduit was so superior, this project was not pursued.

In order to assess the second channel relative to the other channels, the data were treated in a similar manner as in the original holophotal study, described in Chapter 4, where it was shown that the signal/noise ratio was approximately related to the square

root of the light throughput. In Table 5.3 the relative light throughputs, measured as *peak height currents*, are presented, followed by a list of their average for the four different elements. Assuming the square-root relationship holds, the average theoretical S/N_{p-p} is calculated and listed for each channel. This value can then be compared to the actual measured value listed in the last column.

Table 5.3

Relative Light Throughputs (Peak heights, Percent of holophotal)

Channel	Os	Pb	S			P		Avg.	S/N$_{p-p}$	
									Calc^g	Meas
1. Holophotal	100	100	100	100^h	100	100	100	100	100	100
2a. Image conduit	27 (78)	ND^j	14 (37)			27 (57)		23	48 (59)	55
2b. Lens/mirror		ND	13 (36)		2 (8.2)		12 (40)	9	30 (28)	36
Conventional	3 (12)		3 (15)	6 (22)	3 (43)	3 (27)	5 (47)	4	20 (28)	26

[g] Assuming fundamental noise, i.e., square-root dependence of the S/N_{p-p} ratio on light throughput.

[h] Particularly clean detector.

[i] Improvement in signal (peak current) divided by the square root of the corresponding change in noise.

[j] ND = not determined

In Chapter 4 it was suggested that the best correlation between calculated and measured S/N_{p-p} ratios is obtained when the improvement in signal (peak current) is divided by the square root of the corresponding change in noise. These values have been calculated for each channel, as well, and are put in parenthesis in Table 5.3. The average values are listed, also in parenthesis, in the column for calculated S/N_{p-p} ratios.

For either method of calculation the holophotal method is by far the most sensitive. The image conduit ranks second and is surprisingly sensitive, approximately one-half of the holophotal. The sensitivity of the lens/mirror appears slightly larger than the conventional (roughly the same if calculated using the alternate method of calculation) which is about one-fourth to one-fifth of the holophotal.

Again, it must be emphasized that these results are highly dependent on the experimental conditions and the element itself. The minimum detectable amounts shown in Table 5.1, 5.2 and Table 5.4 serve to illustrate this point. The minimum detectable amounts in Table 5.1 and 5.2 were calculated using the definition familiar to chromatographers: $S/N_{p-p} = 2$ For comparison purposes, Table 5.4 has also been included, giving the same detection limits as above but with the condition $S/RMS = 3$, a definition more familiar to spectroscopists. From these MDLs it can be seen that the sensitivity of the holophotal channel is approximately seven to eight times larger than the conventional for osmium and lead, but only two times larger for sulfur and four times larger for phosphorus Detector contamination and chimney effects have already been discussed but flame shapes and positions, jet dimensions and other similar variables can alter the ideal case of light throughput from a constant point source. If the flame was truly

Table 5.4

Minimum Detectable Flows [calculated as -log(mole X/s) at S/σ = 3]

Channel	X							
	Os		Pb		S		P	
1. Holophotal	15.3			14.1	14.2[k]	13.9	15.6	15.5
2a. Image conduit	15.0		ND[l]		14.1		15.3	
2b. Lens/ mirror		ND		13.6		13.3		15.2
Conventional	14.6			13.2	13.9	13.6	14.9	15.0

a point source, then the improvement ratio for all the elements should have been the same.

The better performance of the light guide arrangement over the lens/mirror set-up is in keeping with the higher visible light throughput which can be expected from a comparison of Figures 5.1 and 5.2. The physical construction of the conduit channel is also more simple than that of the lens/mirror. The latter, however, could be expected to perform somewhat better than the quartz rod for emission in the ultraviolet provided a quartz lens were to be inserted.

The holophotal version described in this chapter has been altered only slightly from

---

[k] Particularly clean detector.

[l] ND = not determined.

that described in the preceding chapter. In spite of the small opening drilled *behind* the flame, it has performed essentially just as effectively. Just as troublesome, however, is the increased noise level which, when compared to the second channel, produces a relatively erratic baseline. Since the image conduit is clearly superior to the conventional, it is highly conceivable that the second channel could easily be adapted as a *primary* channel as well. For example, there could be an image conduit on *both* sides of the flame, a design similar to the original dual-channel design of Bowman and Beroza.[19] The easy construction of such a system makes possible the addition of even more conduit-type channels (including one for easy viewing of the flame). This may not be especially practical but it certainly demonstrates the effectiveness and flexibility of this second-channel design.

Chapter 6 MEASUREMENTS OF FPD-ACTIVE ELEMENTS IN THE SMALL STOICHIOMETRIC FLAME

6.1 INTRODUCTION

One of the original topics of research for this thesis was a follow-up investigation of some interesting continua produced by several metals in the FPD. Such continua can often be useful for analytical purposes and as a consequence, their spectroscopic characteristics should be clearly defined. To do this quickly and easily, a variable interference filter that could be adapted to existing apparatus was designed and constructed. It was hoped that this filter *monochromator*, with increased light throughput supplied via holophotal means, would prove helpful for investigating other low-level luminescent phenomena. The discovery of an apparent optimal flow condition for many of the FPD-active elements (see section 3.5 on stoichiometric flames) made it necessary to reinvestigate much of the already established spectral information. Because of the increased sensitivities using stoichiometric flames, many calibrations and minimum detectable limits had to be remeasured and compared to existing data. While investigating these known FPD-active elements, it soon became apparent that there were even more elements that responded to these common flow conditions and tungsten, silicon, bismuth and magnesium were added to the list.

6.2 THE VARIABLE INTERFERENCE FILTER MONOCHROMATOR

There have been produced, using the FPD, a variety of spectra that often appear different from those found in the spectroscopic literature. There is, also, always the chance that a particular spectrum has never been seen or reported, a possibility that increases for elements with low responses. These low-intensity spectra may not be analytically relevant but they may often be *spectroscopically* interesting. The measurement of the spectra of low or intermediate spectra, however, is often difficult using conventional, or grating, monochromators. As an alternative, a variable interference filter monochromator was used that provided higher light throughput, although less spectral resolution. Using this as a foundation, a semicircular variable interference filter was recently assembled that rotated to obtain spectra from chromatographic peaks passing through the FPD. Although this method was very quick and rewarding, it was also relatively complicated with respect to software and hardware. It was low in spectral resolution and was limited to between 400 and 700 nm, the wavelength range of the filter.

Circular filters with a larger range do not appear to be commercially available. Rectangular filters can, however, be purchased but they do not have a *monochromator* housing. An obvious solution, then, was to purchase a wide-range variable interference filter (one that would reach into the near IR) and encase it in a housing that was specially equipped with a reliable filter transport mechanism, adjustable slits, and ports leading to the FPD on one side and the photomultiplier tube on the other. This naturally would produce a longer light tunnel and a much smaller aperture than with the conventional FPD

and consequently less light transmission. The holophotal technique solved this problem, so it was just a matter of assembling a suitable wavelength selector.

6.2.1 Experimental

The spectrometer constructed was a long box with a vernier-controlled helical drive (Small Parts Inc., 6891 N.E. Third Avenue, P.O. Box 381966, Miami, Fl., 33238-1966), which carried, with backstop, a frame holding the 200 x 25 mm variable interference filter (Oriel Corporation, Long Beach Blvd., P.O. Box 872, Stratford, Ct., USA, 06497, item # 57481). The filter had a range of 400-1000 nm, a minimum transmission of 30 % and a mid-range bandwidth (the transmittance FWHM at the center of the coated region) of 42.5 nm according to Oriel specifications.

Initially, the variable filter was calibrated by injecting quantities of tetrabutyltin (emission maxima at 610 nm[56]), ruthenocene (two maxima, 484 and 528 nm[69]) and MMT (maxima at 403 nm[67]) and plotting the emission maximum wavelengths against the corresponding vernier scale reading. For a more reliable calibration the variable filter assembly with PMT was temporarily connected to the exit port of a Jarrell-Ash model 82-415 quarter-meter grating monochromator. A light bulb source was attached to the entrance port and at selected wavelengths on the grating monochromater the corresponding maxima for the filter were determined using the response measured with the Shimadzu millivolt recorder. Excellent agreement was obtained with the two different calibrations. Figure 6.1 shows a wavelength calibration plot as well as plots for bandpass and transmission (determined using the Jarrell-Ash model 82-415 quarter-meter grating monochromator). The calibration plot was perfectly linear from 400 to almost 800 nm
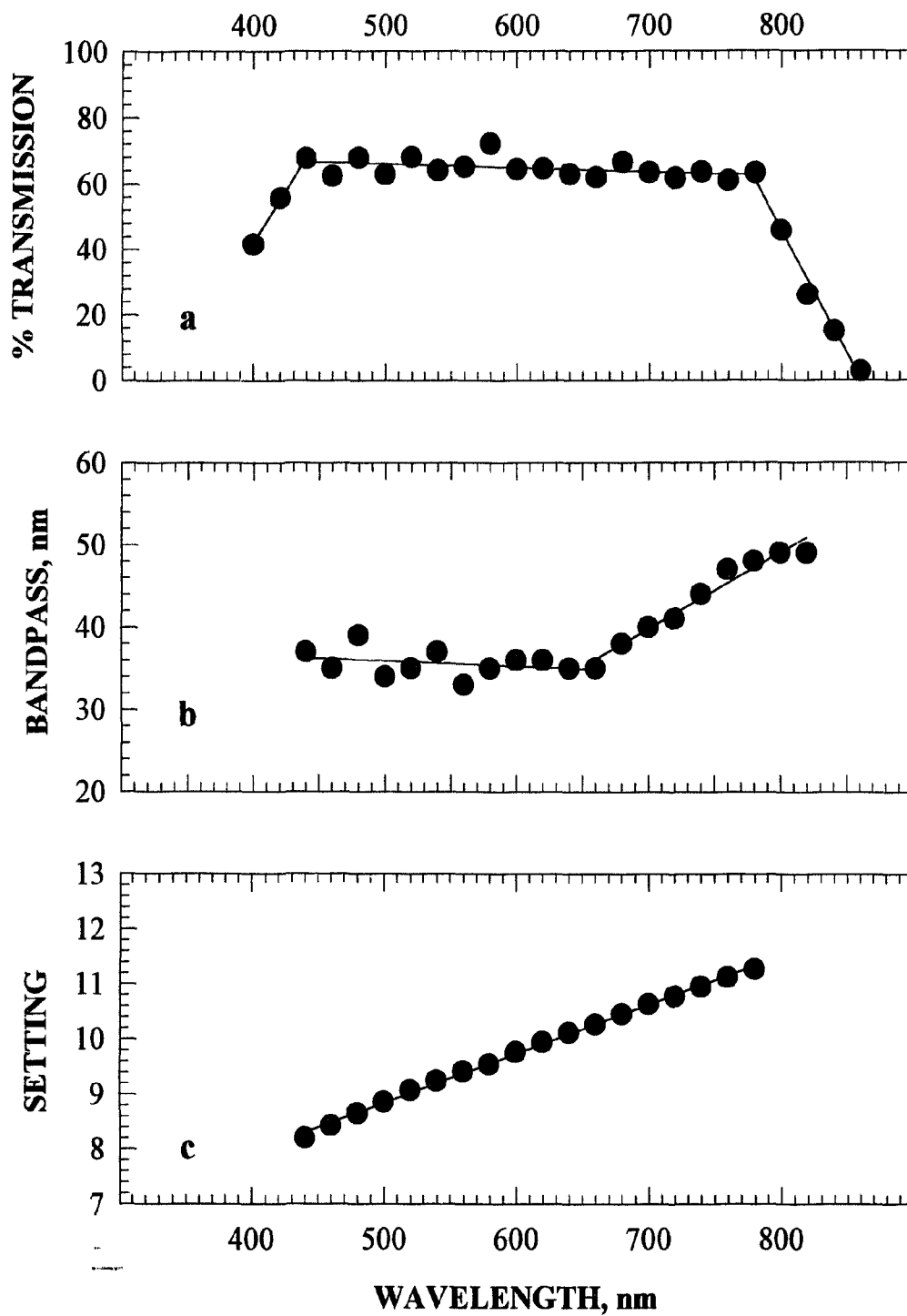
Figure 6.1   Calibration of variable interference filter: **a.** % transmittance
b. bandpass **c.** vernier drive.

and the bandpass was approximately 34 nm from 440 to about 700 nm, where it rose

gradually to about 49 nm at 800 nm. The percent transmission averaged about 65 % until

800 nm where it began to drop sharply, reaching zero transmission well before 900 nm.

A pair of non-coordinated sliding slits could be controlled from the outside by

verniers but, for most measurements, the slits were left wide open. A piece of paper with

cut-out aperture, about 6 mm, was then inserted in front of and very close to the variable

filter. The backside port of the spectrometer allowed a photomultiplier tube housing to

slide as close to the filter as the slit arrangement would allow. The lab-constructed PMT

housing for most experiments carried a Hamamatsu R-1104 or R-2228, already described

in Table 2.1. Figure 6.2 provides a schematic of the optical layout with indications of the

light path using the parabolic mirror of the holophotal system. (The complete second

channel set-up can be seen in Figure 5.2.)

6.3   RESPONSE CHARACTERISTICS AND SPECTRA

6.3.1   Experimental

With the unexpected discovery that the very small *stoichiometric* flame gave the

best signal to noise ratio for several metals, difficult and lengthy optimizations were now

an exception. Sulfur, phosphorus and tin did not respond as well as with higher, more

hydrogen-rich flames, but these elements were already well-documented and were not

included as a formal part of this study. In general, the elements that did respond were

subjected to a visual examination, a calibration, an MDL determination and then a spectral

C

I

```
0  1  2  3  4  5 cm
```

W   T   L   S   VF   PMT
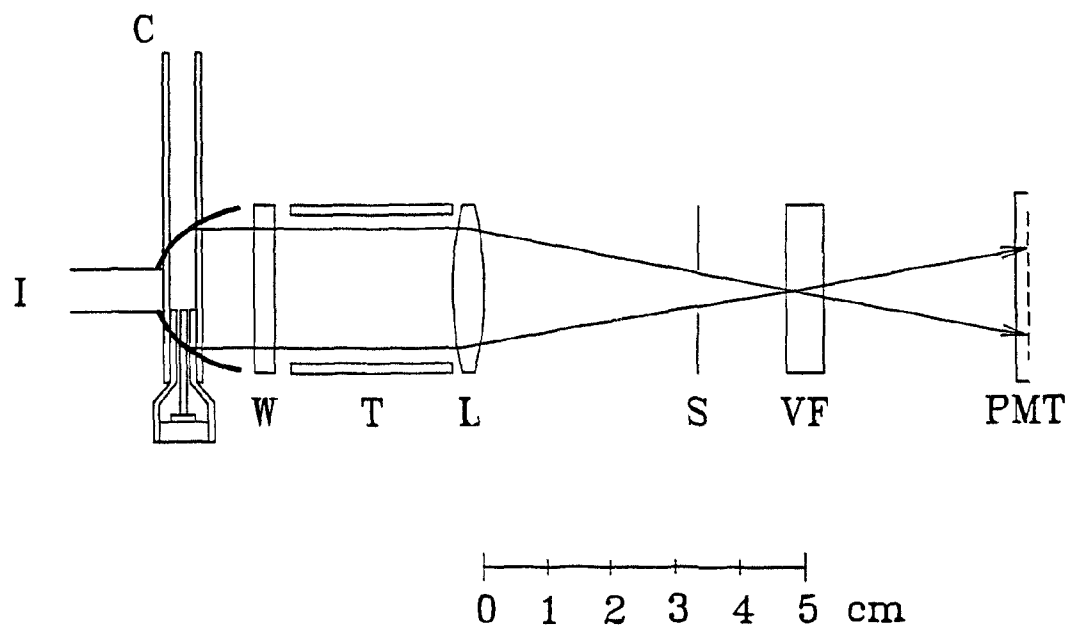
Figure 6.2 Variable interference filter and the optical layout: PMT = photocathode of a head-on photomultiplier tube; VF = variable filter; S = 6 mm slit; L = double-convex lens; T = light reflecting aluminum tunnel; W = quartz window; C = quartz chimney; I = image conduit to second channel.

measurement.

The holophotal parabolic arrangement described in Chapter 4 was used almost exclusively, except for part of the osmium study where experimentation with the circular first-surface mirror and a larger centered jet showed very little difference between the two mirrors (see Table 4.3). Also, one of two tungsten calibrations was done with the mirror. The GC, the column, the electronic filter, the carrier and flows, etc., all described in Chapter 2, remained essentially the same for all test compounds as shown in Table 6.1. Column temperatures were chosen so that analyte peaks would elute at a suitable time, roughly 2 minutes, and not too close to the solvent peak. The consistent cleaning regime

Table 6.1

Elements, Analytes and Experimental Calibration Conditions

Element	Compound	Col Temp (°C)	H$_2$ mL/min	Air mL/min	N$_2$ mL/min	Filter nm	PMT -V
C	dodecane	130	16	40	20	475	540
Si	Si(C$_2$H$_5$)$_4$	80	16	40	20	455	540
Pb	Pb(C$_2$H$_5$)$_4$	110	16	40	20	455	540
As	As(C$_6$H$_5$)$_3$	230	16	40	19	455	500
Sb	Sb(C$_6$H$_5$)$_3$	235	16	40	19	455	540
Bi	Bi(C$_6$H$_5$)$_3$	270	16	40	20	475	540
Mg	Mg(C$_5$H$_5$)$_2$	60	16	40	20	455	540
Cr	Cr(CO)$_6$	48	16	40	16	455	540
Mo	Mo(CO)$_6$	48	16	40	17	455	540
W	W(CO)$_6$	60	14	44	28	455	560
Mn	C$_5$H$_4$CH$_3$-Mn(CO)$_3$	130	16	40	20	455	540
Re	Re$_2$(CO)$_{10}$	150	16	40	20	455	540
Fe	Fe(C$_5$H$_5$)$_2$	140	16	40	20	455	540
Ru	Ru(C$_5$H$_5$)$_2$	160	16	40	20	455	500
Os	Os(C$_5$H$_5$)$_2$	170	16	40	20	475	540
Ni	Ni(C$_5$H$_5$)$_2$	130	16	40	20	455	

discussed in section 5.3 was followed after the completion of study on each element or more frequently if necessary.

Visual observations of analyte emission were usually made at night with a dark-adapted eye. A darkened room, however, was sufficient for most of the stronger emissions. The PMT was simply removed and the eye centered at the end of the aluminum light tube so that the flame could be seen. During daylight hours the flame itself was difficult to distinguish but the reflection from the parabolic mirror in the flame chamber made it possible to determine the location of the flame.

To establish a reliable measure of linear range, calibrations were carried out on a *well-conditioned* system, i.e., a number of injections of moderately large amounts of analyte were chromatographed until consistent results were obtained. Upon using a freshly cleaned detector, often the first few injections did not produce *normal* peaks. Instead, the peak would form in a positive direction, then dip sharply in the negative direction, as if being quenched. Although dependent on analyte, this would gradually improve with repeated injection until perfectly positive, well-shaped peaks appeared. During measurements in the lower region of the calibration curves, periodic injections, of solvent only, were made to ensure that there was no undue influence from previously-injected large amounts. Measurements of MDL were made under the same conditions as the calibration curve so that the MDL could be read directly from the plot as well. The values were usually consistent with the actual peak size and were all recorded as -log(mole element/s) with $S/N_{p-p} = 2$.

Spectra were obtained using the variable interference filter and/or the quarter-

meter grating monochromator. In order to make relevant comparisons, the same PMT

(R-1104) with close to the same voltage (-540 V), was used each time. Again, like the

calibration conditions in Table 6.1, there were slight variations. The response, recorded as

coulombs/mole, could therefore be used as an approximate measure of relative analyte

sensitivity. The derivation of this C/mole ordinate is given in detail in Appendix I. Any

measurements with the quarter-meter were done using 2 mm slits which resulted in a band

pass of about 6.7 nm. All spectra were obtained by repeated injection of the compound

dissolved in acetone, while manually advancing the wavelength setting. The second

channel was installed and used as an injection control system so repeated injection, at one

wavelength, was unnecessary. Conditions were highly reproducible using this system,

thus, measurements for a single detailed spectrum could be continued reliably over a

period of several days.

6.4 RESULTS AND DISCUSSION

To remain consistent with the format introduced in the first chapter, results for

elements determined to be FPD-active will be classified according to group or family and

compared with previously recorded data. All new elements that responded will also be

identified with their appropriate group. The main group 14 will be discussed first since

carbon constitutes a major portion of the compounds introduced and is used as a standard

upon which selectivity can be determined.

6.4.1 Carbon

Stoichiometric flows with the holophotal channel have produced some interesting

results for the carbon group. Sensitivity has been increased to the point where positive

results have been obtained for *silicon*, a new FPD-active element. Because carbon

sensitivity has also improved, the response of silicon is only about 10 times larger than that

of carbon as shown in Figure 6.3. The carbon plot was obtained by assuming that tetra-

ethylsilane was a carbon compound with eight carbons and the corresponding plot of

-log(mol C/s) versus log S/N_{p-p} was made. Therefore, it was possible that part, or all, of

the luminescence from this compound could have been caused by carbon.

Also from the calibration plot, the linear range for tetraethylsilane was determined

to be roughly over two orders of magnitude. Lead, however, was linear over four orders

and can now be detected as low as 200 pg. In Figure 6.4 the actual peaks are shown for

the smallest amounts of the lead and silicon compounds that were injected to determine

the MDL. A minimum peak for dodecane is included as well. Calculated as flows (-log

[mole element/s]) with $S/N_{p-p} = 2$, the best value of carbon was 10.2 and for silicon it was

11.9 (assuming no contribution from carbon). Lead had improved from 12.5 to 13.8, over

twenty times better.

It should be noted at this time, that all the MDLs reported in this chapter have, for

the most part, been determined using a 455 nm (LP) filter. This was used initially to help

decrease high background noise inherent in this small, stoichiometric flame. Any

elements, then, with emissions around or before 450 nm are probably even more sensitive

than actually measured. The obvious solution would have been to increase the bucking
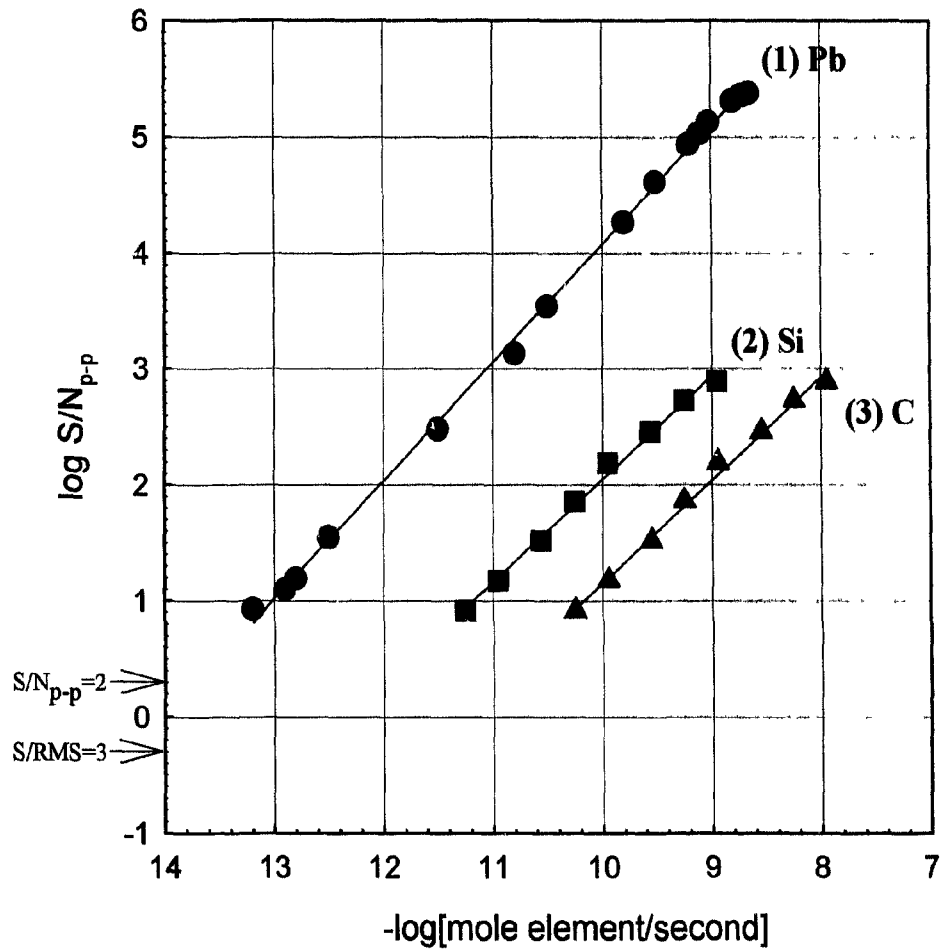
Figure 6.3 Calibration curves at stoichiometric conditions, holophotal channel, R-1104. (1) tetraethylead: - 540 V, column 110 °C, 455 nm (LP) (2) tetraethylsilane: -500 V, column 80 °C, 455 nm (LP) (3) carbon (see text).

200 ng dodecane
column 130 °C
gas flows (mL/min)
nitrogen 20
hydrogen 16
air 40
-log(mol C/s) = 10.2

50.0 ng tetraethylsilane
column 80 °C
gas flows (mL/min)
nitrogen 20
hydrogen 16
air 41
-log(mol Si/s) = 11.9

200 pg tetraethyllead
column 110 °C
gas flows (mL/min)
nitrogen 21
hydrogen 16
air 41
-log(mol Pb/s) = 13.8

time, minutes
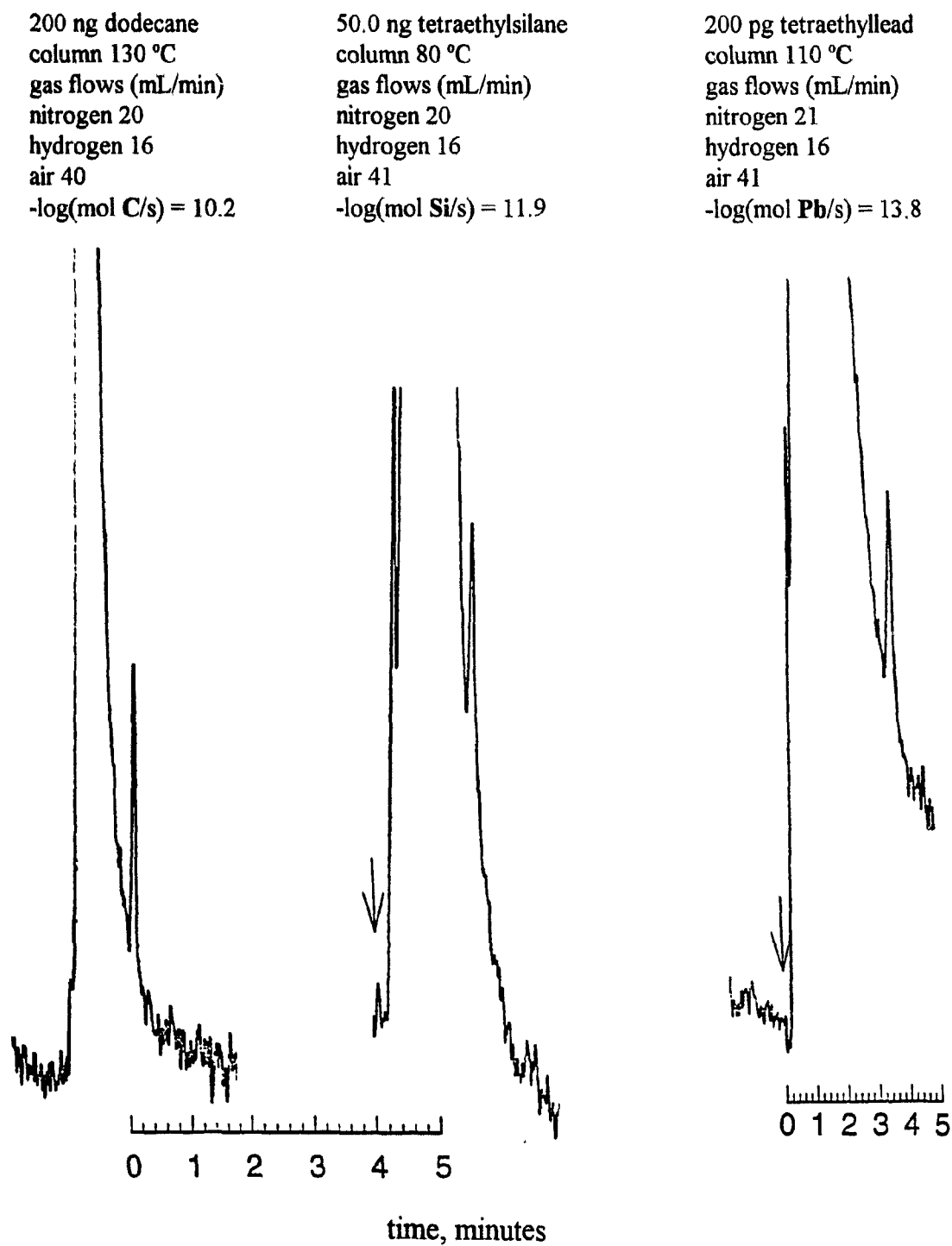
Figure 6.4   MDL peaks and values calculated as -log(mole element/s) for Si, Pb and C:
holophotal channel; R -1104, -540 V; 455 nm (LP); RC time constant 1 second.

range of the electrometer or even lower the PMT voltage (usually ~ -540 V). However, much of the spectral analysis had already been done with the variable interference filter, whose effective lower range just begins around 420 to 450 nm. It was decided, therefore, that consistency of operating parameters for comparative purposes took priority over searching for still lower detection limits.

The three spectra in Figure 6.5 show marked similarity with the major emission occurring between 430 and 450 nm. Great care must be taken when identifying maxima with absolute wavelength numbers as they are highly dependent both on the device used to measure the wavelength and on the photomultiplier. The increase in response from 400 to about 430 nm may be real but the percent transmission of the interference filter is also increasing (see Figure 6.1a). The range of the R-1104 photomultiplier used is perfectly sensitive in this area but for the R-2228, the sensitivity is not as high.

Although the resolution is limited by the rather large bandpass of the variable interference filter, the use of the second channel as a control for all spectral measurements reduces the possibility of injection errors. This means that for lead there is another distinct feature around 610 nm, extending well past 650 nm, and possible less defined features at approximately 500 and 550 nm. Visual examination of the lead emission (done before the spectral measurement so as not to unduly influence the observation) revealed a "fuzzy" bright bluish-green ball at the tip of the burner. The bluish luminescence was very similar to that of the solvent but not nearly so intense.

The lead spectrum bears some likeness to that previously recorded[53] which shows several bands (superimposed upon a continuum) around 530, 610 and 660 nm. The strong
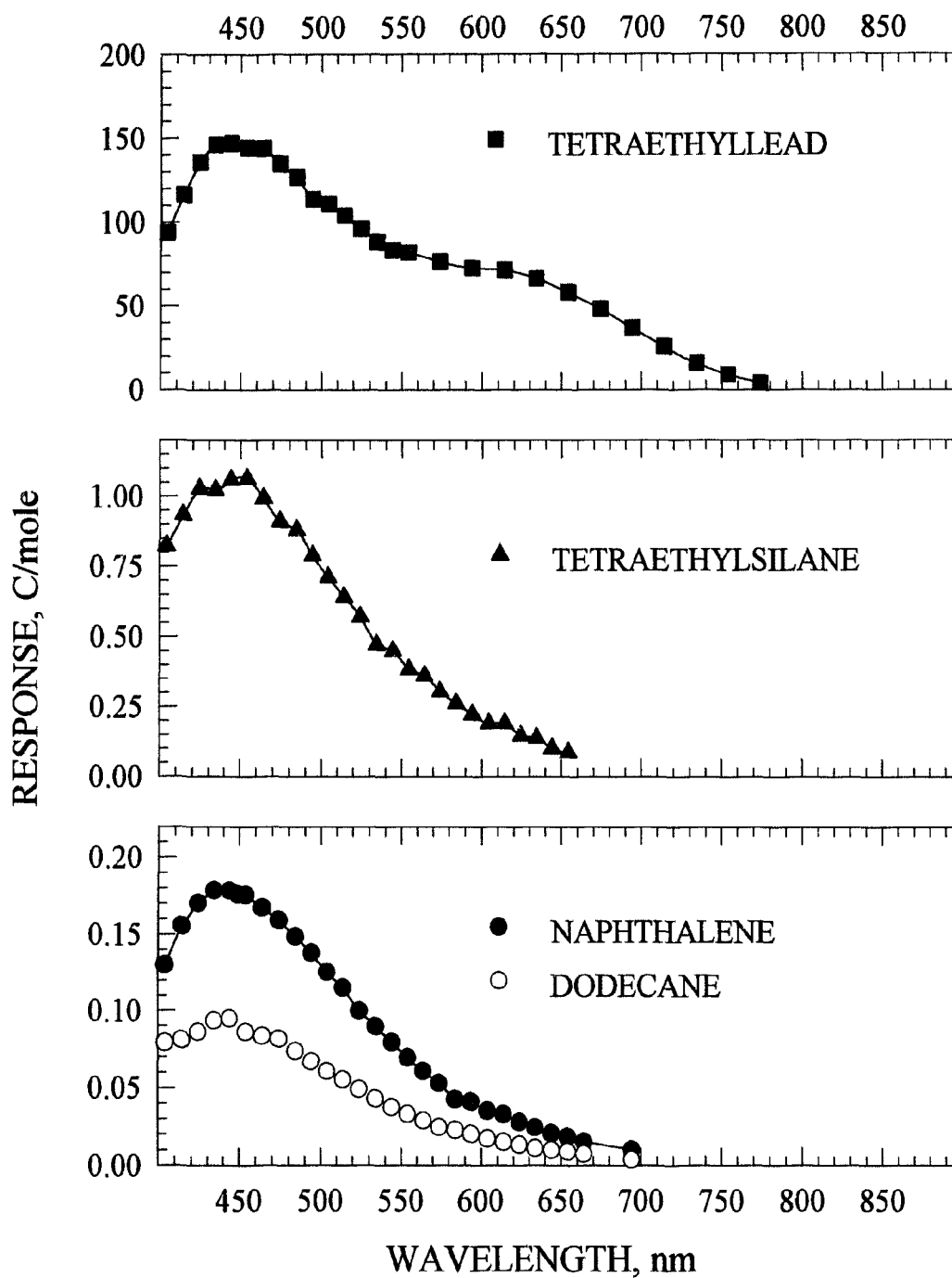
Figure 6.5   Spectrum obtained from tetraethyllead, tetraethylsilane, naphthalene and dodecane: variable wavelength selector; bandpass ~ 36 nm; 6-mm slit; R-1104, -540 V; holophotal channel; stoichiometric flows.

emission in Figure 6.5 around 450 nm, however, is different. The limitations of the filter

-prevent any conclusion about the presence of the 405.8 nm line used by Kaskin and

Milliken[80] in their detection of lead in gasoline samples with an oxyhydrogen flame. It was

suggested that PbH bands or the B system of PbO may be responsible for emissions in the

earlier spectrum and the 450 nm response may also involve a contribution from PbO.[53,81]

Now that the light level has been markedly improved, better resolution can be obtained.

Data from previous work[53,73] and continuing study with lead will hopefully yield more

information.

The luminescence from the tetraethylsilane is very weak, roughly ten times better

than dodecane and only six times better than naphthalene. (This is not unusual as

aromatics do give a slightly larger response in the FPD than aliphatics.[54]) Consequently, it

would be even more difficult to identify possible emitters. Pearse and Gaydon[81] list several

band systems which could be considered, including SiH, SiO or possibly SiO_2 which has a

strong group of bands between 421.5 and 430.0. The only other band system listed in that

region is for Si_2 (a weak system) which is unlikely. The carbon spectra, although obtained

with slightly less resolution, appeared quite similar to those obtained earlier. The main

feature was, again, attributed to CH at 431 nm with little evidence of the Swan bands.

6.4.2   Nitrogen

Nitrogen itself was not investigated but other members of this family proved to be

some of the more interesting and sensitive elements for FPD analysis. As phosphorus

(with sulfur) has made up the bulk of the FPD literature, little more was added except to

improve the overall detection limit from a -log(mole P/s) of 14.8 to 15.1, but only with a

hydrogen rich flame. It is noteworthy, however, that some phosphorus compounds were somewhat difficult to chromatograph. Samples such as triethylphosphate, triethylphosphite, tributylphosphite and dibutylphosphite produced wide tailing peaks and often seemed to decompose on injection. To overcome these difficulties, tris(pentafluoro-phenyl)phosphine, abbreviated tris-P, was used with much improved results. It gave sharp, well-shaped peaks and was quite sensitive but it also produced a high background. A similar problem was encountered with other elements in this group, using stoichiometric flows, and often the available bucking range was exceeded.

Calibration curves of arsenic and antimony were very similar in sensitivity, so they were plotted separately in Figures 6.6 and 6.7 to illustrate their peculiar shapes. Each point is an average value and the calibrations were repeated on several different days. This, hopefully, ensured the plots were reproducible under the indicated experimental conditions. At low concentrations the calibrations appeared linear for about two orders of magnitude, then the slope started to increase, especially the portion of the curve just before the bend-off. The tendency toward second-order kinetics, however, seemed more pronounced for antimony than arsenic. Both plots bore more resemblance to calibration curves of some tin compounds[35] rather than to some earlier linear calibrations of triphenylarsine and triphenylantimony.[49,60,61]

A three-point calibration plot of triphenylbismuth was presented previously as well, but the bismuth response was very weak and later attempts to confirm these results met with failure.[49,53] It was found in this study, however, that, other than coping with the high background, it was much easier to calibrate triphenylbismuth than the corresponding
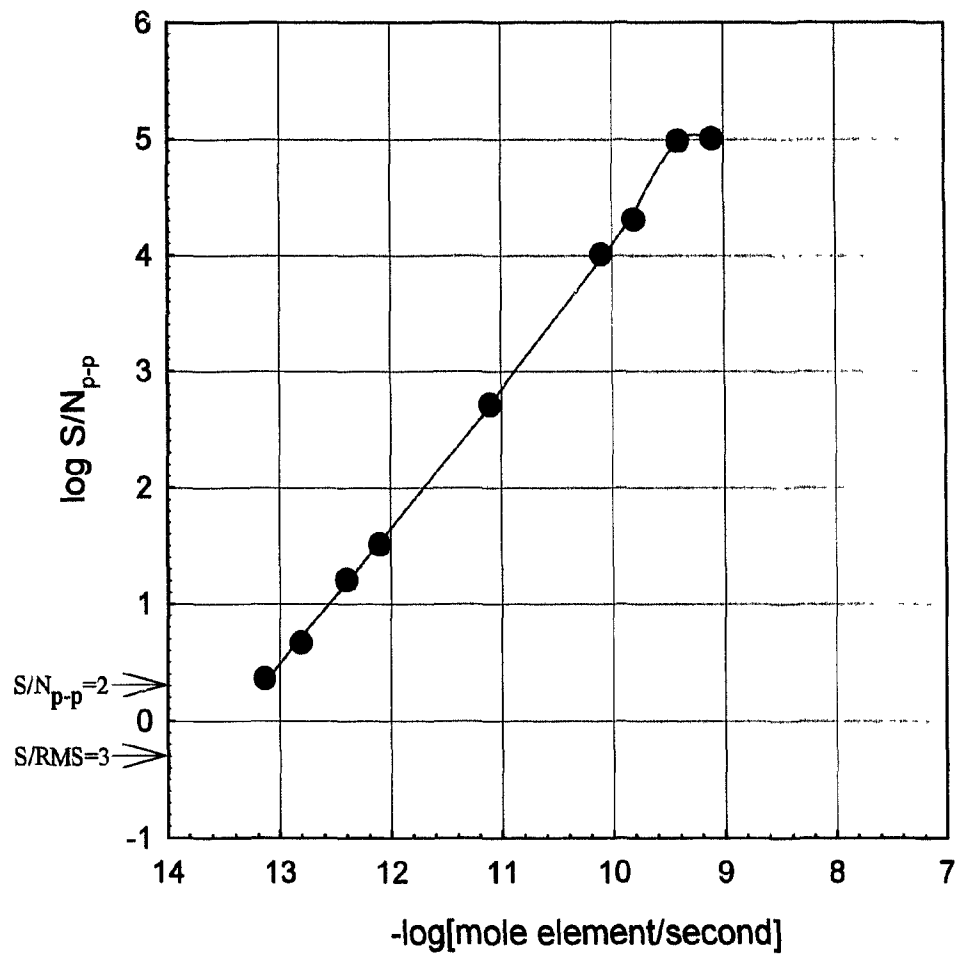
Figure 6.6 Calibration curve of triphenylarsenic: R1104, -540 V; 455 nm (LP); holophotal channel; stoichiometric flows; column 230 °C.
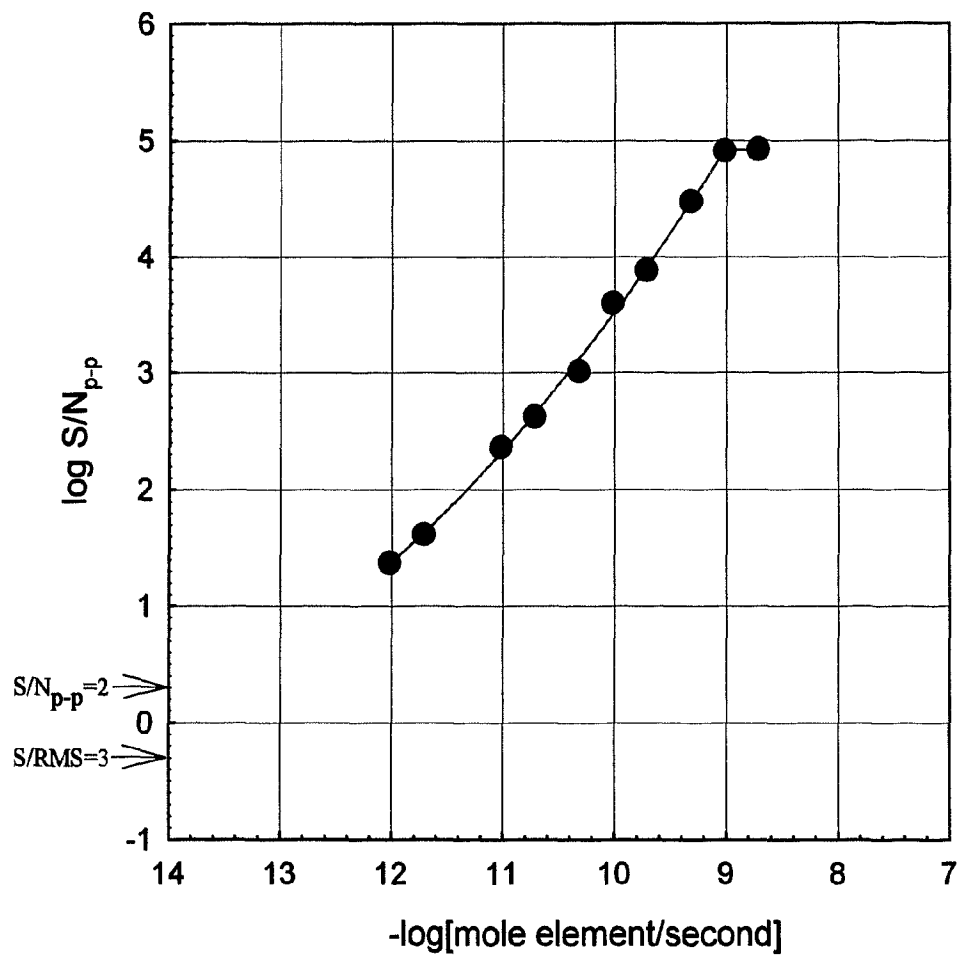
Figure 6.7   Calibration curve of triphenylantimony: R1104, -540 V; 455 nm
(LP); holophotal channel; stoichiometric flows; column 235 °C.

compounds of arsenic and antimony. The column temperature was very high, 270 °C, which caused some column bleed, and the peaks were wide and tailing but the results were very reproducible and gave a perfectly linear plot shown in Figure 6.8. The range was good, over three orders of magnitude, when with an injection of 2 μg the curve dropped sharply. Again, this was completely reproducible. The loss of bucking control prevented injection quantities less than 2 ng but the MDL, as -log(mole Bi/s), estimated from the plot, was around 14.0.

This value was surprisingly large when compared to only 13.3 for arsenic and about 13.2 for antimony. Because of the lack of linearity of the plots and the limitations imposed by the high background, these values were calculated using the smallest injection quantity. The arsenic was rather disappointing as it was slightly less than the previously recorded result of 13.5, based on the work of Kapila and Vogt[60], but the antimony was substantially superior to a previous value of 11.9, i.e., it was over 20 times better. The bismuth response was even more sensitive. In fact, both in numbers and in actual experimental properties, the bismuth seemed to resemble lead more than the members of group 15. The extraordinarily high background could be attributed to the excessive bleed from the column at such high temperatures, and the large white deposit found on the chimney after repeated injections seemed to support this idea.

Before measuring the spectrum of arsenic, 1 μg of triphenylarsenic was injected and the emission observed by a dark-adapted eye. The hazy, yellow-gold luminescence was not as completely round as that produced by most analytes under these conditions. It was more flame shaped and there appeared to be more reflection off the sides of the
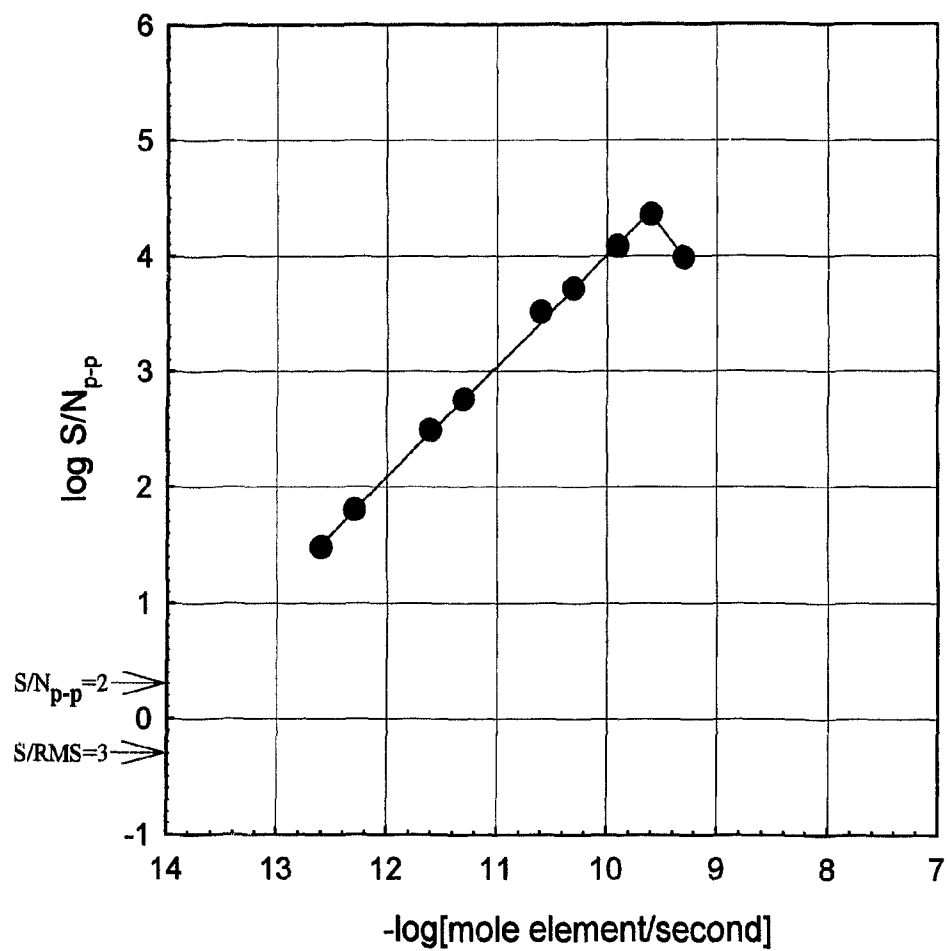
Figure 6.8 Calibration curve of triphenylbismuth: R1104, -540 V; 475 nm (LP); holophotal channel; stoichiometric flows; column 270 °C.
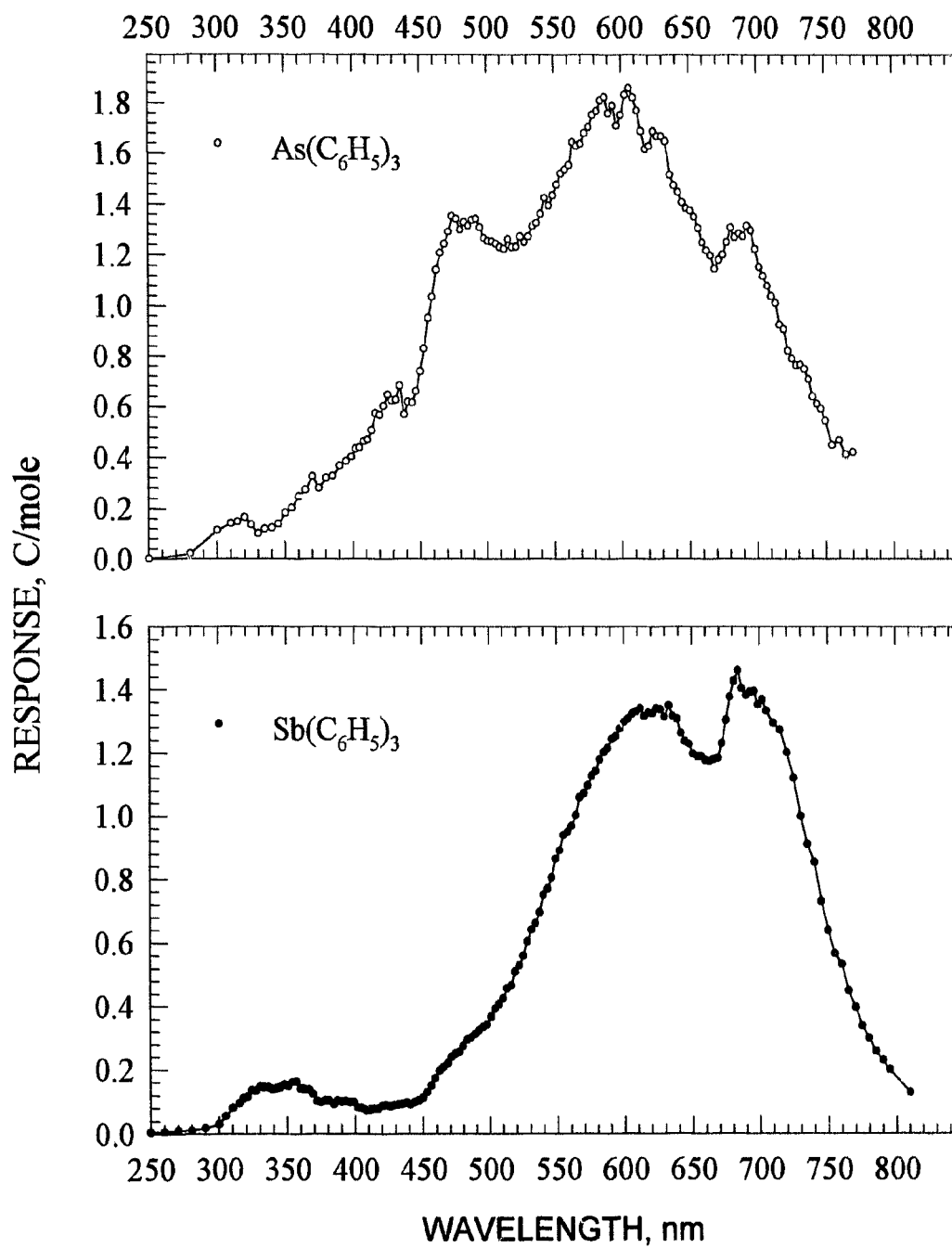
Figure 6.9   Spectrum from triphenylarsenic and triphenylantimony: grating mono-chromator; 6.7 nm bandpass; R-1104, -540 V; holophotal channel; stoichiometric flows.

parabolic mirror. The measured spectrum given in Figure 6.9 confirmed the visual

experiment. It appeared to be similar to earlier spectra[53, 59-61] which showed a broad

continuum between 400 and 700 nm. The species responsible for the emission is reported

to be unknown but Fujiwara and coworkers[82], using gas-phase chemiluminescence

spectroscopy, attribute emissions from 240-300 nm to AsO. In the lower wavelength

regions (225-430 nm), there is also a well-known, extensive system of As_2 which, because

of the non-linearity of the calibrations, may be a possibility.[81] The 420-500 nm region

could correspond to the AsO G system while the AsO A system is known from 580 - 640

nm.[81]

The *feature* observed at 680 to 700 nm, which has appeared in many spectra

recorded by the quarter-meter grating monochromator used in this study (and in other

work by this research group), is presumably an anomaly in the monochromator and is not

considered a true feature. To confirm this, spectra of rhenium were compared using a

filter monochromator (bandpass 28 nm), the variable interference filter built for this study,

and then the quarter-meter grating monochromator. The latter was the only one that

showed the deviation around 700 nm in an otherwise smooth continuum. Appropriate

wide band filters were used to try and isolate the problem but it was neither a "light leak"

nor was it due to second order. For a final check, a *light bulb* spectrum was measured,

first using the variable interference filter and then the quarter-meter grating

monochromator (see Figure 6.10). The variable filter gave the typical broad continuum of

glowing tungsten (a "grey" body), while the quarter-meter again displayed the strange

phenomenon around 700 nm.
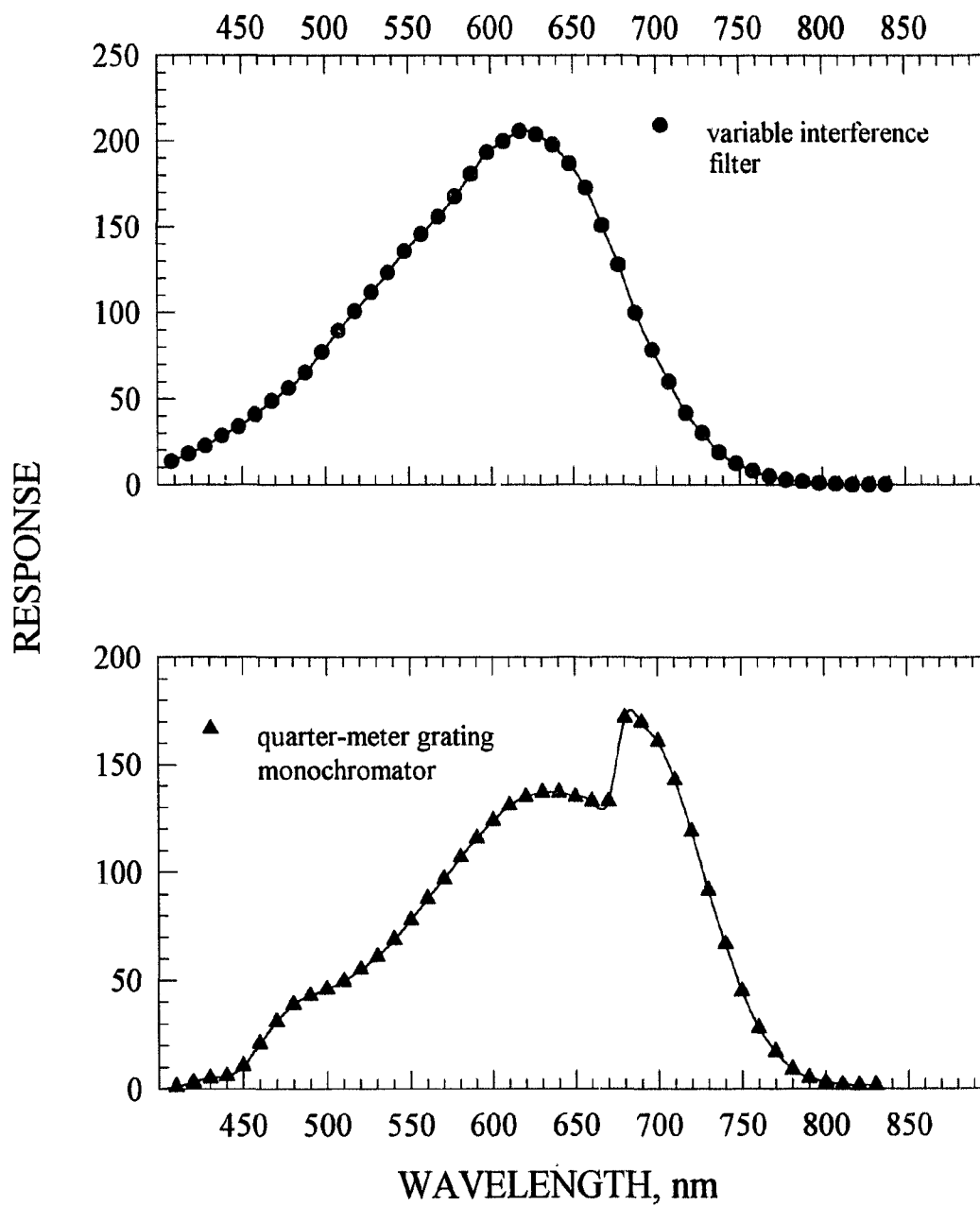
Figure 6.10 Comparison of *light bulb* spectra using the variable interference filter and the quarter-meter grating monochromator.

Oriel[83] describes such anomalies as "sudden increases or decreases in the efficiency versus wavelength curve" that occur "as a result of the interaction of the electric fields of incident and diffracted beams with each other and with the metal coated grooves of the grating. They were first documented by Wood and so are sometimes called Wood's Anomalies." The explanation continues by saying "they are not a defect of the grating but an inescapable consequence of the diffraction physics of blazed gratings". If this is, indeed, the correct explanation, then the spectral features of the quarter-meter were not distorted but their intensity simply was suddenly increased.

The phenomenon is clearly evident in the spectrum of triphenylantimony, however, the remainder shows the same featureless, broad continuum with maxima around 600 nm, as seen before[53,59] and was attributed to the A system of SbO. No conclusive evidence for Sb_2 was obtained from the literature as reported bands for this species were about 217-230 nm.[84] Other SbO systems may account for the features between 300 and 400 nm.[81]

This anomaly did not appear in the very different spectrum of triphenylbismuth shown in Figure 6.11. The detection of triphenylbismuth by eye revealed an intense, but out-of-focus luminescence that was a deep blue in color with a touch of green appearing towards the end of the peak. In the measured spectrum there does appear to be a strong, fairly sharp emission from about 340 to 550 nm, quite unlike those of arsenic and antimony. There were three defined maxima around 390, 420 and 470 nm after which the intensity fell abruptly, well before 600 nm. The intensity was comparable to that of nickel and ruthenium, two of the most sensitive elements in the FPD. This, again, draws attention to the rather poor choice of filter for the calibration plot of triphenylbismuth.
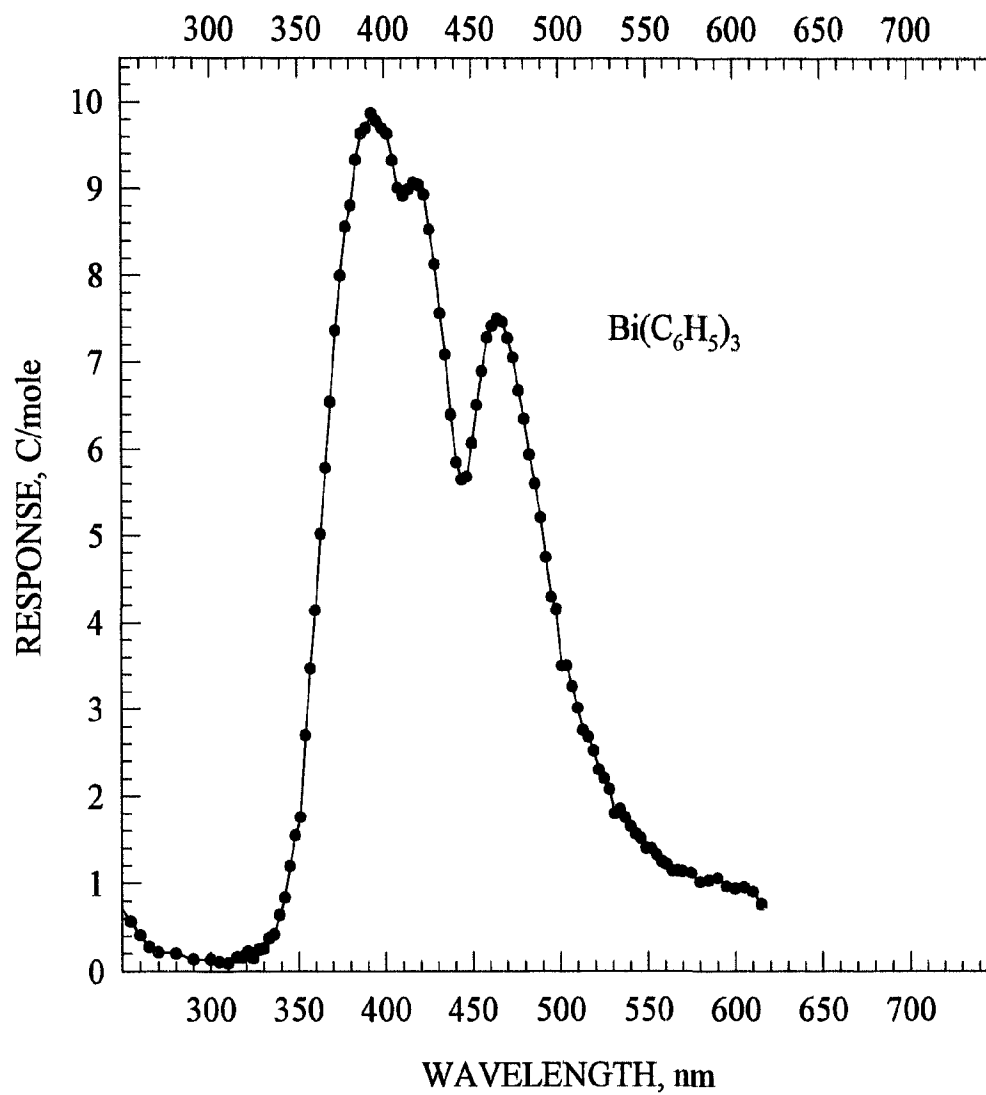
Figure 6.11   Spectrum from triphenylbismuth: grating monochromator; 6.7 nm bandpass; R-1104 -540 V; holophotal channel; stoichiometric flows.

The 455 nm (LP) filter cut off a significant portion of the emission and the actual MDL should have been much better than presented above. The emission at around 465 nm could correspond to a strong atomic line at 472.2 nm or to the BiH "469.8 nm system" which are very close.[85,81] The largest maximum, at 390 nm, remains unidentified.

6.4.3 Group 13 and 17

No attempt was made to examine compounds of boron but aluminumhexafluoro-acetylacetonate was checked very quickly by temperature-programmed chromatography from 60 to 230 °C. While there seemed to be no immediate response, a large peak did appear after about 20 minutes. The sample, however, was not homogeneous: the white powder-like solid dissolved easily in acetone but beige granules remained at the bottom of the solution. It was decided, therefore, to try some volatile halogen compounds instead. The only observed response came from decafluorobiphenyl which showed very poor selectivity against carbon (F/C ~ 3) and, consequently, this was abandoned too.

6.4.4 Magnesium

Although elements in groups 1 and 2 have not been known to respond in the FPD, possibly the main reason, as previously mentioned, is the lack of suitably volatile compounds. A sample of calcium bis(2,2,6,6-tetramethyl)3,5-heptadionate, which was not very soluble in acetone, gave no response at all, nor did magnesium hexafluoroacetyl-acetonate. A final attempt was made with magnesocene which was highly pyrophoric and both air and moisture sensitive. All solutions had to be prepared and stored under nitrogen. A surprisingly good response was observed when this compound was chromatographed at 60 °C. Unfortunately, solutions of less than 100 ng showed no

response, probably due to irreversible adsorption and/or premature decomposition. A full, reliable calibration curve could not be made, however, Figure 6.12 gives an indication of good sensitivity. The larger concentrations posed no problem, either for injection or for storage purposes. It was possible, then, to obtain the spectrum using both the variable interference filter and the quarter-meter grating monochromator, as shown in Figure 6.13.

Preliminary visual examination of the magnesium emission revealed a hazy, bluish-green ball of moderate intensity, not as strong as bismuth. The spectrum, measured with the variable interference filter, showed a maximum around 440 nm (the transmission starts to decline at this point) and dropped to a low level before 600 nm. The more detailed spectrum had corresponding peaks around 430 and 475 nm and there was evidence, as well, of another peak at 340 to 350 nm. The most interesting feature, however, was a very sharp peak around 310 nm. The profile at 620 nm was suspected to be second order which was confirmed by repetition of the spectrum, in this area, using a 550 nm (LP) filter. The spectrum appeared to be different from the literature descriptions and identification of emitters is speculation only. There is a known strong atomic line of magnesium at 285 nm[86] and a complex system of MgO bands in the region 364 to 396 nm.[84] The features between 400-500 nm could be attributed to several bands of MgH reported in that area[81]. The sharp peak around 310 nm does not correspond to any atomic line of magnesium, however, there is the 306.4 nm system of OH with strong 0,0 transitions at 306.36, 306.72, 307.8 and 308.9 nm.[84] Perhaps the OH is, in some way, promoted by the magnesium.
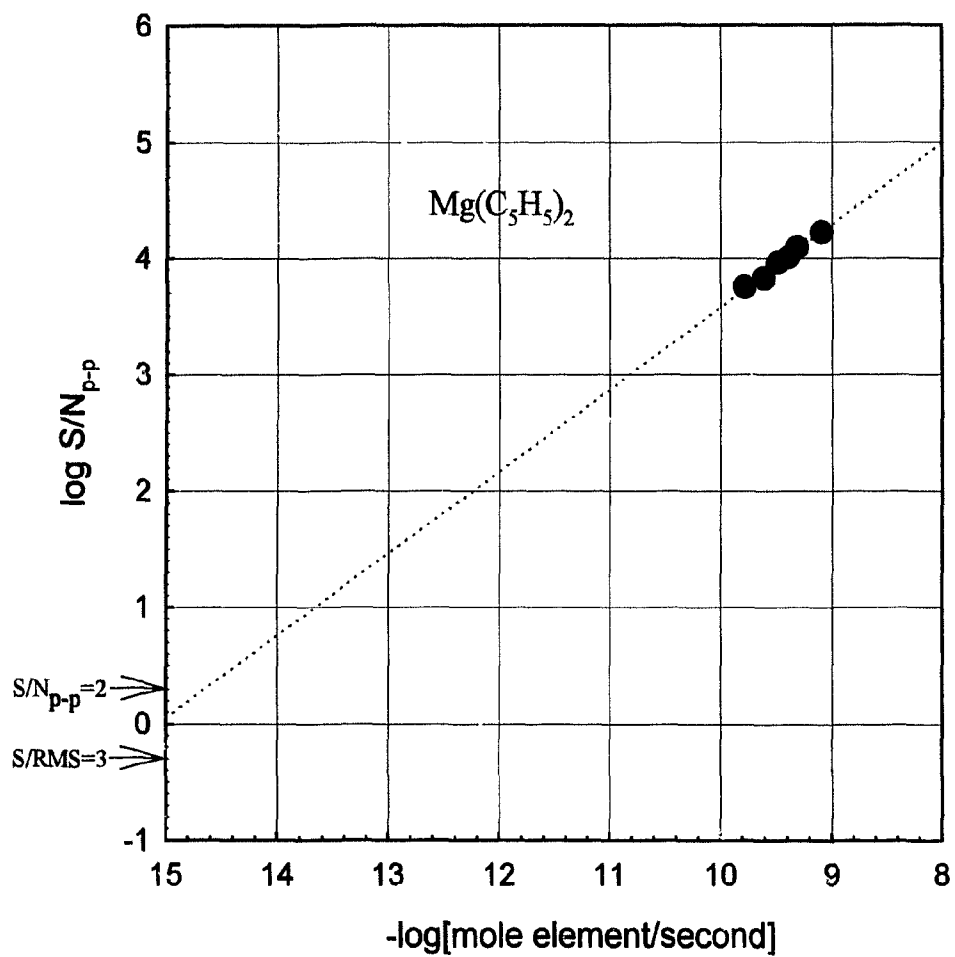
Figure 6.12 Calibration curve of magnesocene: R-1104, -540 V; 455 nm (LP); holophotal channel; stoichiometric flows; column 60 °C.
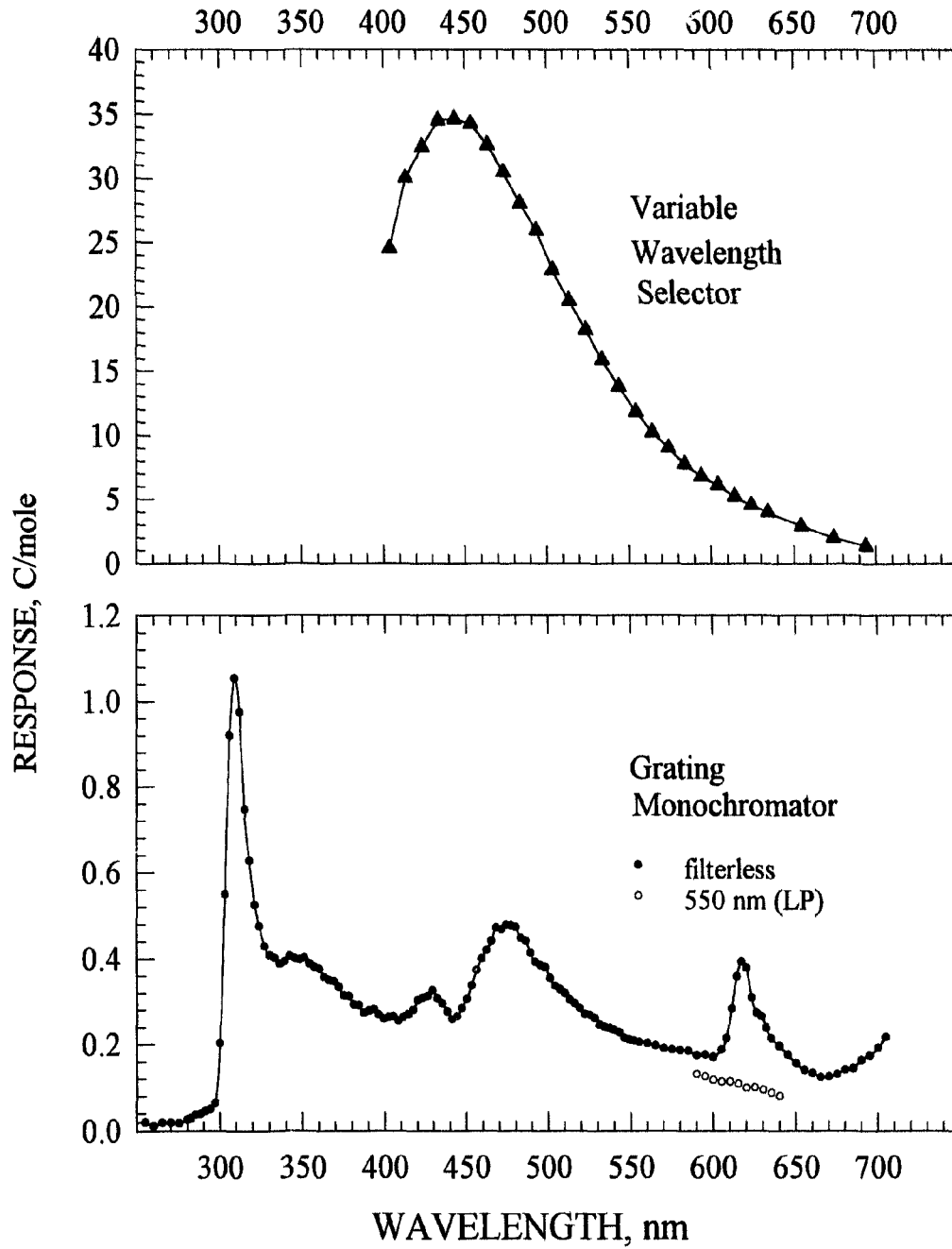
Figure 6.13   Spectra from magnesocene: R-1104, -540 V; holophotal channel; stoichiometric flows:

▲   variable wavelength selector, bandpass ~ 36 nm, 6-mm slit;

•   grating monochromator, 6.7 nm bandpass, no filter;

°   grating monochromator, 6.7 nm, 550 nm (LP) filter.

6.4.5   Group 6

Magnesium was the last metal in the study of the main groups. The first of the

transition metals, in order of the periodic table, to respond favorably to the FPD was Cr.

(It was also historically the first transition metal to be successfully analyzed by the FPD.[65])

The hexacarbonyl derivative was found to be much more stable than benzene chromium

carbonyl, which decomposed in a matter of hours. Both chromium hexacarbonyl and

molybdenum hexacarbonyl were easy to chromatograph under the exact same conditions

and produced linear calibration plots with 2 to 3 orders of magnitude (see Figure 6.14).

The sensitivity of the chromium was slightly disappointing, with -log(mole Cr/s) = 14.0 ,

compared to a previously recorded value of 14.7. This may have been, in part, due to the

poor MDL determination shown in Figure 6.15, where the chromium peak was eluted well

before the solvent peak returned to the baseline and quenching could have occurred. The

calibration plot, however, indicated a similar value, so the more likely reason was, again,

the poor choice of filter used to reduce the background noise. The MDL for

molybdenum, on the other hand, improved significantly, from 11.7 to 12.6, almost an

order of magnitude (Figure 6.15). This marked increase was supported by the calibration

curve of molybdenum also given Figure 6.14.

After calibration of chromium and molybdenum, solutions of tungsten were

prepared and injected using the same stoichiometric conditions, but with the column

temperature raised to 60 °C. Tungsten responded quite well at close to the same

conditions, but more air-rich: hydrogen 14 mL/min and air 44 mL/min. The nitrogen was

also increased to 28 mL/min. Figure 6.16 shows the calibration curve of tungsten
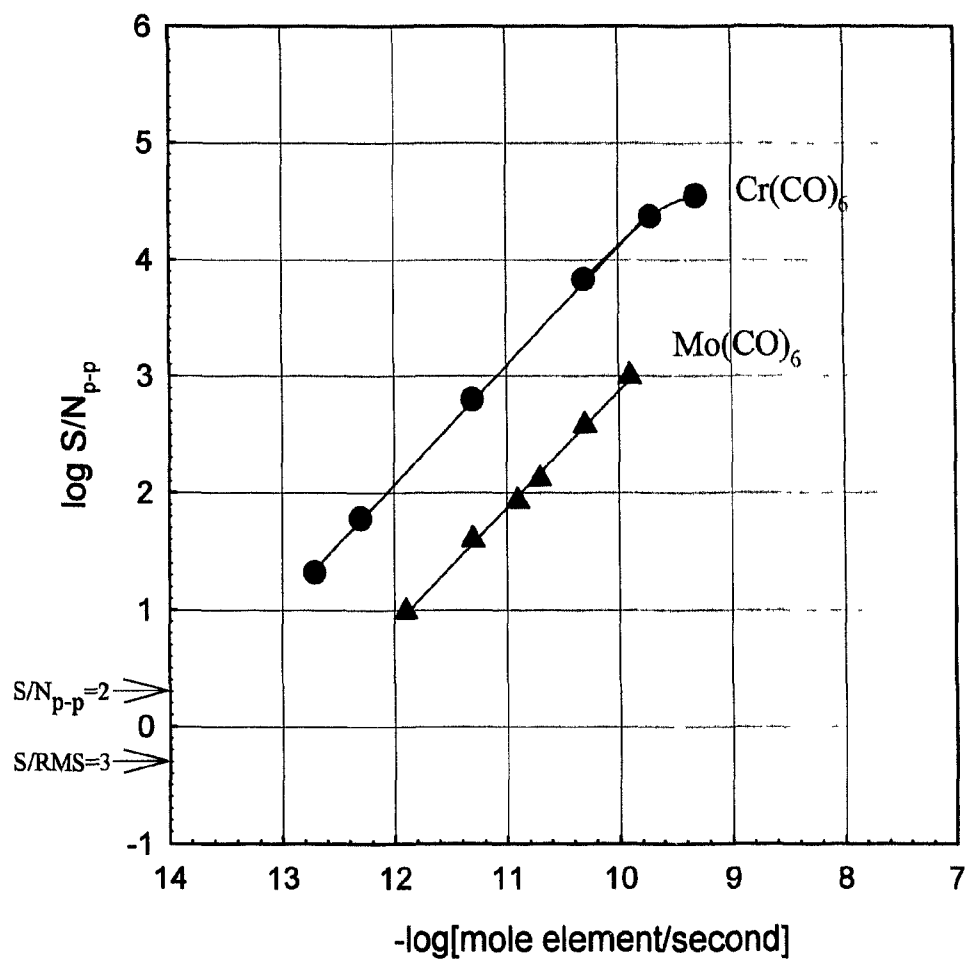
Figure 6.14   Calibration curves for chromium hexacarbonyl and molybdenum hexacarbonyl: stoichiometric flows; holophotal channel; R-1104, -540 V; 455 nm (LP); column 48 °C.

200 pg Cr(CO)$_6$
-log(mole Cr/s) = 14.0

5.0 Mo(CO)$_6$
-log(mole Mo/s) = 12.6

0 1 2 3 4 5

time, minutes

0 1 2 3 4 5

time, minutes
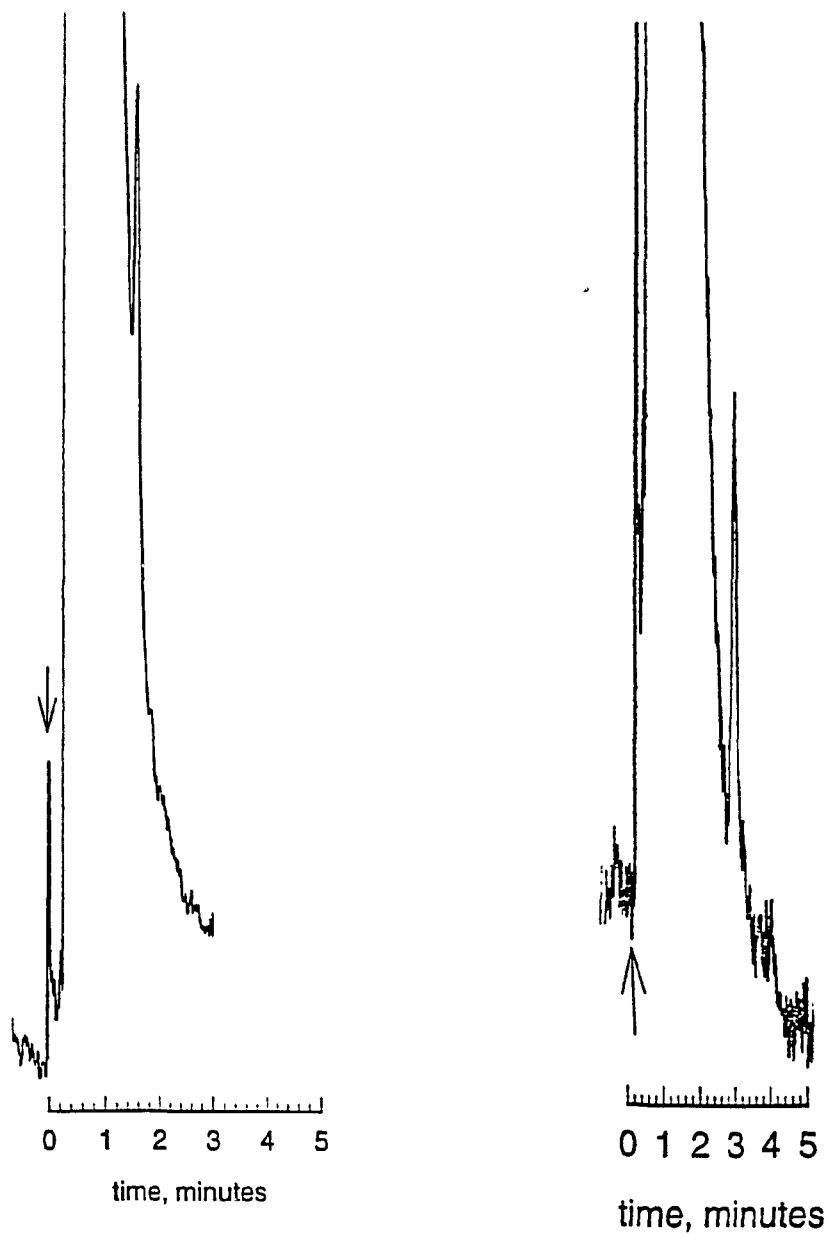
Figure 6.15   MDL peaks and values for Cr and Mo: R1104, -540 V; 455nm (LP); stoichiometric flows; nitrogen 16 mL/min for Cr and 17 mL/min for Mo; column 48 °C; RC time constant 1 second.
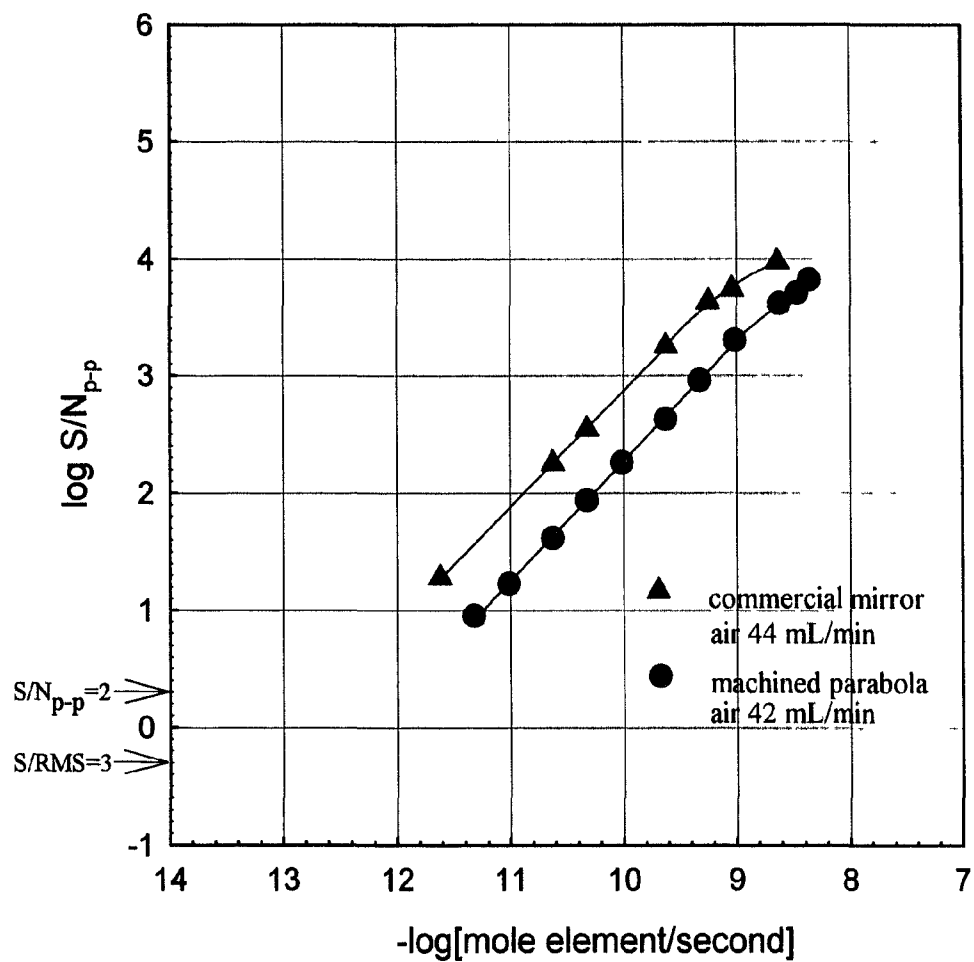
Figure 6.16 Calibration curves for tungsten hexacarbonyl: holophotal channel; R-1104, -540 V; 455 nm (LP); H_2 14 mL/min; column 60 °C.

measured at these flows. It also gives another calibration plot, more sensitive, done with the commercial mirror but with slightly different flows. The increase in sensitivity was probably due more to the gas flows than to the difference in mirrors, assuming that the mirror comparisons presented in Table 4.3 were correct. The corresponding MDL determinations are given in Figure 6.17. The best value of 12.8 was quite gratifying, in view of the fact tungsten had previously been considered unresponsive in the FPD.

The chromium emission was the brightest for the visual examination and was a slightly yellow color. Injection of 2 μg hexacarbonyl tungsten exhibited only a very faint emission but 10 μg produced a distinctly gold-colored, round emission. The spectra of Cr, Mo and W, measured on the variable interference filter, are given in Figure 6.18. The resolution was limited by the filter but they all appeared to be broad continua from approximately 400 to over 700 nm. The largest maximum for chromium occurred at about 470 nm but there was evidence of other features between 450 and 550 nm. There also was another lower peak area around 600 nm. There appeared, however, to be no confirmation of chromium's strongest emission line (425.435 nm) used by Ross and Shafik[65] for their FPD determination of chromium and earlier by Juvet and Durbin[87] in their hot, oxygen-rich system. A more recent FPD spectrum of Cr also displayed a distinct maximum at about 427 nm. (It should be noted that the large feature around 700 nm in this latter spectrum may be actually the *quarter-meter anomoly* discussed on page 118). The maximum around 480 nm and the broad features up to 700 nm, all unidentified, seem to agree with the most recent work.[54] It is possible, however, that the emission in the higher wavelength region could be due to CrO which has strong heads at 579.44 (1,0),

(1) MDL = 12.2   (2) MDL = 12.8

0 2 4 6 8
time, minutes

0 2 4 6 8
time, minutes

Figure 6.17   MDL peaks and values for tungsten hexacarbonyl: R-1104, -560 V; 455
nm (LP); H_2 14 mL/min; N_2 28 mL/min; column 60 °C; RC time constant 1 second.
(1) 10 ng $W(CO)_6$, air 44 mL/min, -log(mole W/s) = 12.2.
(2) 5 ng $W(CO)_6$, air 42 mL/min, -log(mole W/s) = 12.8.
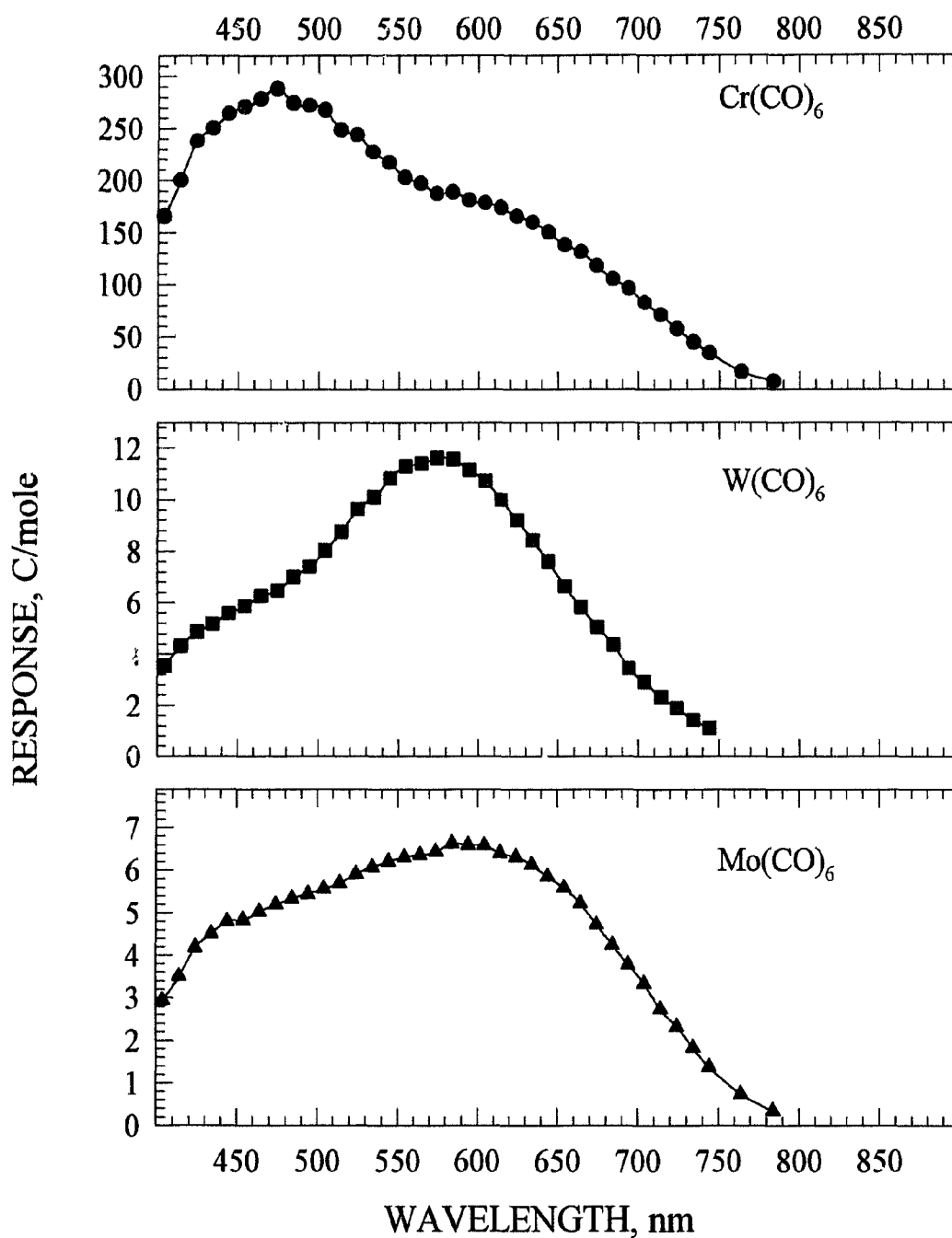
Figure 6.18 Spectra obtained from hexacarbonyl compounds of chromium, molybdenum and tungsten: variable interference filter; R-1104; holophotal channel.

● $Cr(CO)_6$: -540 V; H_2 16 mL/min, air 40 mL/min; column 50 °C.

■ $W(CO)_6$: -600 V; H_2 14 mL/min, air 42 mL/min; column 60 °C.

▲ $Mo(CO)_6$: -540 V; H_2 16 mL/min, air 40 mL/min; column 50 °C.

605.16 (0,0) and 639.43 (0,1) nm.[81]

The molybdenum response for the spectral measurement appeared to be approximately two orders of magnitude larger than that for the corresponding carbon compound which helped to confirm that there really was a molybdenum emitter. Unlike the previous investigation, however, there was no distinct evidence of a sharp peak at 420 nm (possibly due to atomic lines, 414.355 and 418.832 nm).[54] Instead, there was a broad profile that was already quite pronounced around 400 nm, the limit of the variable interference filter. There was a slight feature around 450 nm, and then the continuum reached a maximum around 600 nm which did seem to correspond to the earlier work. Little information is available, but there appears to be some evidence for a system of MoO in that area.[84]

That the tungsten response was also sufficiently larger than that of carbon suggests that there was, indeed, a tungsten emitter. The spectrum was an almost symmetrical, smooth continuum with maximum around 580 nm. There are approximate measurements reported for a WO system with a strong head at 470.94 nm.[84] No distinct spectral feature appeared in this region, only a change of slope in the continuum around 470 nm. There were also several other systems recorded for WO, one of which had a head at 586.52 nm (1, 0) which may be applicable.[84]

6.4.6   Group 7

Flame photometric analysis has already been shown to be an excellent analytical method for determining trace amounts of manganese. The purpose of this study was to use the known response of this metal to further investigate the capabilities of the tiny,

stoichiometric flame. Rhenium, reported to be not nearly as sensitive, was also selected as

part of this investigation. The information obtained, then, could be compared to

previously obtained results.

The 455 nm (LP) filter, selected for the calibration of almost all the elements, was

used once again for consistency, in spite of prior knowledge of the strong atomic emission

of manganese at 403 nm. The sensitivity, however, was surprisingly good for manganese

and rhenium both. From Figure 6.19, it can be seen that the linear range was about four

orders of magnitude for (methylcyclopentadienyl)manganese tricarbonyl or MMT but was

almost five for rhenium in the form of dirheniumdeccarbonyl. There were few problems

like excessive background noise or peak-to-peak fluctuation, and the MDL measurements

were relatively easy (see Figure 6.20). The 50 pg injection of MMT gave a -log(mole

Mn/s) value of 14.3 which was ten times better than the previous work.[54] The MDL for

rhenium, described as "not a very strong emitter", was measured at 14.2, an improvement

of two *orders* of magnitude.

Emissions of both Mn and Re were examined visually. MMT produced a

luminescence that changed from green to yellow with perhaps a touch of red at the end of

the peak, but the emission by this time was very weak. Dirheniumdecacarbonyl was

yellow-orange with a gold color at the brightest point.

With the variable interference filter monochromator, it was possible to detect a

portion of the strong atomic line of manganese at 403 nm as shown in Figure 6.21. An

earlier spectrum[67] showed strong evidence of another atomic contribution at 540 nm

which did not appear distinctly in Figure 6.21 unless it was part of the maximum at
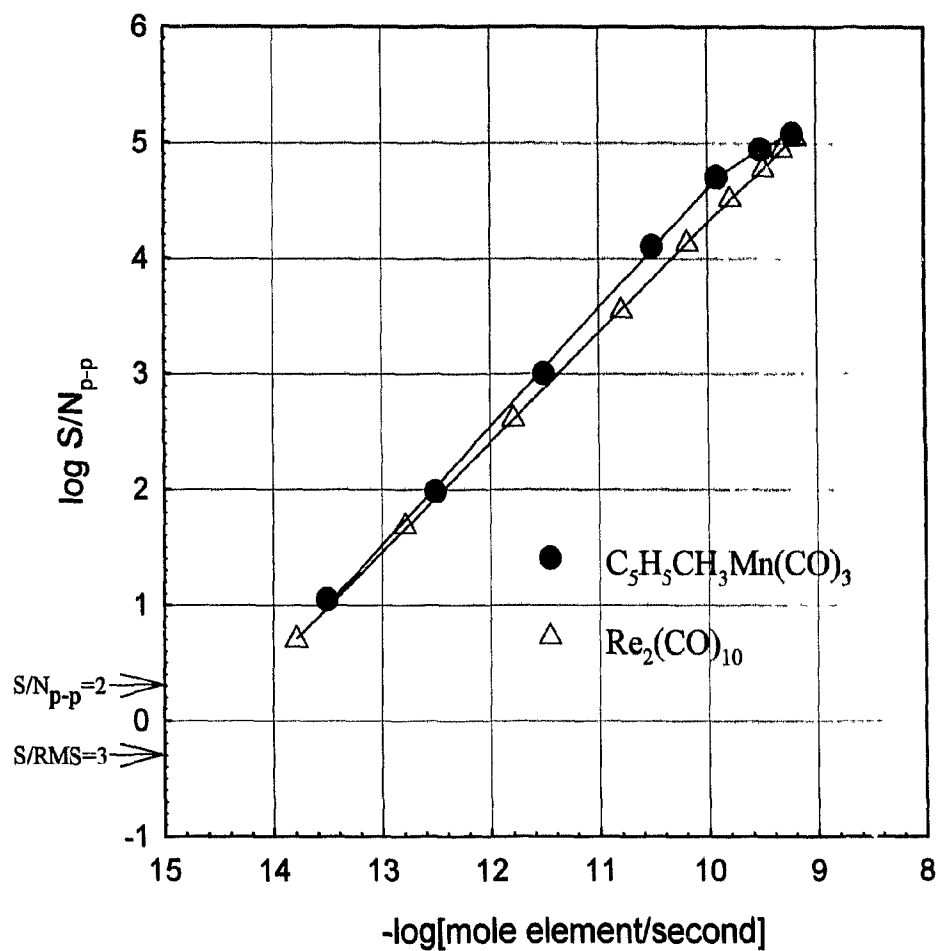
**Figure 6.19**   Calibration curve of MMT, (methylcyclopentadienyl)manganese tricarbonyl and dirheniumdecacarbonyl: holophotal channel; R-1104, -540 V; 455 nm (LP); stoichiometric flows; column temperatures: $Re(CO)_{10}$ 150 °C and MMT 130 °C.

50 pg MMT
-log(mole **Mn**/s) = 14.3

50 pg Re₂(CO)₁₀
-log(mole **Re**/s) = 14.2

0 1 2 3 4 5
time, minutes

0 1 2 3 4 5
time, minutes
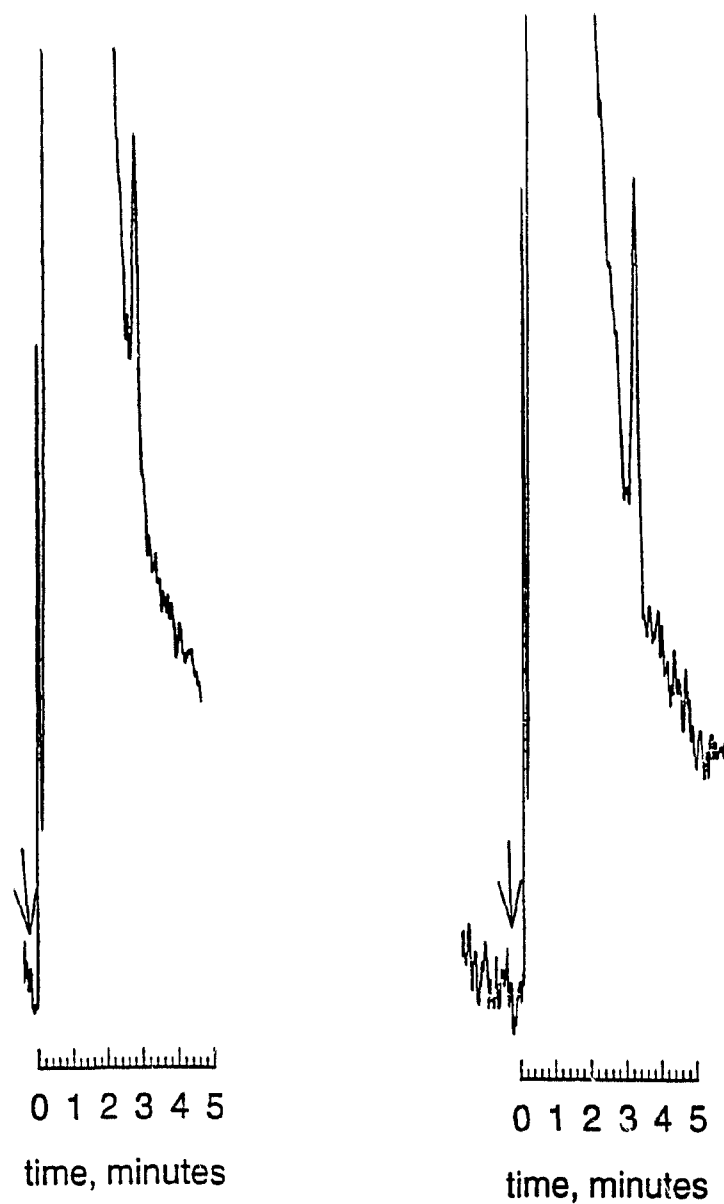
Figure 6.20   MDL peaks and values for (methylcyclopentadienyl)manganese tricarbonyl (MMT) and dirheniumdecacarbonyl: holophotal channel; stoichiometric flows; R-1104, -540 V; 455 nm (LP); column temperatures: $Re(CO)_{10}$ 150 °C and MMT 130 °C.
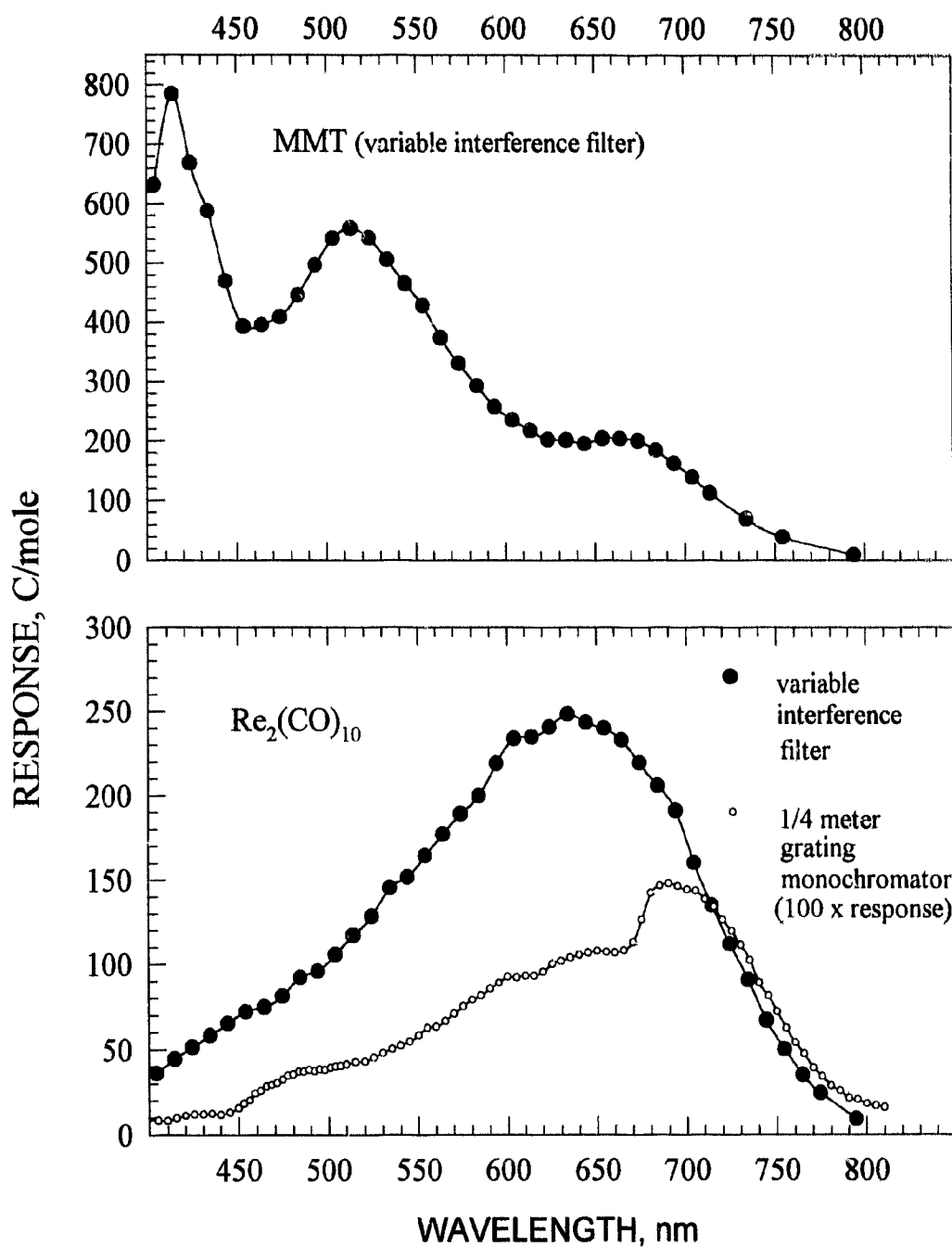
Figure 6.21 Spectra from (methylcyclopentadienyl)manganese tricarbonyl and dirheniumdecacarbonyl: holophotal channel; R-1104, -540 V; stoichiometric flows.

515 nm. There was another definite feature that peaked at about 660 nm which also was not seen earlier in the more resolved spectrum. There have been reported some strong bands of MnO in both these regions.[81] As a final note on manganese, it should be pointed out that the overall response is approximately 2 to 3 times larger than that of Re, as shown in the lower part of Figure 6.21, confirming that the MDL for Mn could have been even better without the 455 nm filter.

The spectrum of dirheniumdecacarbonyl was measured both using the variable interference filter and the quarter-meter grating monochromator. The quarter-meter spectrum, with the exception of the anomaly at about 700 nm, was essentially the same as the spectrum obtained with less resolution. It was also very similar to spectra obtained previously, both for a cool hydrogen-rich flame and for a hotter flame with more oxygen.[54,59] Again, there was no response in the 300 to 400 nm region so the atomic lines around 346 nm were not involved. A system of ReO bands[81] that exists between 606 and 609 nm may have made some contribution, but the maximum of the rather featureless spectrum seemed to be at about 630 to 650 nm. The response, therefore, remained basically unidentified.

6.4.7 Group 8

The iron family, including ruthenium and osmium, soon became one of the more interesting groups. Certainly, they were the initial metals that responded to the stoichiometric conditions and, therefore, much more time was devoted to the study of their behavior in this (for an FPD) unusual flame. Osmium was also used as a major test element in both the development of the holophotal technique and the second-channel

work.[71,74]

Figure 6.22 gives the calibration plots of the metallocenes of iron, ruthenium and

osmium, all at stoichiometric flows and with the same 455 nm (LP) filter. Not

unexpectedly, they all had excellent linear range, at least four orders of magnitude. The

MDL for ruthenium as -log(mole Ru/s) was 15.4, determined either from the calibration

curve or the minimum injection of only 2 pg of ruthenocene (Figure 6.23). This was just a

slight improvement from the previously recorded value which may have been due to the

stoichiometric flows or the holophotal technique or a combination of both. Because of

ruthenium's high response, the PMT voltage had to be lowered to -500 V from -540 V in

order to keep the signal within the range of the attenuation on the electrometer. Iron also

had been discovered to be relatively sensitive in the FPD[48] but with stoichiometric

conditions the MDL was increased from 13.3 to 14.6. The ferrocene peak in Figure 6.23

shows the response to just 20 pg of analyte. It was osmocene, however, that showed the

greatest improvement, from 12.8 to 14.9. The response had increased over a hundred

times.

At lower flows that were still stoichiometric, i.e., hydrogen 10 mL/min and air 25

mL/min, visual observation of the emission was made for the three metallocenes.

Ferrocene produced a round, pale greenish-yellow response that was surrounded by an

orange rim. Ruthenocene also had the orange rim but the interior was a creamy-white

color. Osmocene resembled ferrocene except there was no rim. With flows of hydrogen

16 mL/min and air 40 mL/min, the ferrocene appeared as a yellow-white ball with a darker

yellow rim. At 190 °C the emission of osmium was an orange, rimless ball but at 150 °C
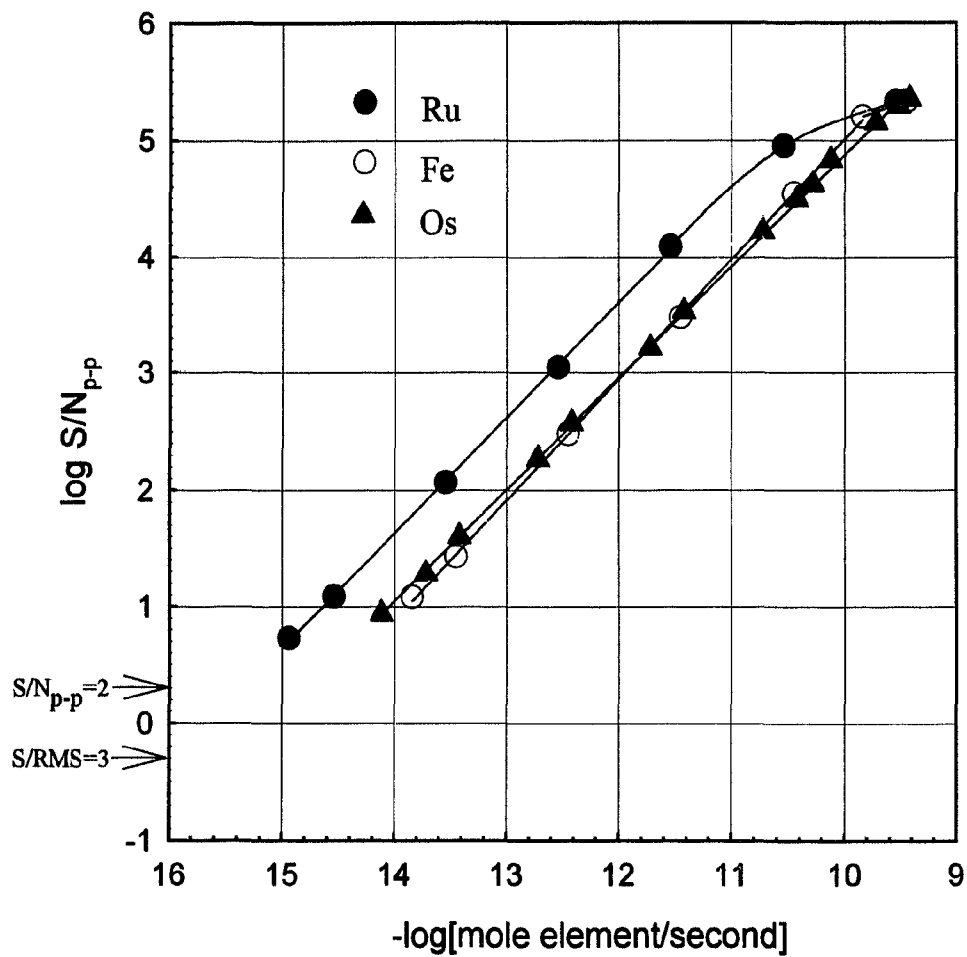
Figure 6.22   Calibration curve of ferrocene, ruthenocene and osmocene:
hohophotal channel; stoichiometric flows; R-1104.
●   -500 V; 455 nm (LP); column 160 °C.
○   -540 V; 455 nm (LP); column 140 °C.
▲   -540 V; 475 nm (LP); column 170 °C.

20 pg ferrocene
-log(mole **Fe**/s) = 14.6

2 pg ruthenocene
-log(mole **Ru**/s) = 15.4

10 pg osmocene
-log(mole **Os**/s) = 14.9

0 1 2 3 4 5

time, minutes

0 1 2 3 4 5

time, minutes

0 1 2 3 4 5

time, minutes
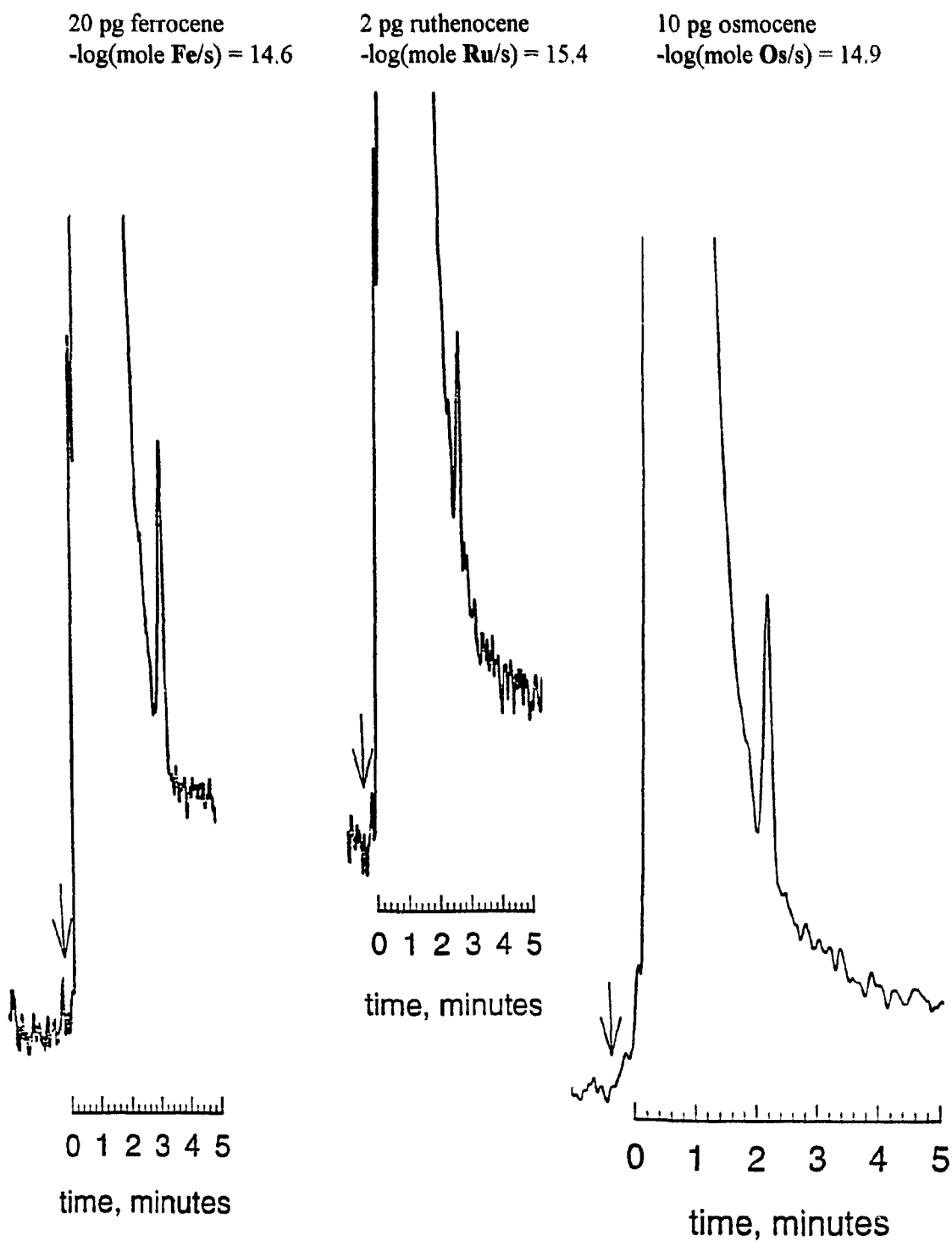
Figure 6.23   MDL peaks and values for ferrocene, ruthenocene and osmocene:
holophotal channel; R-1104, -540 V; 455 nm (LP); stoichiometric flows.

it was much lighter in color and the glow seemed to last longer. The ruthenocene

luminescence no longer had the distinct rim but was lighter around the edge of the small

sphere that was blue at first with a touch of red at the end of the emission. At higher,

more hydrogen-rich flows, the colors of the emissions were slightly varied and the shape

of the flame was more traditional, as opposed to the small sphere.

Because of the excellent sensitivity of these three metallocenes, the spectral

measurements were done on both the variable filter and the quarter-meter grating

monochromator. Figure 6.24, however, just provides the measurements from the latter as

they show much better resolution. Because there were more features present, the anomaly

from the quarter-meter grating monochromator was not as obvious as with rhenium;

nevertheless, it did seem to be present around 690 to 700 nm. Long pass filters were used

to remeasure portions of each spectrum to check this anomaly once more, and also to

eliminate features due to second order. With a bit of imagination, the three profiles did

appear similar: a well-defined peak at 340-360 nm, followed by a small feature which

turned into a sharp rise, reaching a maximum around 480 nm. The remainder of each

spectrum varied slightly, but essentially, it was a broad continuum (with a few fine

features) that ended between 750 and 800 nm.

The ferrocene spectrum bears a marked resemblance to the automatic scan, also

done at stoichiometric conditions but with higher flows (hydrogen 45.5 mL/min and air 75

mL/min).[68] The fairly sharp peak, just over 360 nm, has less resolution than the scanned

spectrum which shows sharper, more defined peaks at 359 and 367 nm. It is suggested

that atomic lines may be responsible but that there also exists two groups of bands in this

25
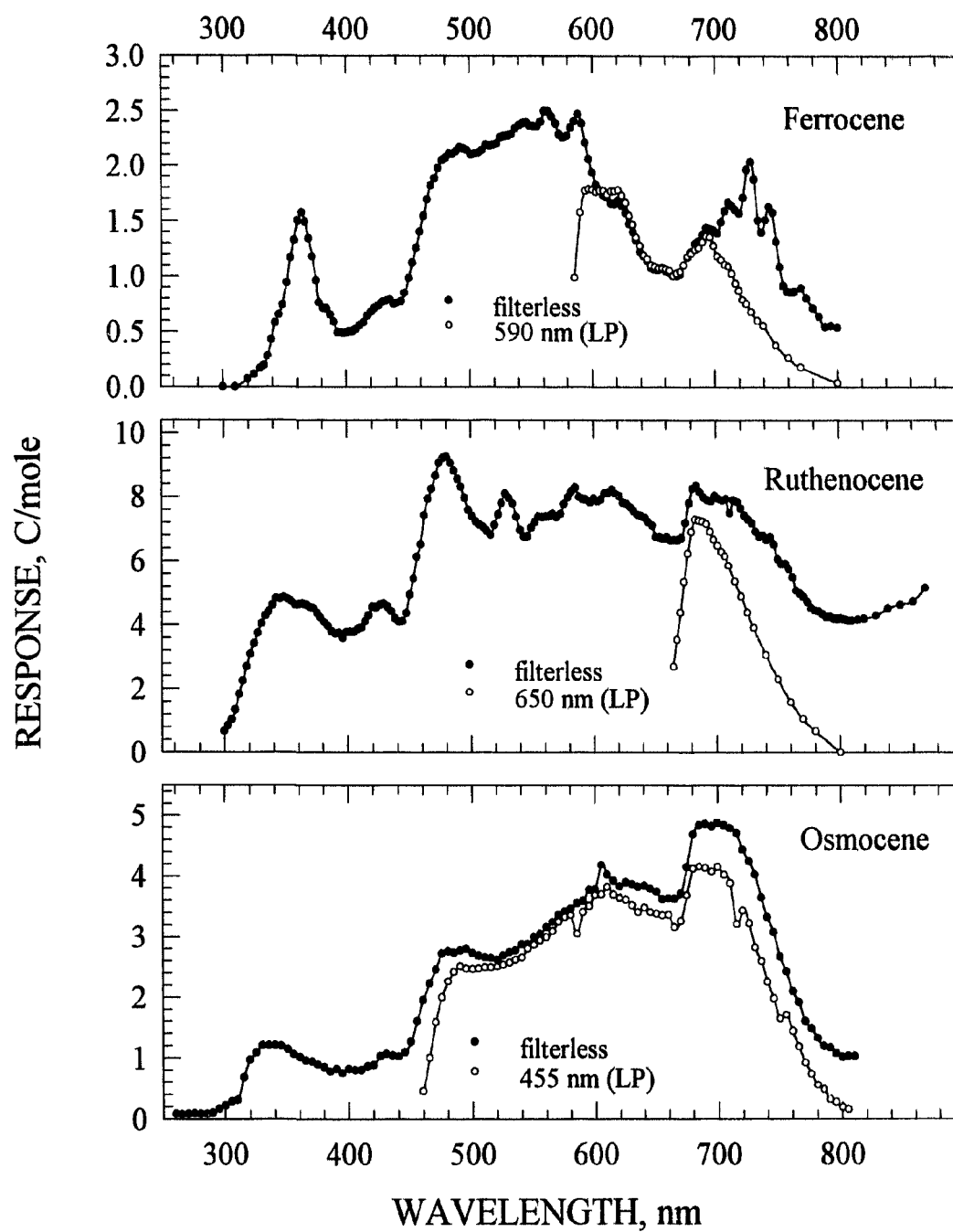
Figure 6.24 Spectra obtained from ferrocene, ruthenocene and osmocene: quarter-meter grating monochromator; 6.7 nm bandpass; holophotal channel; stoichiometric flows; R-1104, - 540 V.

area, possibly from FeOH: one from 353.0-358.0 nm and the other from 363.0-367.5

nm.[68,81] Bands attributed to FeO[68,81] (344, 358, 383, 388, and 393 nm) were discussed but

it was pointed out that some prominent atomic lines occur in this region as well.[85] There

was some speculation about the origins of the large, featureless portion of the spectrum

from 460 to almost 600 nm (including FeO and FeH) but this region remained

unidentified.

The spectrum of ruthenocene in Figure 6.24 exhibited many of the main features of

an earlier, detailed spectrum, measured with a larger, hydrogen-rich flame.[69] The broad

area, between 350 and 400 nm, probably corresponded to some atomic lines, all involving

transitions to the ground state (349.9, 372.8, and 379.9 nm).[69] The sharp emissions at 484

and 528 nm, which were so pronounced in the early spectrum, were still evident,

especially the 484 nm peak, but they were much smaller. Since their origin was suspected

to be RuH, the reduction in size was not surprising, considering the much smaller,

stoichiometric flame. It was also noticed that the present spectrum extended farther into

the red although it is difficult tell quantitatively because of the artificial rise seen in this

region (see page 117). In any case, emitters from approximately 550-700 nm remained

unidentified.

The spectral features of osmocene in Figure 6.24 did not resemble previous work[70]

as much as those of ferrocene and ruthenocene, perhaps because the emission in the

present study was much stronger. In the earlier study the luminescence could only be

observed at wavelengths greater than 400 nm but in Figure 6.24 there was a definite

feature around 330 nm. Atomic emission was suspected for ferrocene and ruthenocene in

this region but there is a possible resonance line of osmium at 330.156 nm. Between 650

and 900 nm in the original spectrum, there was an enormous broad peak that did not

resemble the *anomaly*, nor was it present in this newer spectrum. There was also no

obvious spectral explanation why osmium was more responsive with stoichiometric

conditions. There is a reported atomic line[85] at 442.047 nm, about 2.8 eV, but the only

clear feature close to this was a sharp rise starting at about 450 nm which then came to a

plateau between 460 and 480 nm. The broad continuum which reached a maximum

around 620 nm and continued to fall gradually until 750-800 nm also remained

unidentified.

6.4.8 Nickel

Nickel was the last of the transition metals that was responsive to FPD

determination. The compound used, bis(cyclopentadienyl)nickel or nickelocene, was

slightly unstable so it was prepared and stored under nitrogen, eliminating the problem of

decomposition. It responded very well to the stoichiometric flow conditions with a large

linear range and log(mole Ni/s) = 14.6, calculated from the calibration curve given in

Figure 6.25. This was slightly more sensitive than the earlier recorded value of 14.0. The

spectrum was measured using both the variable interference filter and the quarter-meter

but only the latter is given in Figure 6.26. However, also shown in Figure 6.26 is the

original spectrum from the 1992 study in order to illustrate the remarkable similarity. The

only real difference, apart from a very slight improvement in resolution, was that the peak

at 345 nm (attributed to atomic lines from 330 to 360 nm) appeared to have almost

doubled in intensity. The earlier paper gives a detailed interpretation of the emission(s)
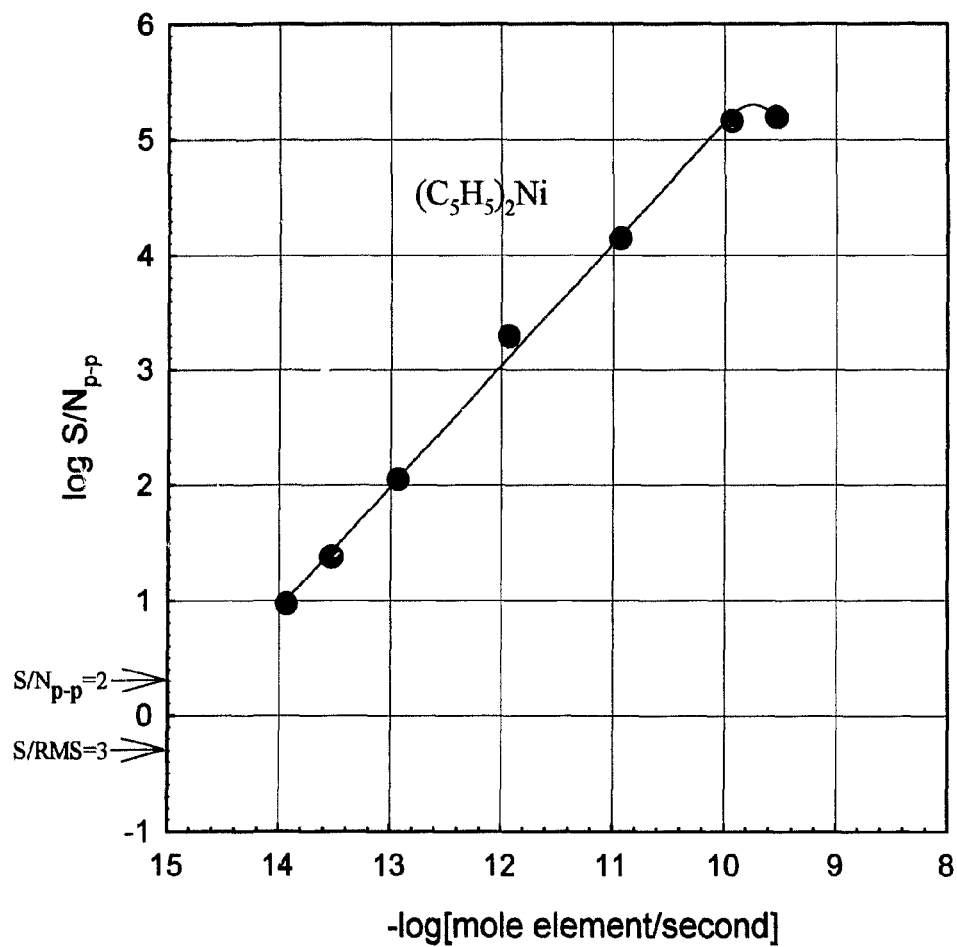
Figure 6.25 Calibration curve of dicyclopentadienylnickel: R1104, -540 V; 455 nm (LP); holophotal channel; stoichiometric flows; column 135 °C.
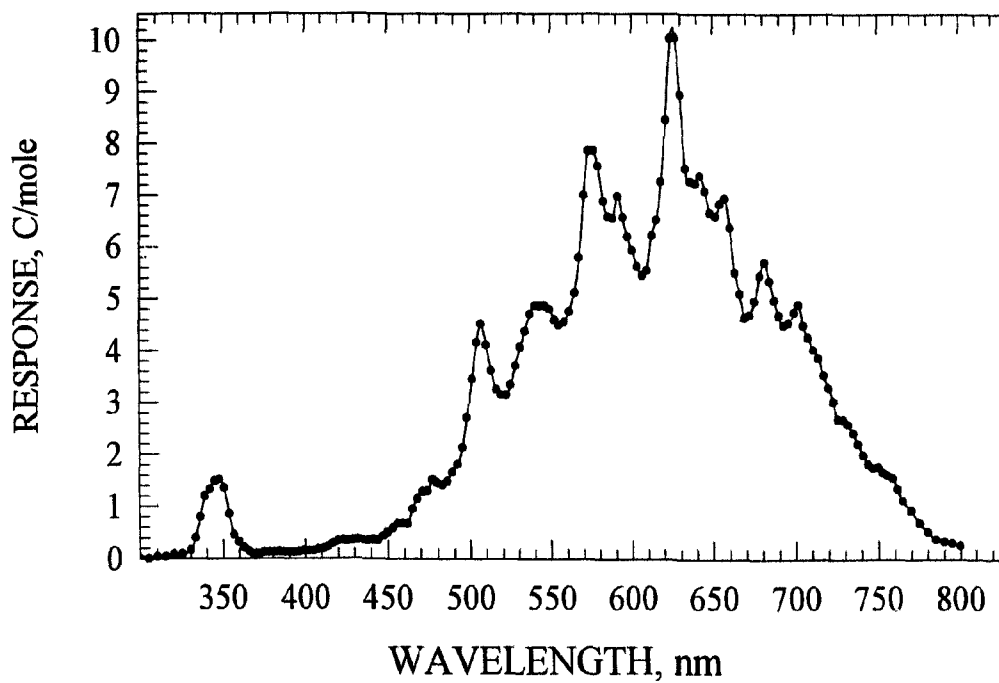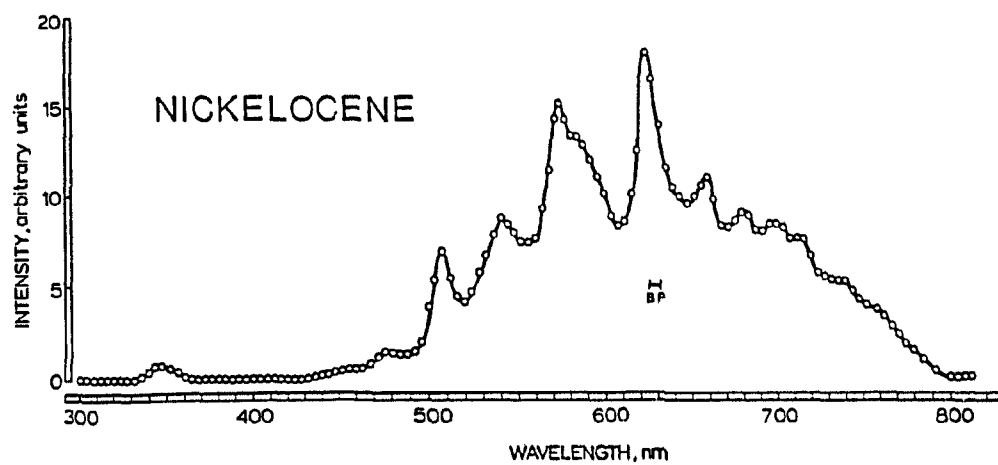
Figure 6.26   Spectra from nickelocene: R-1104, -540 V column 130 °C; quarter-meter grating monochromator; 2.1 mm slits; bandpass 6.7 nm.
Top: hydrogen 300 mL/min; air 55 mL/min.
Bottom: stoichiometric conditions; holophotal channel.

between 450 and 800 nm, citing several possible NiO systems from about 470 to 550

nm.[54,81] It was also suggested that NiH could be an emitter for several of the sharper

bands at 574 and 626 nm or even at 507 nm. NiH was considered to be perhaps the more

likely origin of much of the emission but the stoichiometric spectrum added support to the

systems of NiO as well.

6.4.9 Group 11

It was hoped, in view of nickel's excellent response, that compounds from group

11 metals would behave in a similar manner. (1,5-cyclooctadiene)silver(I), known to be

light-sensitive, dissolved readily in acetone to make a $2\mu g/\mu l$ solution. It was both

refrigerated and stored under nitrogen but injection of large quantities only produced a

small response at 60 °C. Copper(II) hexafluoroacetylacetonate also dissolved readily in

acetone but only a negligible response was obtained at 230 °C.

6.5   SUMMARY

In a 1991 paper a summary is given of "best" FPD detection limits in the literature

in -log(mole element per second), all detected using hydrogen-rich, "typical GC-FPD

flames".[48] A portion of this chart has been reproduced in Figure 6.27 with all the

stoichiometric-holophotal measurements entered as the second number, in bold type and

under the appropriate element symbol. The halogens which were detected originally as

copper or indium halides were omitted from this table while group 2, with magnesium,

was added. Although not determined at stoichiometric conditions, sulfur and phosphorus

													B 11.0 -	C 9.2 10.2	N 11.6 -	
Mg - ~14												Al (stripe)	Si - 11.9	P 14.4 15.1*	S 13.2 13.7*	
Ca (stripe)			V (stripe)	Cr 14.7 14.0	Mn 13.3 14.3	Fe 13.3 14.6	Co 11.6 -	Ni 13.9 14.6	Cu (stripe)	Zn (stripe)			Ge 16.0 -	As 13.5 13.3	Se 12.7 -	
	Y (stripe)	Zr (stripe)		Mo 11.7 12.6		Ru 15.0 15.4			Ag (stripe)	Cd (stripe)			Sn 17.3 -	Sb 11.9 13.2	Te 12.4 -	
				W ? 12.8	Re 12.2 14.2	Os 12.8 14.9			Hg (stripe)	Tl (stripe)		Pb 12.5 13.8	Bi - 14			

Figure 6.27 Comparison of minimum detectable limits, obtained using the holophotal channel and stoichiometric conditions, with some "best" literature values, all calculated as -log (mole element per second) at $S/N_{p-p} = 2$. Diagonal stripe or ? indicates no significant response. The first number under the symbols corresponds to the literature MDL while the second number is taken from this study and appears in dark print. "New" elements also appear in dark print. MDLs with * were measured with non-stoichiometric flows.

were measured using the holophotal technique. Their recorded numbers can also serve as an interesting contrast to the earlier values.

With the original chart there was a precautionary note to the effect that different sources, different detectors, etc., can often be misleading. This, once again, must be emphasized. The *improvement* recorded for phosphorus, using the holophotal technique, cannot be applied to sulfur as the shape of the sulfur emission is very different and consequently, the method is slightly less effective. This means, as well, the improvement of MDL values cannot be specifically attributed to either the stoichiometric flame or the holophotal technique separately. Each measurement would have had to have been done *separately*. Even then it was found, particularly with the components of the holophotal apparatus, that improvements do not necessarily add up linearly. Nevertheless, it is safe to say that the stoichiometric flame was effective in improving the detection limits of the organometallics. Chromium was the one main exception, and this may have been due to the selection of a cut-on filter to reduce noise (although this did not seem to be a factor in the similar case with manganese) or perhaps the original value for chromium was already quite high. Arsenic, too, failed to respond as well as most of the elements. The detection of the new FPD-elements, silicon and tungsten was interesting but not of much analytical value. The limit for silicon was barely significant. Spectral information for tungsten revealed nothing new or useful and the emission was still relatively weak. On the other hand, the discovery that magnesium and bismuth both showed sensitive response, was much more analytically relevant.

Bismuth compounds were traditionally used for medicinal purposes and although

their consumption has declined in recent years, pharmaceutical use in the US is still as high

as 20 %.[88] Cosmetics, catalysts, industrial pigments, electronics, and, particularly, a host

of different alloys make use of various bismuth compounds. Several recent medical

reviews on the toxicology of certain bismuth compounds and analysis-related problems

reveal a need for a reliable and sensitive method for the detection of bismuth.[89,90] Trace

amounts of bismuth have been detected by a chromatographic-atomic fluorescence

spectroscopy method, using a microwave-excited electrodeless discharge lamp, a carbon

rod atomizer and dispersive optics.[91] The detection limit was reported to be 10 pg. Other

sensitive methods are also available such as atomic absorption spectrometry[90] but

sensitivity is not the only criterium, although it is important. Quantity of available sample,

simplicity of analysis and cost requirements are also key factors. Furthermore, recent

work with a variety of organobismuth derivatives[92] indicates that GC-FPD analysis of

bismuth is worthy of further investigation.

The detection of magnesium is also of biological importance (blood, urine, tissue

etc.) but lack of magnesium is the problem, not toxicity. Graphite furnace detectors have

been used in conjunction with high temperature GC separations for inorganic compounds

of magnesium but little has been reported with respect to organometallic derivatives.

Traditional methods usually rely on atomic absorption spectroscopy and have been used

extensively. Nevertheless, the discovery of the unusual magnesium spectrum, while

perhaps not analytically useful, was spectroscopically very interesting.

Chapter 7. SPECTRA DETERMINED WITH NON-STOICHIOMETRIC FLAMES

7.1 "SHIFTING SPECTRA"

During the early stages of the investigation of the small stoichiometric flame, much of the research centered on osmium, primarily for two reasons. First, the sensitivity of osmium detection had increased so dramatically and second, the maximum of the spectra seemed to shift with different air to hydrogen ratios. Figure 7.1 illustrates this peculiarity of osmium contrasted with the weaker, but consistent, rhenium spectra. The maximum of the osmocene spectrum changes from approximately 580 nm to 650 nm. At the time, the holophotal technique was in its *pre-parabola* stage. Consequently, the second channel had not been developed and injection of rhenium and osmium, together for spectral measurements, provided some measure of control over injection error. The maximum for the dirheniumdecacarbonyl at 630 nm did not change.

Unfortunately, the air/hydrogen ratio of 47/10 was difficult to reproduce as the flame became very unstable at these flows. The osmocene spectrum, however, was checked again, but at a constant air flow of 40 mL/min as shown in Figure 7.2. As the hydrogen is changed from 90 mL/min to 14 mL/min, the maximum seems to change from 575 nm to approximately 610 nm. The shape of the spectrum was less regular as well. Independent injection of dirhenium decacarbonyl at varying hydrogen flows confirmed that
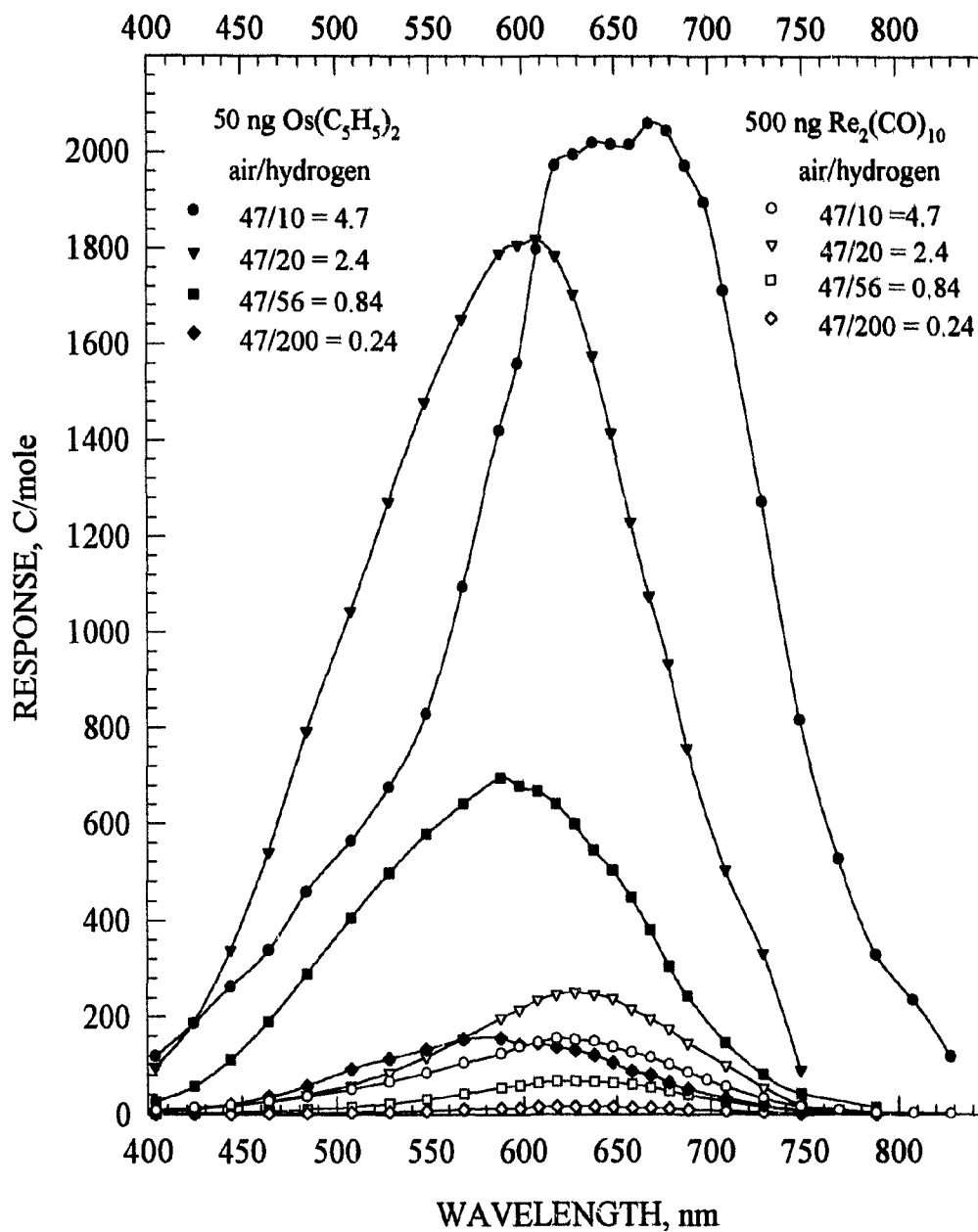
Figure 7.1 Spectra of osmocene and dirheniumdecacarbonyl at different flame gas conditions: variable wavelength selector; bandpass ~36 nm; R-2228, -900 V; nitrogen 20 mL/min; column 190 °C; mirror; tall/wide jet; lens; Al tube.
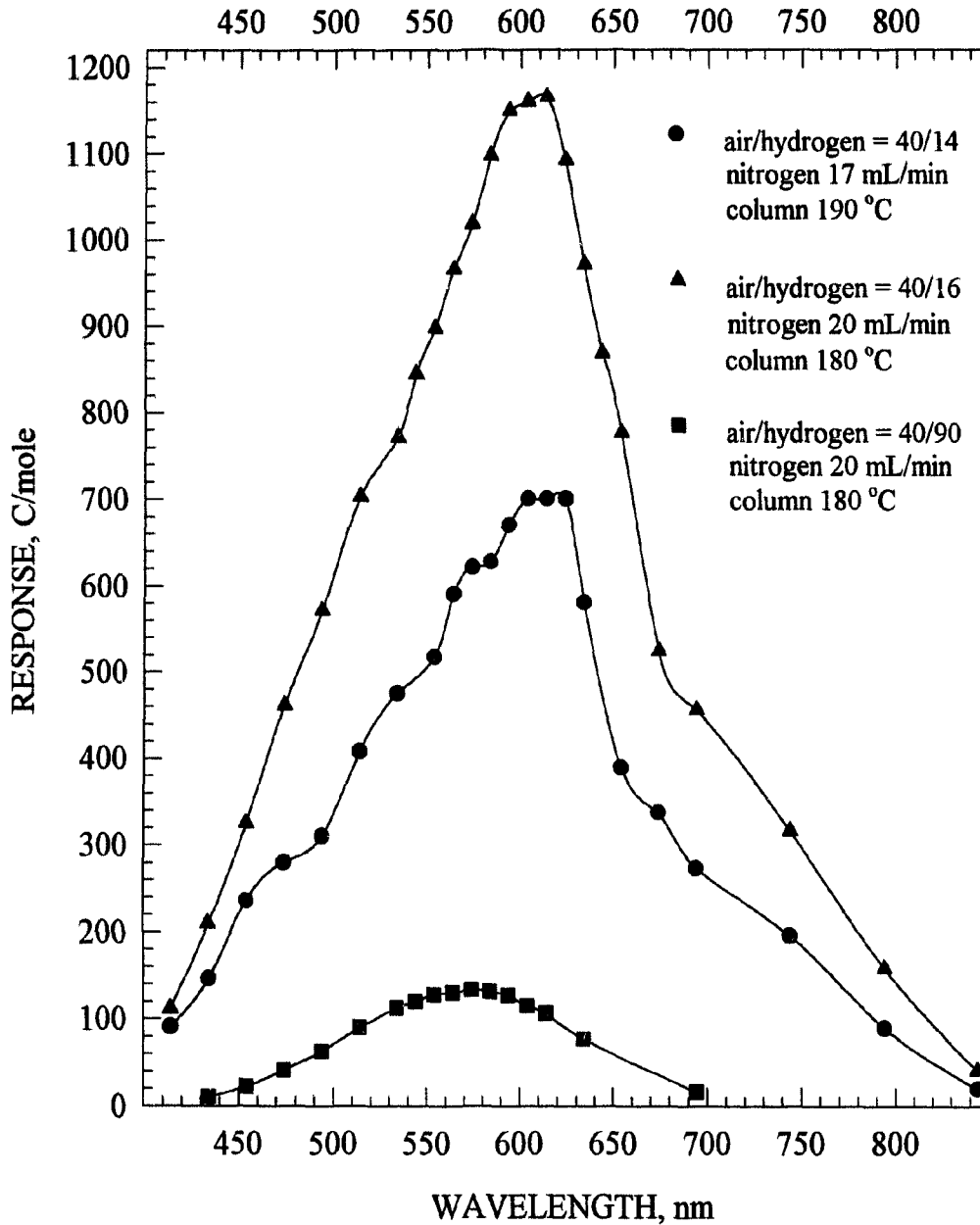
Figure 7.2   Spectra of osmocene at different flame gas conditions: variable interference filter; mirror; lens; Al tube; large/wide jet; R2228, -900 V.

this spectrum (not shown) did not change except for intensity. While the shift was not as dramatic as in the first figure, it provided enough incentive to search for other *shifting spectra* and to discover the nature of this shift. Was it an actual shift or was it a change in intensity of already existing features?

Spectra of tungsten and molybdenum, acquired at different times and quite different flows, are presented in Figure 7.3. The comparisons, however, are not without some ambiguity since two different photomultipliers were used, as well as different mirrors (circular and parabolic). A number of different studies showed that the mirrors had little effect on the spectra themselves but the photomultiplier tubes did have some influence. The R-2228, which was red extended, was slightly less sensitive in the 400-500 nm range than the R-1104, but at 600 nm they were essentially the same, according to the radiant sensitivity plots provided by Hamamatsu. This provided some speculation as to whether any changes were due to the different tubes or were as a result of the changes in gas flows. The non-symmetrical portion of the tungsten in the lower plot was probably partly due to the greater sensitivity of the R-1104 in that region, but the fact remained that the maximum was located at 575 nm while in the upper plot the maximum appeared to be around 605 nm. The spectra for molybdenum, also shown in Figure 7.3, experienced a similar change in maximum accompanied by a definite change in shape.

A search through files of recorded spectra provided two more examples of changes, again, not without some ambiguity. In Figure 7.4 are given several spectra of chromium and manganese, both stronger emitters than molybdenum and tungsten and also with more spectral features. The top spectra are chromium hexacarbonyl measured at an
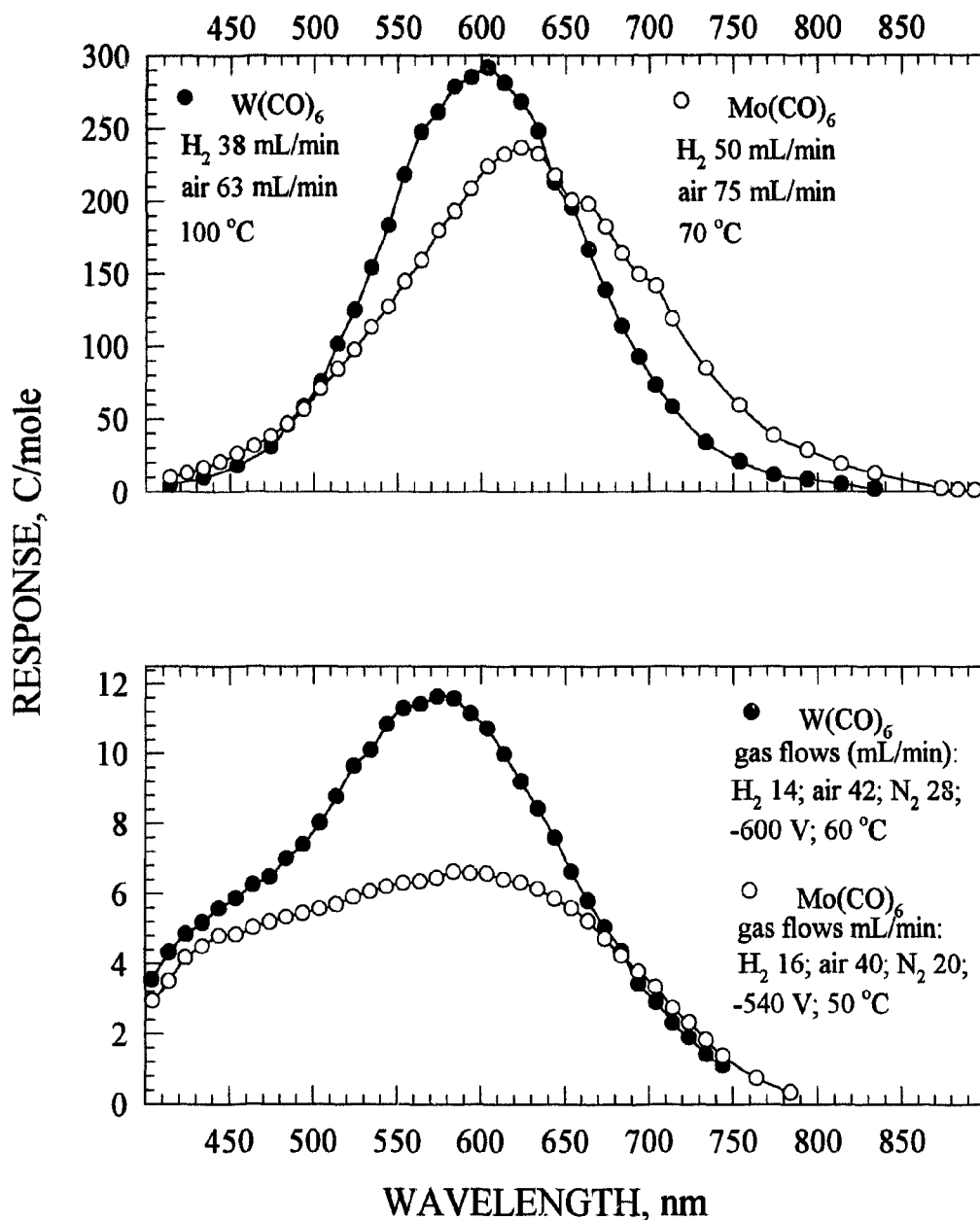
Figure 7.3 Comparison of spectra of molybdenum and tungsten at different air to hydrogen ratios. Top: R-2228, -900 V; variable interference filter; mirror; lens; Al tube; nitrogen 23 mL/min. Bottom: R-1104; holophotal channel; variable interference filter.
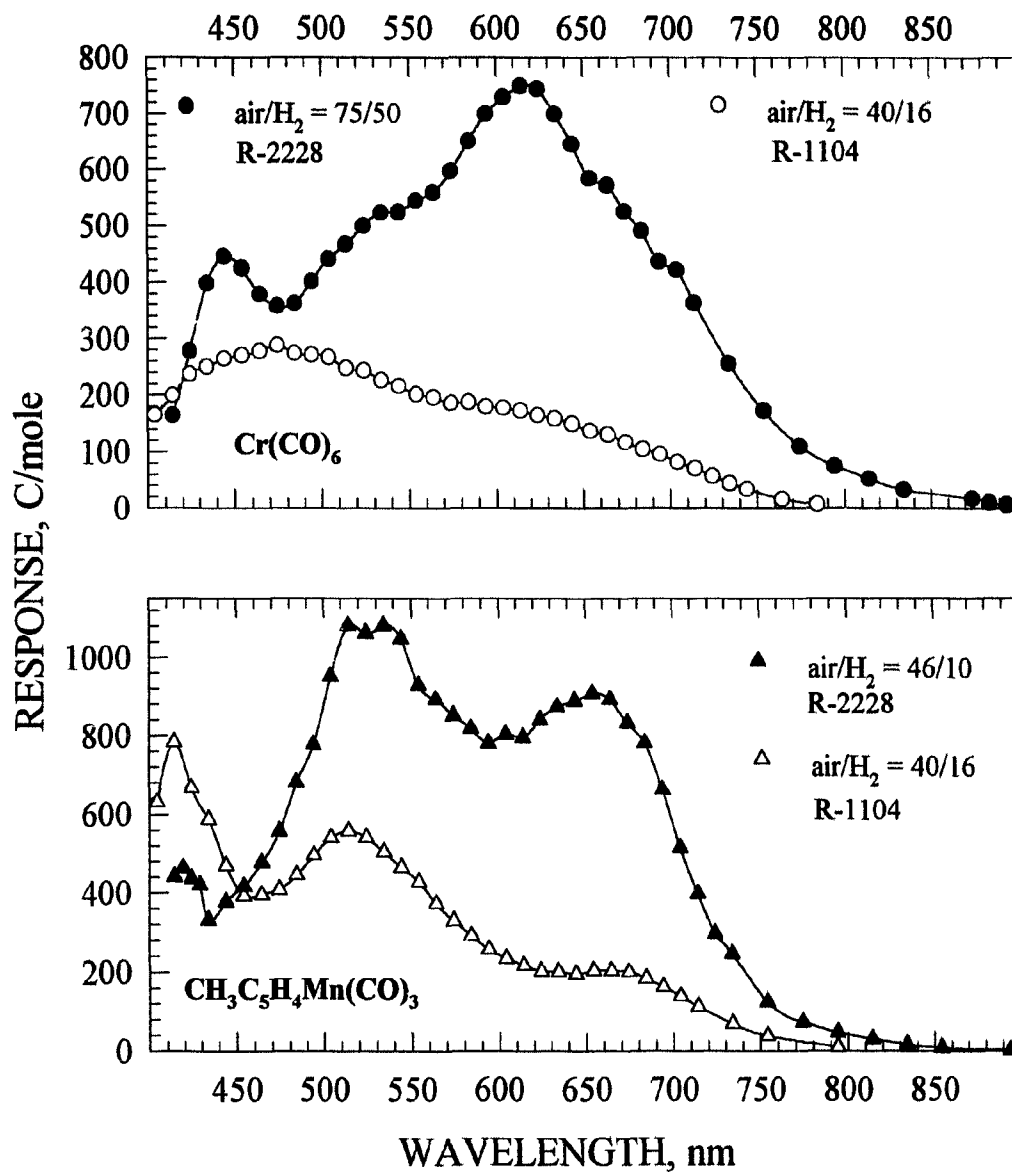
Figure 7.4 Comparison of spectra of chromiumhexacarbonyl and MMT at different air to hydrogen ratios using the variable interference filter; lens; Al tube.

● -900 V; nitrogen 23 mL/min; column 70 °C; circular mirror.

○ -540 V; nitrogen 20 mL/min; column 50 °C; parabolic mirror.

▲ -900 V; nitrogen 20 mL/min; column 150 °C; circular mirror.

△ -540 V; nitrogen 20 mL/min; column 130 °C; parabolic mirror.

air/hydrogen ratio of 75/50 using the R-2228 tube along with the same compound at an

air/hydrogen ratio of 40/16 using the R-1104 photomultiplier tube. It should be noted

that, in the first case, the commercial lens was used while in the latter the parabola was

used but, as mentioned above, this had previously been shown to have no effect on the

spectrum. Also, the rough comparison of spectra with different photomultiplier tubes is

possible but the comparison between intensity scales is not. The unit, C/mole, was valid

for comparisons only when the exact same tube and voltages were used.

The chromium spectra showed some interesting changes. The peak between 430

and 440 nm was detected using the R-2228 tube which is *less* sensitive in that region,

indicating that the more hydrogen-rich flame with higher flows could have been

responsible. The limits imposed by the filter and by the photomultiplier tube at this

wavelength make it difficult to interpret, but this peak could be attributed to the strong

transitions to the ground state at 425.435, 427.480 and 428.972 nm.[85] The maximum at

615 nm was present in the 40/16 version of the chromium spectra but was just barely

discernable. CrO, as a possible emitter, was suggested earlier (in section 6.4.5) but this

maximum was essentially unidentified. The manganese spectral features changed slightly

but not significantly. Any change in relative size, for example, the intensity of the

maximum at the lower range, could be attributed to the difference in tubes.

With relatively small changes in air and hydrogen flows the spectra of lead also

appeared to vary. In the top half of Figure 7.5 there are two spectra of tetraethyl lead,

both measured with the R-2228 photomultiplier tube. At air flows of 45 mL/min and

hydrogen 10 mL/min, the response was quite good with a large continuum peaking at
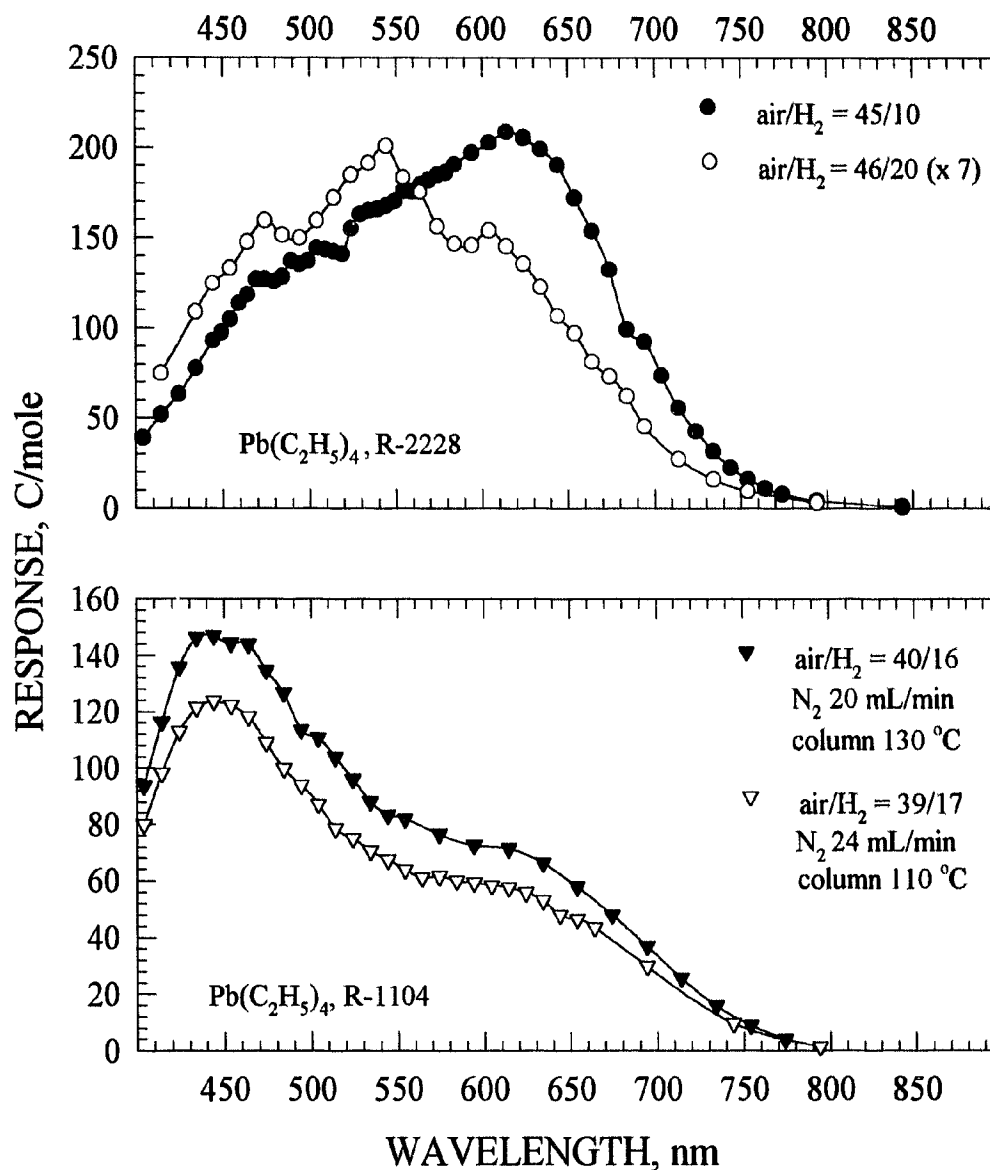
Figure 7.5 Comparison of spectra of tetraethyllead at different air to hydrogen ratios: variable interference filter; lens; Al tube.
Upper: R-2228, -900 V; circular mirror; nitrogen 20 mL/min; column 150 °C.
Lower: R-1104, -540 V; parabolic mirror.

about 615 nm. With the hydrogen doubled and the air almost the same, the sensitivity dropped drastically (the plot has been scaled to seven times its size) and three maxima appeared, at 470, 545 and 600 nm. The same features seemed to be present in each spectrum but the intensity varied with more air corresponding to a higher peak around 600 nm. The lower plots, which were both close to optimal conditions for lead, were very similar to each other. They did, however, agree with the trend in the upper plot, i.e., the stoichiometric flame, as opposed to the air-rich, produced a less dominant 600 nm feature.

As a final example of the *shifting spectra*, a collection of spectra of ferrocene and ruthenocene were selected and compared. For ferrocene, spectrum changes with alterations in air/hydrogen ratios is not new. An unidentified *shoulder* from 460 and 580 nm developed as the flame became stoichiometric. In Figure 7.6 spectra at various flame gas conditions were examined for the region between 450 and 800 nm. From the three plots with dark symbols, it appears that the peak around 560 nm (possibly due to FeO) gets larger with higher air. These three spectra were measured with the exact same conditions except for the variation in hydrogen, so the comparison is valid. The second peak at about 670 nm seems to coincide with higher hydrogen but relative sizes cannot be compared because of the different photomultiplier tubes. In any event, the peak at 560 nm did not appear to shift.

In a similar manner, the ruthenium spectra, shown in Figure 7.7, also seemed to have at least two, and maybe more, features that become more resolved or less, depending on the air to hydrogen ratios. The plots with the three dark symbols seemed to suggest that at more hydrogen-rich conditions, there was a feature around 545 nm that was
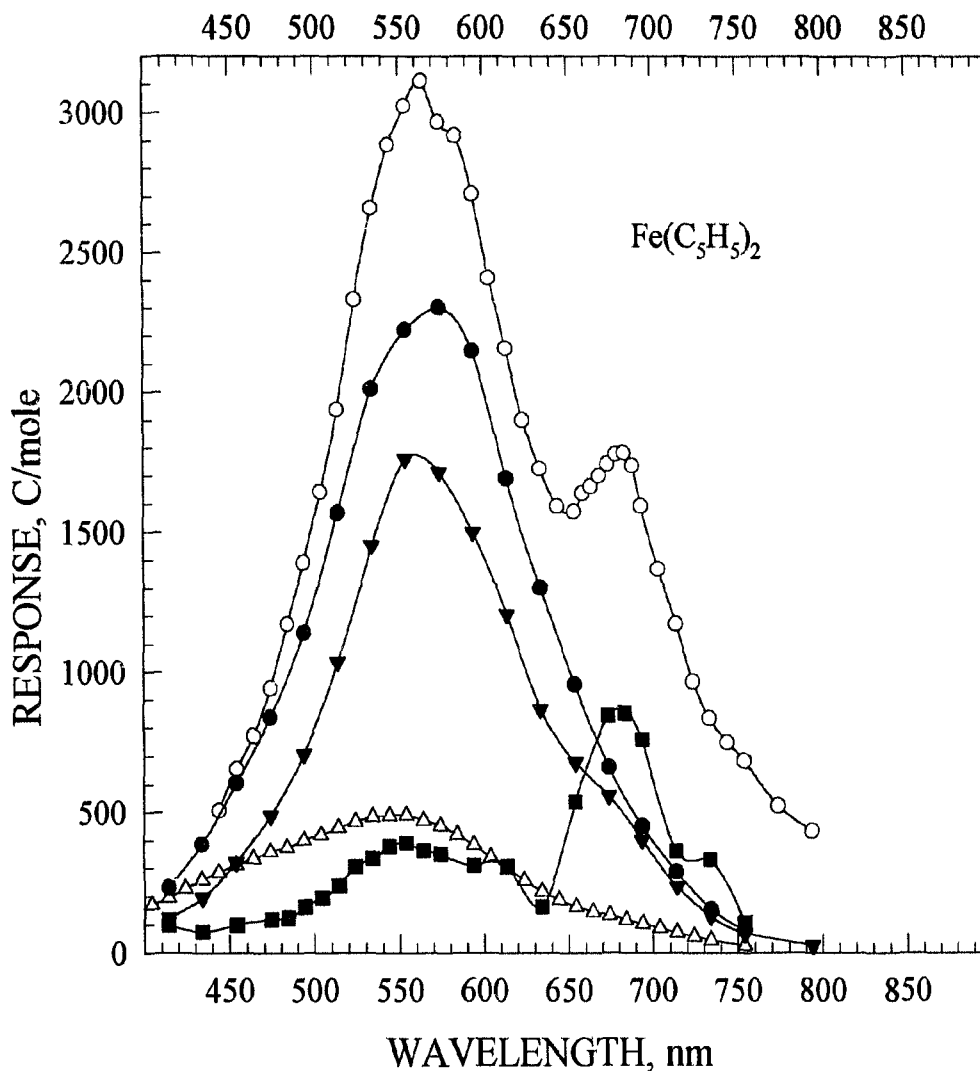
Figure 7.6 Comparison of spectra of ferrocene at different air to hydrogen ratios: variable interference filter and holophotal channel.

△ R-1104, -540 V; N_2 20 mL/min; H_2 16 mL/min; air 40 mL/min; column 140 °C.
○ R-2228, -900 V; N_2 25 mL/min; H_2 15 mL/min; air 34 mL/min; column 140 °C.
● R-2228, -900 V; N_2 20 mL/min; H_2 10 mL/min; air 47 mL/min; column 170 °C.
▼ R-2228, -900 V; N_2 20 mL/min; H_2 20 mL/min; air 47 mL/min; column 170 °C.
■ R-2228, -900 V; N_2 20 mL/min; H_2 46 mL/min; air 47 mL/min; column 170 °C; (x 5).
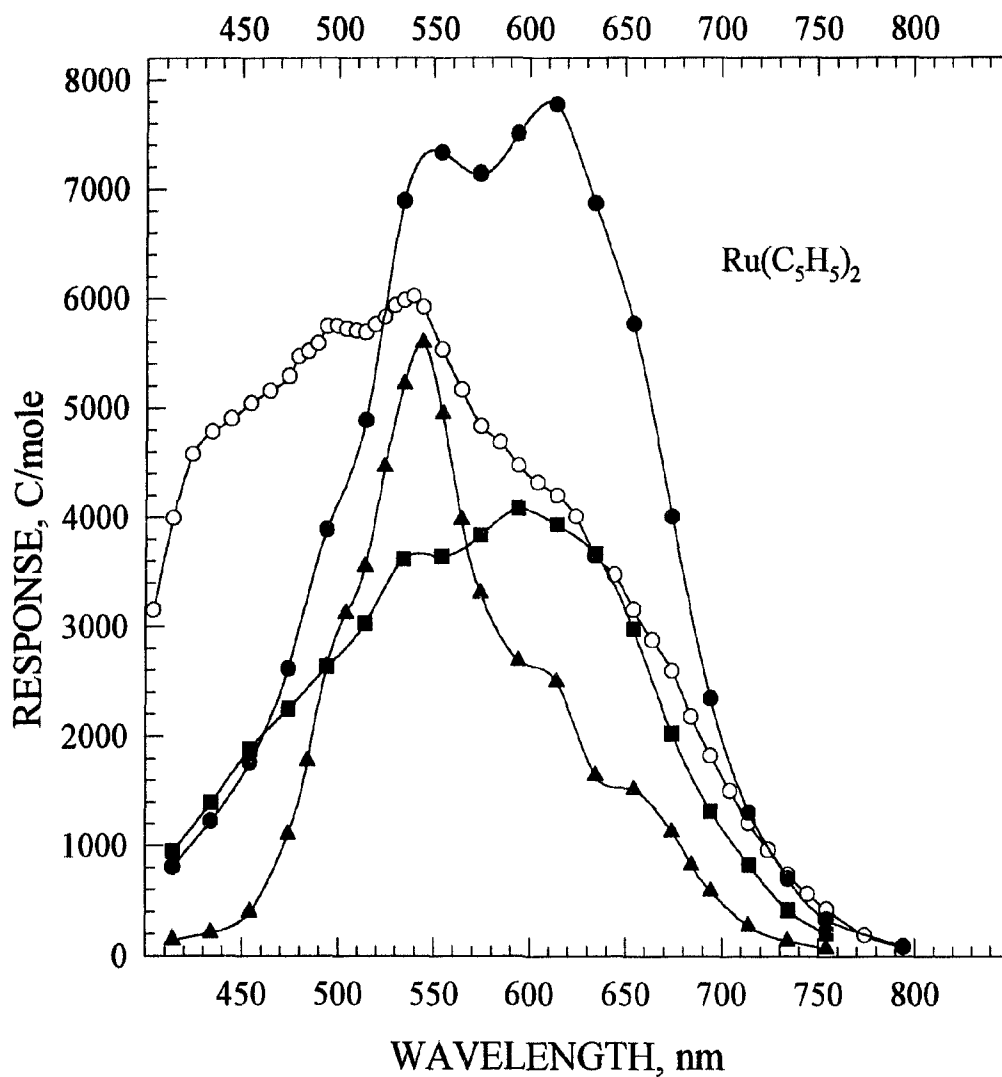
Figure 7.7   Comparison of spectra of ruthenocene at different air to hydrogen ratios: variable interference filter and holophotal channel.

○   R-1104, -540 V; N_2 20 mL/min; H_2 16 mL/min; air 40 mL/min; column 160 °C.

■   R-2228. -900 V; N_2 20 mL/min; H_2 10 mL/min; air 47 mL/min; column 170 °C.

●   R-2228, -900 V; N_2 20 mL/min; H_2 20 mL/min; air 47 mL/min; column 170 °C.

▲   R-2228, -900 V; N_2 20 mL/min; H_2 46 mL/min; air 47 mL/min; column 170 °C.

dominant, while with less hydrogen and air-rich flows there is another large peak around 615 nm. This was not as evident in the spectra obtained with the R-1104 but this was obtained at a lower temperature and stoichiometric flows. (It should be noted that the actual sensitivity for the stoichiometric plot was the highest of the four spectra but it was measured with the R-1104 photomultiplier tube and, therefore, cannot be compared to those measured with the R-2228.)

It seems, then, for all the spectra that have just been examined, that there really was not a shift of a continuum with changes in gas flows. There was, rather, a change in the features or maxima that make up the profile. There is the possibility of different emitters that respond to different air/hydrogen ratios and as the ratios change, so does the response. In the spectra of dirheniumdecacarbonyl perhaps there was only one species responsible for the emission, whereas for the spectra for many of the other compounds, there could be two or more emitters. These examples of spectra, however, were a sampling of data already accumulated for other purposes. More controlled experimentation of spectral changes with different air/hydrogen could lead to possible methods for more selective detection. These examples also emphasize the need to know the relevant emission spectra for the detector conditions, i.e., the conditions at which the actual analysis is done.

7.2   FLAME SPECTRA

After the repeated introduction of sample for detailed spectra, the detector often

became very dirty. Chimneys became permanently stained, there was often a deposit on the jet, and even without visible signs of contamination, the sensitivity of the instrument would be reduced. Very often injections of large quantities of tetraethyllead left larger-than-normal black deposits, so after a spectrum of tetraethyllead was finished, a quick scan of the wavelengths was made without injection. This *flame spectrum* (see Figure 7.8), measured at stoichiometric conditions and with the holophotal channel, revealed two main peaks, one around 430 nm and one around 715 nm. The intensity of two peaks was fairly significant but all spectra were done by injection so that this background would not be a factor. Figure 7.8 also shows similar scans taken after spectral measurements of manganese, silicon and nickel. Ironically, the flame profile after lead injections was the smallest while after silicon and manganese it was much higher.

The detector had been thoroughly cleaned in between each spectrum and care was taken to use the same experimental conditions other than column temperature. There was, however, almost always a black ring around the tip of the jet after each spectrum, possibly due to a carbon deposit which could explain the emission at 430 nm. The flame spectra observed subsequent to injecting organolead and organonickel compounds were almost identical. The after-silicon flame spectrum was also similar except for a small rise around 580 nm of unknown origin. Manganese was the only metal that seemed to have contaminated the detector, creating a large rising continuum from 450 nm to the feature at 700 nm. The peak around 700 nm was believed to have been caused by a species present in the stoichiometric flame and unrelated to any analyte injected. In an attempt to confirm this, the flame profile was recorded for four different air/hydrogen ratios. As shown in
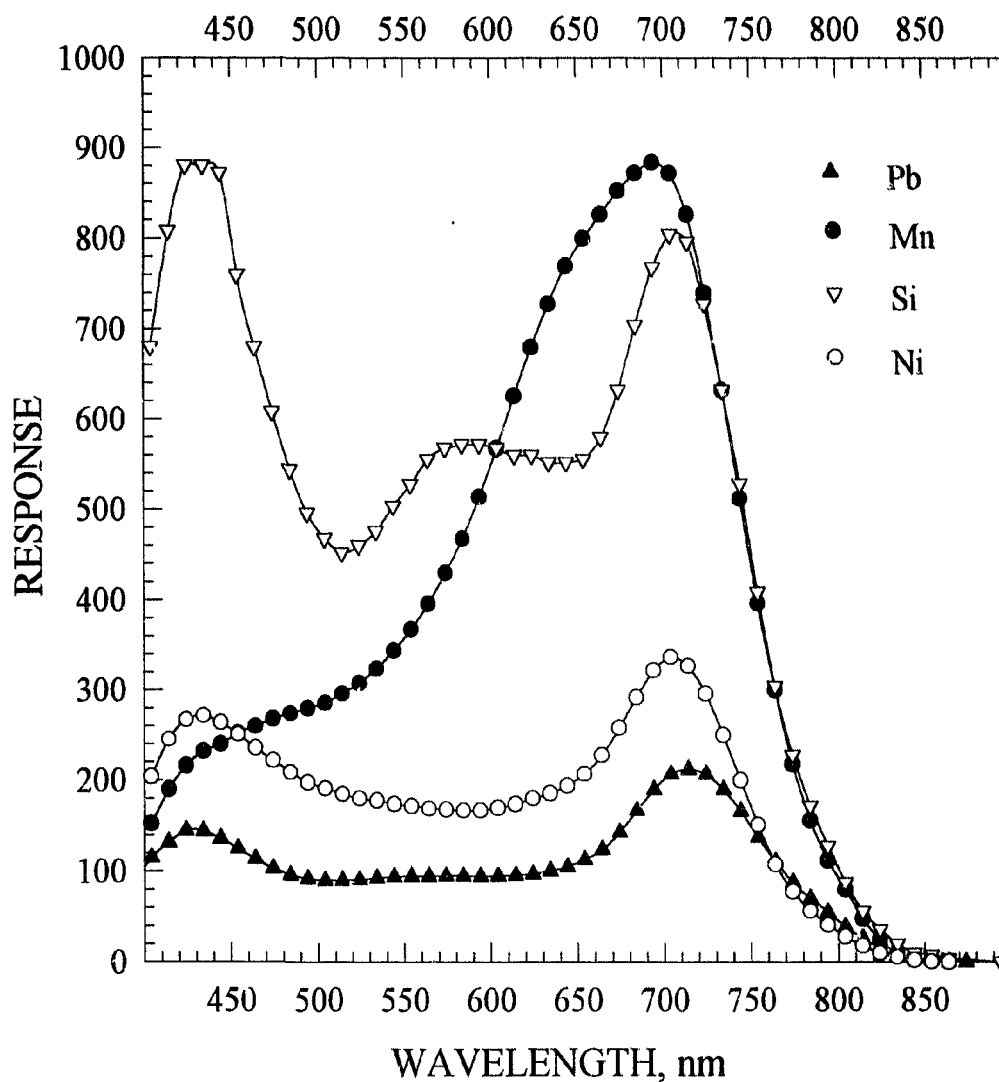
Figure 7.8 Comparison of *flame spectra* measured following the spectrum of tetraethyllead, (methylcyclopentadienyl)manganese, tetraethylsilane and nickelocene: holophotal channel; variable interference filter; R-1104, -540 V; N_2 20 mL/min; H_2 16 mL/min; air 40 mL/min; column temperatures: Pb and Mn 130 °C, Si 80 °C, Ni 140 °C.
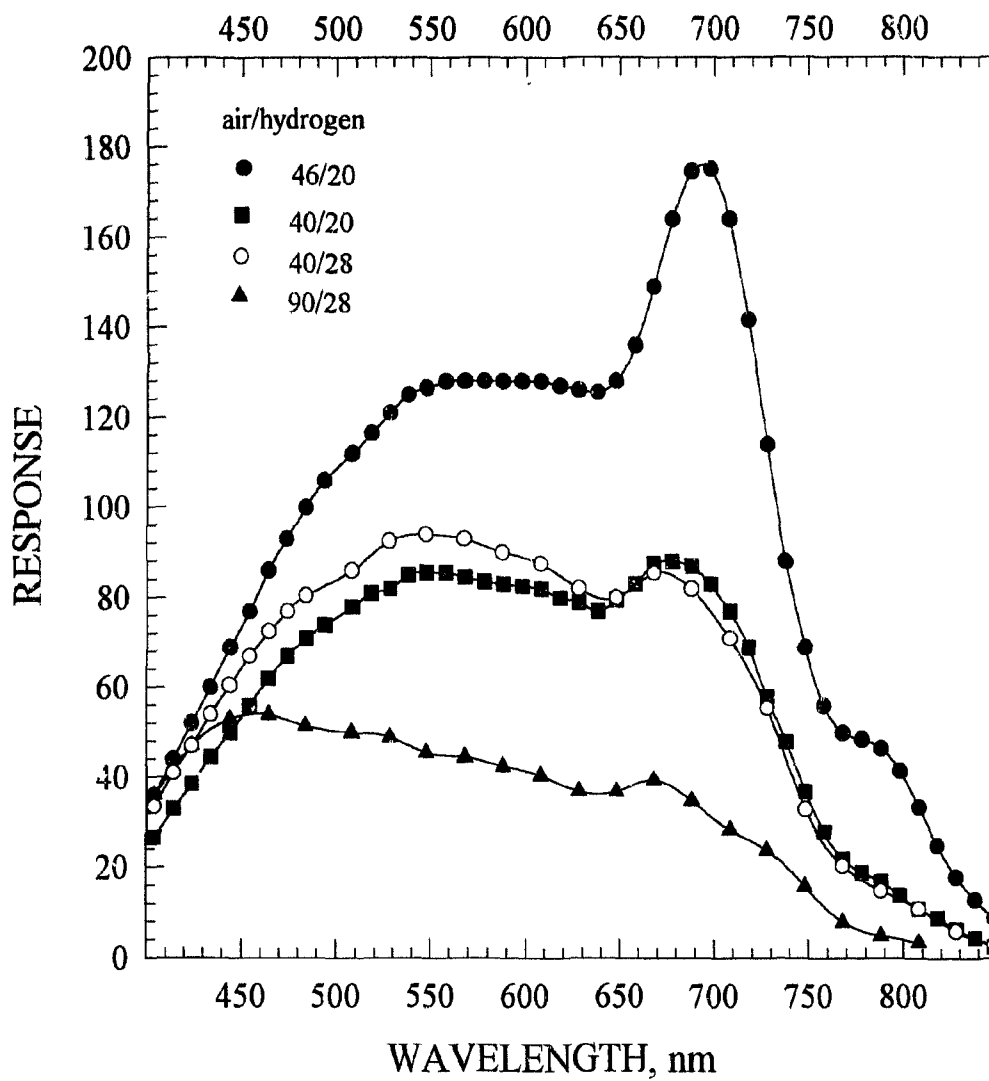
Figure 7.9   *Flame spectra* at different air to hydrogen ratios: variable interference filter; mirror; lens; Al tube; R-2228, -900 V; nitrogen 20 mL/min; column 150 °C.

Figure 7.9, the largest emission at the 700 nm wavelength occurred with the almost

stoichiometric conditions and fell with both the more hydrogen-rich conditions and for the

air-rich. Extensive cleaning failed to change the appearance of this maximum, either in

shape or size and it was found that the air/hydrogen ratio of 40/16 seemed to produce the

largest maximum.

In a table of persistent bandheads of molecular spectra there are two values for

H_2O : 716.45 and 692.20 nm. They are described as being "part of the vibration-rotation

spectrum of H_2O". "The visible bands are weak and are best given by a flame of oxygen

burning in hydrogen." These two particular heads, however, are descr.. ..d as outstanding

and their intensity is "probably due to bunching of lines".

CONCLUSION

Flame studies with a GC-FPD have shown that diffusion-type flames were superior to premixed flames. The possibility remained, however, that the flame gases were not completely premixed before reaching the flame. This problem could easily be checked by mixing the hydrogen and air more rigorously, well before entering the detector. However, enough convincing evidence was presented under a variety of experimental conditions to confirm that the diffusion flame was truly superior. In particular, a diffusion flame was used that was both very tiny and stoichiometric. For a large number of organometallics, optimal flows were hydrogen 16 mL/min and air 40 mL/min. Apart from the increased sensitivities of most of the compounds tested, advantages can include greater safety, lower cost and more convenience. Also, in multielement analysis, the chances of overlooking a key element, because of non-optimum conditions, would be reduced.

Not enough information can be obtained from this present work to determine exactly why the stoichiometric flame produced such significant improvement in detection limits. The drastically reduced hydrogen flows, in addition to the stoichiometric ratios of air to hydrogen, would most likely favor any molecular oxide emissions but lack of spectral data in the literature makes this difficult to confirm. It might prove interesting to check some well-known systems such as the BO and BO_2 bands which have previously been determined to be sensitive to flame gas conditions[53]. It is also noteworthy that the stoichiometric flame produced not only the very best responses for many organometallics

169

but also for the flame spectrum itself, suggesting that formation of OH may be an important factor. Perhaps the species responsible for the formation of the vibration-rotation spectrum of water is also responsible for the some of the organometallic emissions.

Significantly better detection limits were also obtained when this stoichiometric flame was combined with the new holophotal modifications. Because the S/N_{p-p} increased with the square root of the light throughput from the flame, the addition of a parabolic mirror, an appropriate lens and a light-conducting aluminum tube improved both linear range and detection limits. The measured improvement for osmium detection was 7.2 times and 9.7 times for lead. Because of the increased background noise using this system, improvement in detection limits (especially for some of the weaker emitters) was often restricted by the bucking control. Increased bucking and reduction in background noise would be obviously worth pursuing for future work.

The new, lab-constructed second-channel, either the light-guide or the lens-mirror version, proved to be superior in sensitivity to the conventional channel of the GC-FPD and provided lower detection limits for compounds of sulfur, phosphorus, osmium and lead. However, unlike the more sensitive holophotal channel, it had a very steady baseline which made it often the channel of choice, not just for a practical control but also for traditional measurements.

Using these modifications to the FPD plus the stoichiometric flame, calibrations, calculations of minimum detectable limits and spectral measurements were carried out for a variety of organometallic compounds. In almost all cases the minimum detectable limits

improved, especially for compounds of Mn, Mo, Re, Pb and Sb. These were enhanced by at least an order of magnitude while the response of Os was found to be over one hundred times better than previously determined values. Of all the organometallics tested only the MDL for chromium was less than accepted literature values (see Figure 6.27). It would be interesting to repeat the measurements with this metal using more appropriate filters to see if the detection limit could be improved as well.

Also, as a result of increased sensitivities from the modifications and/or the small stoichiometric flame, four *new* elements were added to the list of FPD-responsive elements: Si, W, Mg and Bi. Si was a very weak emitter while tungsten was found to be slightly more sensitive than Mo. Mg and Bi, however, were both detected with significant responses of about 1×10^{-14} mole/s ($S/N_{p-p} = 2$) and are, therefore, probably more deserving of further investigation. Since solutions of less than 100 ng of magnesocene in acetone gave no response, perhaps a different solvent or a fresh supply of magnesocene may overcome this problem. There may be even another volatile compound of magnesium, commercially available, that may be less difficult to handle. Similarly, other derivatives of bismuth that do not require such high temperatures to chromatograph should be checked. Further examination of the spectra of both Mg and Bi should also be made at different flame gas conditions, i.e., slightly more and slightly less stoichiometric , to observe the effect on the dominant spectral features. It would be especially interesting to look at any changes in the sharp emission of Mg around 310 nm which was so close to the strong OH system.

In summary, there appear to be many possibilities for future work. Besides

completing existing study on magnesium and bismuth, there is also a large quantity of data

assembled by this group on lead compounds, data which should be analyzed and

supplemented with stoichiometric measurements. As mentioned above, previously

determined boron compounds may be worth investigating (and perhaps nitrogen as well)

to help explain the function of the stoichiometric flame. Certainly, in view of the success

with magnesium, more attention should be given to derivatives of other Group 1 and 2

elements, especially any metallocenes and carbonyls as opposed to the acetylacetonates

which did not seem to chromatograph as well in this system. Finally, no study would be

considered complete unless the system is investigated with respect to quenching.

APPENDIX I

Long Pass Optical Filters from Ditric

(Spectral measurements done in lab)

570 nm (LP)

WAVELENGTH, nm

590 nm (LP)

WAVELENGTH, nm

SIGNAL

620 nm (LP)

WAVELENGTH, nm

SIGNAL

630 nm (LP)

WAVELENGTH, nm

SIGNAL

640 nm (LP)

WAVELENGTH, nm
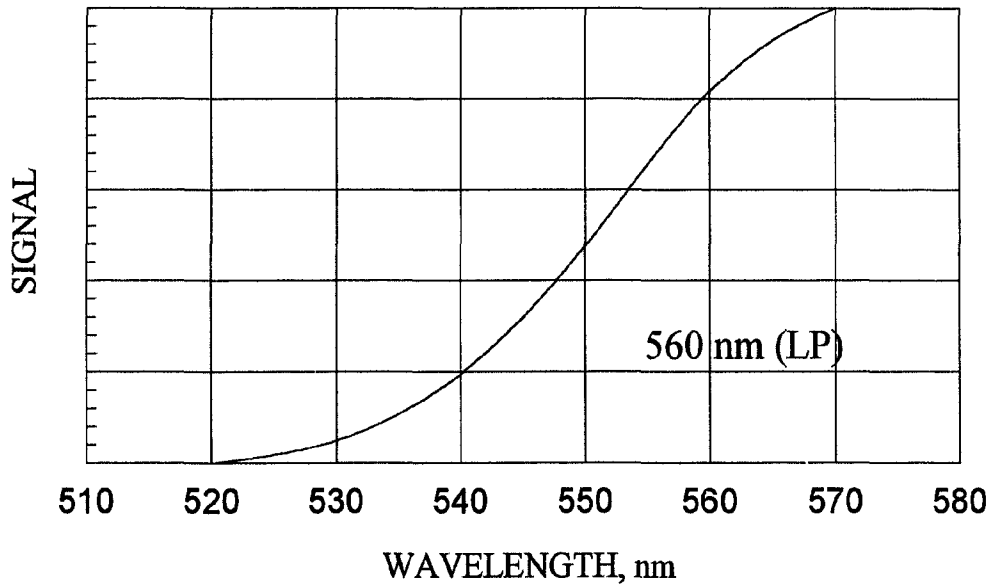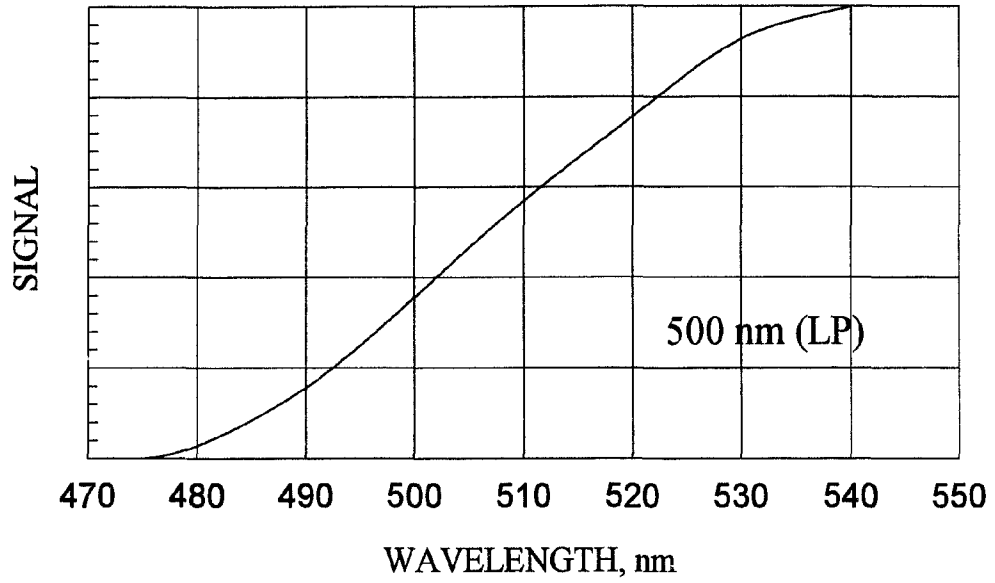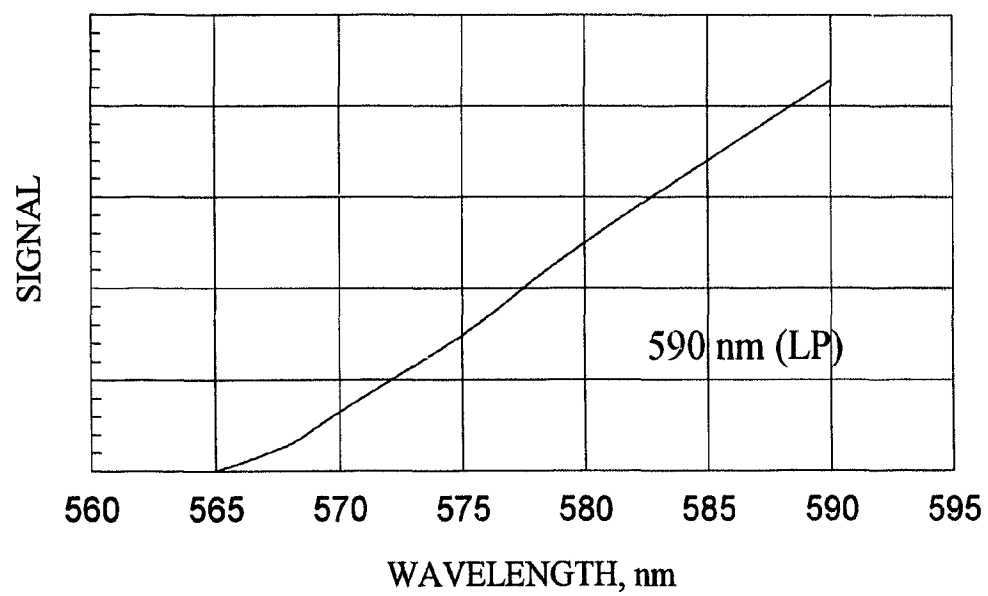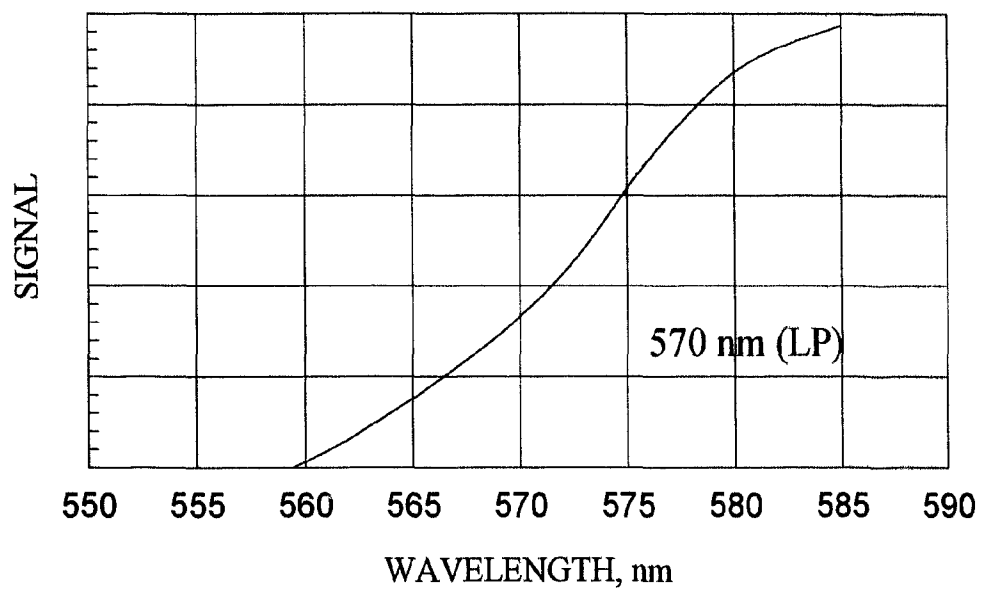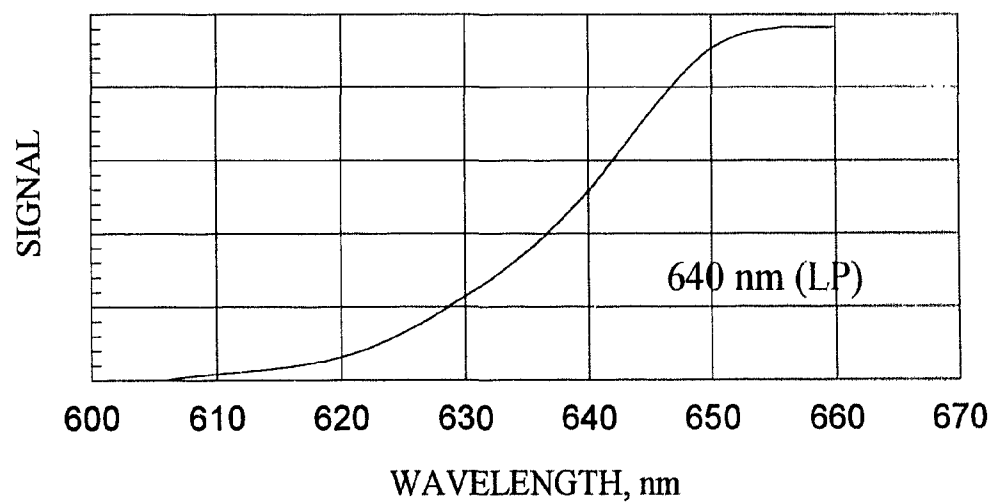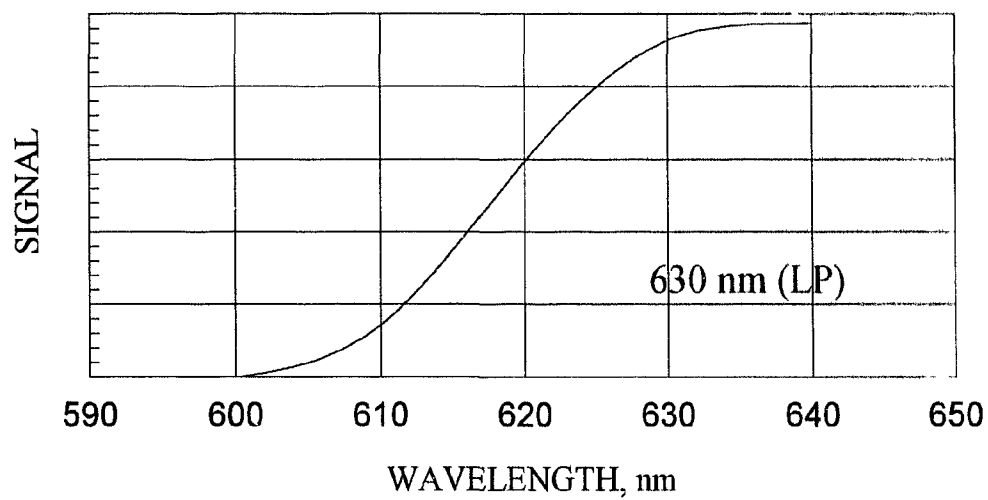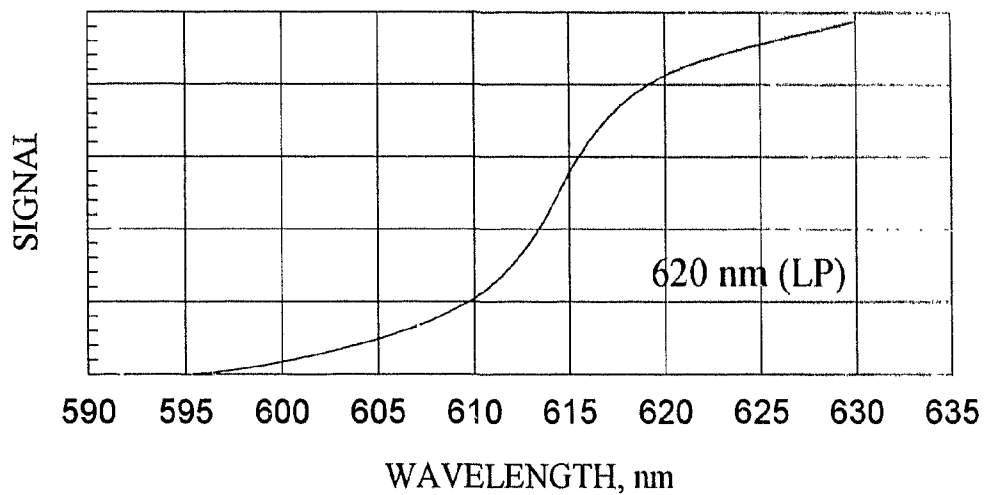
Long Pass Optical Filters from Oriel
(Plots provided by manufacturers)

Filter 51284, 455 nm (LP)
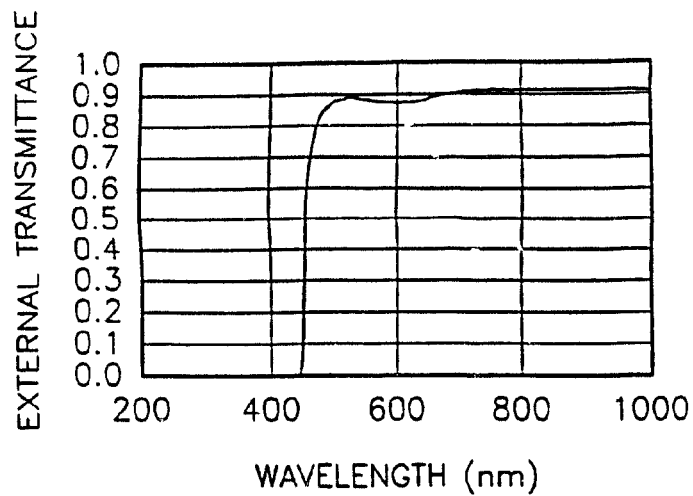
Filter 51290, 475 nm (LP)
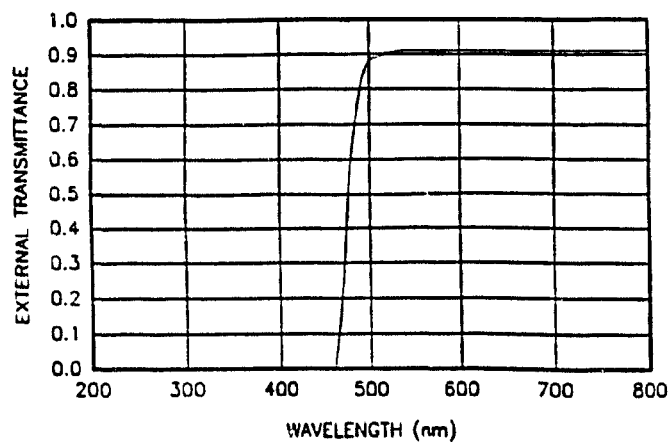
APPENDIX II

Determination of C/mole Ordinate

The response ordinate for all spectra was recorded as coulombs/mole or C/mole.

It was determined from the following equation:

$$(h_p) \cdot (C_{E\&R}) \cdot (Att) \cdot (2\sigma_{peak}/mole\ X) = C/mole$$

where:

h_p = peak height in mm - see Figure A-1

$C_{E\&R}$ = a constant in amperes/mm for given electrometer and recorder (at the highest sensitivity setting of the electrometer, i.e., 10^{-10} A, the recorder full-scale response was 227 mm) - see figure A-2

Att = attenuation (of highest sensitivity)

$mole\ X$ = # moles of analyte

$2\sigma_{peak}$ = width of the peak in seconds (at 60 % of its height) - see Figure A-1
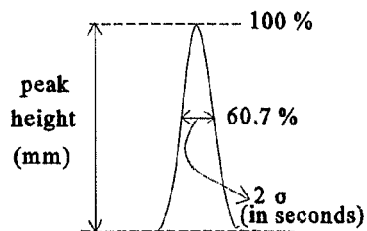
Figure A-1
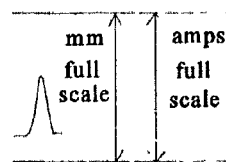
Figure A-2

Dimensional analysis of whole equation:

C/mole =
mm (peak height) • amp/mm • attenuation • 2σ (s)/moles of analyte • C/amp.s

(where amp/mm is constant and C = amp.s is by definition)

Note 1: One value of 2σ will do for a particular run. It stays ~ constant if experimental conditions are not changed.

Note 2: The C/mole allows any cross-comparison only for the same FPD, optics, PMT and PMT voltage conditions.

Note 3: Any "arbitrary unit" scale converts linearly (by a simple factor) to the C/mole scale. Just convert one point and scale.

REFERENCES

1. S.S. Brody and J.E. Chaney, J. Gas Chromatogr., **4** (1966) 42.

2. S. Kapila, D.O Duebelbeis, S.E. Manahan and T.E. Clevenger, Flame Photometric Detectors, from Environmental Analysis Using Chromatography Interfaced with Atomic Spectroscopy, edited by R.M. Harrison and S. Rapsomanikis, Ellis Horwood Limited, Chichester, 1989.

3. W. Thornburg and H. Beckman, Anal. Chem., **41** (1969) 140 R.

4. M. Krejci and M. Dressler, Chromatogr. Rev., **13** (1970) 1.

5. W.A. Aue, Advances in Chemistry Series, **104**, (1971) 39.

6. M. Selucky, Chromatographia, **4** (1971) 425.

7. D. Natusch and T.M. Thorpe, Anal. Chem., **45** (1973) 1184 A.

8. W.A. Aue, J. Chromatogr. Sci., **13** (1975) 329.

9. E.R. Adlard, CRC Critical Reviews in Analytical Chemistry, May (1975) 13.

10. S.O. Farwell and R.A. Rasmussen, J. Chromatogr. Sci., **14** (1976) 224.

11. L.S. Ettre, J. Chromatogr. Sci , **16** (1978) 396.

12. S.O. Farwell, D.R. Gage and R.A. Kagel, J. Chromatogr. Sci., **19** (1981) 358.

13. S.O. Farwell and C.J. Barinaga, J. Chromatogr. Sci., **24** (1986) 483.

14. R.F. Zainullin and V.G. Berezkin, Critical Reviews in Analytical Chemistry, **22** (1991) 183.

15. R.S. Hutte and J.D. Ray, Sulfur-Selective Detectors, pp.193-218, from Detectors for Capillary Chromatography edited by H.H. Hill and D.G. McMinn, Chemical Analysis Series, 121, John Wiley and Sons Ltd., 1992.

16. J. Sevcik, Detectors in Gas Chromatography, pp.145-164, J. Gas Chromatogr. Lib., Vol. 4, Elsevier, Amsterdam, 1986.

17.   M. Dressler, <u>Selective Gas Chromatographic Detectors</u>, pp. 133-160, J. Chromatogr. Lib., **36**, Elsevier, Amsterdam, 1986.

18.   F.M. Zado and R.S. Juvet, Anal. Chem., **38** (1966) 569.

19.   M.C. Bowman and M. Beroza, Anal. Chem., **40** (1968) 1448.

20.   H.W. Grice, M.L. Yates and D.J. David, J. Chromatogr. Sci., **8** (1970) 90.

21.   J. Sevcik, Chromatographia, **4** (1971) 195.

22.   M.F. Crammer, J. Gas Chromatogr., **6** (1968) 352.

23.   H.A. Moye, Anal. Chem., **41** (1969) 1717.

24.   P.A. Gibbons and K.A. Goode, Gas J., Oct.9 (1969) (Taken from reference 6).

25.   C.A. Burgett and L.E. Green, J. Chromatogr. Sci. **12**, (1974) 356.

26.   R. Greenhalgh and M.A. Wilson, J. Chromatogr., **128** (1976) 157.

27.   W.E. Rupprecht and T.R. Phillips, Anal. Chim. Acta, **47** (1969) 439.

28.   S. Hasinski, J. Chromatogr., **119** (1976) 207.

29.   V.A. Joonson and E.P. Loog, J. Chromatogr., **120** (1976) 285.

30.   P.L. Patterson, R.L. Howe and A. Abu-Shumays, Anal. Chem., **50** (1987) 339.

31.   P.L. Patterson, Anal. Chem., **50** (1978) 345.

32.   J.F. McGaughey and S.K. Gangwal, Anal. Chem., **52** (1980) 2079.

33.   S. Fredriksson and A. Cedergren, Anal. Chem., **53** (1981) 614.

34.   C.J. Barinaga and S.O. Farwell, J. High Resolution Chromatography and Chromatographic Communications, **9** (1986) 474.

35.   W.A. Aue and C.G. Flinn, J. Chromatogr., **142** (1977) 145.

36.   W.L. Crider and R.W. Slater, Anal. Chem., **41** (1969) 531.

37.   T. Sugiyama,Y. Suzuki and T. Takeuchi, J. Chromatogr., 77 (1973) 309.

38   G. Liu, X. Luo and S. Zhang, J. Chromatogr., **435** (1988) 327.

39.   G.B. Jiang, P.S. Maxwell, K.W.M. Siu, V.T. Luong, and S.S. Berman, Anal. Chem., **63** (1991) 1506.

40.   J.N. Driscoll and A.W. Berger, J. Chromatogr., **468** (1989) 303.

41.   N.I. Wakayama, H. Nozoye and I. Ogasawara, Anal. Chem., **59** (1987) 681.

42.   S. Cheskis, E. Atar and A. Amirav, Anal. Chem., **65**, (1993) 539.

43.   L. Huber and H. Obbens, J. Chromatogr., **349** (1985) 465.

44.   M.D. Muller, Anal. Chem., **59** (1987) 617.

45.   S.V. Olesik, L.A. Pekay and E.A. Paliwoda, Anal. Chem., **61** (1989) 58.

46.   J. Dachs and J.M. Bayona, J. Chromatogr., **636** (1993) 277.

47.   J. Efer, T. Maurer and W. Engewald, Chromatographia, **29** (1990) 115.

48.   W.A. Aue, B. Millier and X.-Y. Sun, Anal Chem., **63** (1991) 2951.

49.   W.A. Aue and C.R. Hastings, J. Chromatogr., **87** (1973) 232 .

50.   C.Th.J. Alkemade, Tj. Hollander, W. Snelleman and P. J. Th. Zeegers, <u>Metal Vapours in Flames</u>, International Series in Natural Philosophy, Vol. 103, Pergamon Press, 1982.

51.   E.J. Sowinski and I.H. Suffet, Anal. Chem., **46** (1974) 1218.

52.   E.J. Sowinski and I.H. Suffet, J. Chromatogr. Sci., **9** (1971) 632.

53.   W.A. Aue, X.-Y. Sun, B. Millier, J. Chromatogr, **606** (1992) 73.

54.   X.-Y Sun and W.A. Aue, Can. J. Chem., **70** (1992) 1129.

55.   C.G. Flinn and W.A. Aue, J. Chromatogr., **186** (1979) 299.

56.   C.G. Flinn and W.A. Aue, Can. J. Spectrosc. **25** (1980) 141.

57. C.G. Flinn and W.A. Aue, J. Chromatogr.Sci., **18** (1980) 136.

58. W.A. Aue and C.G. Flinn, Anal. Chem., **52** (1980) 1537.

59. R.M. Dagnall, B. Fleet and T.H. Risby, Talanta, **18** (1971) 155.

60. S. Kapila and C.R. Vogt, J. Chromatogr. Sci., **17** (1979) 327

61. R. Belcher, S.L. Bogdanski, S.A. Ghonaim and A. Townshend, Anal. Chim. Acta, **72** (1974) 183.

62. W.A. Aue and X.-Y. Sun, J. Chromatogr., **633** (1993) 151.

63. C.G. Flinn and W.A. Aue, J. Chromatogr., **153** (1978) 49.

64. W.A. Aue and C.G. Flinn, J. Chromatogr., **158** (1978) 161.

65. R. Ross and T. Shafik, J. Chromatogr. Sci., **11** (1973) 46.

66. C.A. Burgett and L.E. Green, Spectrochim. Acta, **30B** (1975) 55.

67. W.A. Aue, B. Millier and X.-Y. Sun, Anal. Chem., **62** (1990) 2453.

68. X.-Y. Sun and W.A. Aue, J. Chromatogr., **467** (1989) 75.

69. X.-Y. Sun and W.A. Aue, Can. J. Chem., **67** (1989) 897.

70. X.-Y. Sun and A.W. Aue, Mikrochim. Acta, **I** (1990) 1.

71. W.A. Aue, C.G. Eisener, J. A. Gebhardt and N. B. Lowery, J. Chromatogr. A, **688** (1994) 153.

72. X.-Y. Sun, H. Singh, B. Millier, C.H. Warren and W.A. Aue, J. Chromatogr. A, **687** (1994) 259.

73. J.A. Gebhardt, Masters Thesis, Dalhousie University, Halifax, 1995.

74. W.A. Aue, C.G. Eisener, J.A. Gebhardt and N. B. Lowery, J. Chromatogr. A **699** (1995) 195.

75. W.A. Aue, B. Millier and X. -Y. Sun, Can. J. Chem., **70** (1992) 1143.

76. H. Singh, B. Millier and W.A. Aue, J. Chromatogr. A., **678** (1994) 291.

77.   X.-Y. Sun and W.A. Aue, J. Chromatogr. A, **667** (1994) 191.

78.   W.A. Aue and X.-Y. Sun, J. Chromatogr., **641**, (1993) 291.

79.   B. Millier, X.-Y. Sun and W.A. Aue, J. Chromatogr. A, **675**, (1994) 155.

80.   W.E. Kaskan and R.C. Milliken, J. Chem. Physics., **32** (1960) 1273.

81.   R.W.B. Pearse and A.G. Gaydon, The Identification of Molecular Spectra, 4th edition, Chapman and Hall, London (1976).

82.   K. Fujiwara, J.N. Bower, J.D. Bradshaw and J.D. Winefordner, Anal. Chim. Acta, **109** (1979) 229.

83.   Oriel Instruments: Booklet of Grating Efficiency of Curves, pp 6-8, Oriel Corporation, 250 Long Beach Blvd., Stratford, Ct., USA, 1995.

84.   R.W.B. Pearse and A.G. Gaydon, The Identification of Molecular Spectra, 3th edition, Chapman and Hall, London (1963).

85.   W.F. Meggers, C.H. Corliss and B.F. Scribner. Tables of Spectral Line Intensities Part I. National Bureau of Standards Monograph 145. U.S. Government Printing Office, Washington, D.C., 1975.

86.   M.L. Parsons and P.M. McElfresh, Flame Spectroscopy: Atlas of Spectral Lines, IFI Plenum, New York, 1971.

87.   R.S. Juvet, Jr. and R.P. Durbin, Anal. Chem., **38** (1966) 565.

88.   Kirk-Othmer, Encyclopedia of Chemical Technology, 4th ed., Vol. 4, John Wiley and Sons, 1991.

89.   D. Ws. Bierer, Reviews of Infectious Diseases, **12**, Supplement I, (1990) S3.

90.   A. Slikkerveer and F.A. de Wolff, Med. Toxicol. Adverse Drug Exp., **4(5)** (1989) 303.

91.   G.F. Kirkbright and T.S. West, Chem. Brit., **8** (1972) 428 (taken from reference 2).

92.   Award-Winning Chemistry, Aldrichimica Acta, **23** (1990) 25.